Ben M. Segal

SHOCK WAVE STRUCTURE USING NONLINEAR MODEL BOLTZMANN EQUATIONS

Submitted to
Engineering Division
National Science Foundation
April 1971

The NUCLEAR ENGINEERING LABORATORY
at STANFORD UNIVERSITY
Stanford, California

SHOCK WAVE STRUCTURE

USING NONLINEAR MODEL BOLTZMANN EQUATIONS

by

Ben Maurice Segal

Submitted to

Engineering Division
National Science Foundation

Approved by

Anthony Leonard and Joel H. Ferziger
Principal Investigators

April 1971

Work supported in part by National Science Foundation
Grant No. GK-4251

Nuclear Engineering Division
Department of Mechanical Engineering
Stanford University
Stanford, California

ACKNOWLEDGMENTS

I gratefully acknowledge the valuable contributions made to this work by my adviser Prof. Joel Ferziger. I would also like to thank Prof. Anthony Leonard and Prof. Donald Baganoff for reading the manuscript and offering helpful comments, Prof. Donald Anderson of Harvard University for providing details of his numerical methods, Dr. Sam Schechter of Stanford Research Institute for suggesting the development of a Gauss-Seidel iteration, Dr. George Deiwert of Ames Research Center for providing some essential Monte Carlo solutions, and Prof. Graeme Bird of the University of Sydney for clarifying some of his published Monte Carlo results.

Financial support from the National Science Foundation under Grant GK-4251 and the National Aeronautics and Space Administration under Grant NGR-05-020-420 was also greatly appreciated.

I thank my many colleagues at the Ryan Laboratory, particularly Drs. Michael Hemsch and Gregg Dixon and Profs. Thomas Connolly and Rudolph Sher, for all the stimulating discussions, technical and otherwise, which so enriched my time there. Especial thanks are due to Mrs. Ruth Korb for all the support she gave me as secretary and friend, including the superb typing of this thesis.

Finally I thank my wife Eva for her loving help and encouragement throughout, and my son Adam for many diversions over the last twenty months.

TABLE OF CONTENTS

LIST OF TABLES

LIST OF FIGURES

CHAPTER I

INTRODUCTION AND BACKGROUND

A. Introduction

The structure of a strong plane shock wave in a monatomic rarefied perfect gas is one of the simplest problems able to be posed in kinetic theory, and one of the hardest to solve. Its simplicity lies in the absence of solid boundaries, geometrical complications, or internal molecular energy. Its difficulty arises from the great departure of the gas from equilibrium within the shock, which invalidates many of the techniques used successfully elsewhere in kinetic theory.

In addition to this theoretical challenge, the modern development of ballistics and hypersonic flight has helped to stimulate extensive theoretical and experimental interest in the shock problem. The experimenters in turn have encountered great difficulties on account of the very small physical dimensions of shocks. In fact, until very recently indeed, any close comparisons of theoretical and experimental shock structure results have been rather unprofitable due to inadequacies of both theory and experiment.

During the last few years this situation has been appreciably improved by development of the Monte Carlo method. This allows idealized "experiments" to be performed on large computers instead of in wind tunnels, using a known intermolecular force law. The most developed of these methods has been shown to be equivalent theoretically to the Boltzmann equation and to give results which agree extremely closely with measurements of high accuracy. Thus Monte Carlo results not only form the

soundest basis for our present theoretical knowledge of shock wave structure, but, for purposes of developing other theories, can also be considered a very valuable experimental resource. However, such results remain very expensive to obtain.

In this thesis we develop more economical kinetic theory methods for the approximate prediction of shock structure, and compare our results with those of the Monte Carlo method.

B. Background

A shock wave represents a disturbance in a gas that propagates with a speed higher than that of sound transmission. In front ("upstream") of the wave front, the gas is in its undisturbed equilibrium state, and behind ("downstream") the gas attains a different equilibrium state with a higher temperature and pressure than before. The physical extent of the transition zone between the two states is very small, being of the order of a few mean molecular free paths in the gas (about 10^{-4} cm. for a moderate shock in air). It is the detailed description of this transition zone in the case of an infinite plane shock front far from any boundaries that we refer to here as the plane shock structure problem.

Shock waves are associated physically with explosive detonations or objects of greater than sonic speed passing through the gas. Such conditions are characterized by the "Mach number", M, taking on values greater than unity. For M close to unity we speak of "weak" shock waves, in which the states on either side of the front are only slightly different and the gas never moves far from an equilibrium state. For higher values of M, above about 3, we speak of "strong" shock waves, in which the state parameters n (density), u (flow velocity), and T (temperature)

differ widely across the front and the gas departs strongly from equilibrium in the transition zone. It is this latter case of strong shocks which primarily interests us in this work, as the theory of weak shocks was satisfactorily completed many years ago.

The laws of thermodynamics, as was shown in the 19th century, permit only compressive shocks, the type described above, and forbid the existence of a rarefaction shock (in a perfect gas) for which the wave would advance from a lower into a higher pressure zone. It is convenient to use coordinates moving with the shock front. In this frame, which we shall use throughout this work, the shock wave is a time-independent change of state of the gas from one condition of equilibrium flow upstream, with state parameters (n_1,u_1,T_1), to another equilibrium state downstream (n_2,u_2,T_2), where $n_2 > n_1$, $u_2 < u_1$, and $T_2 > T_1$; u_1 is the front speed in the observer's frame of coordinates.

C. Previous Theoretical Approaches

The theoretical approaches to the shock problem up to the present time have fallen into five main categories:

1. Application of the continuum equations of fluid dynamics.
2. Solutions of the Boltzmann equation by either the Chapman-Enskog or Grad expansion about equilibrium.
3. Approximate solutions of the Boltzmann equation using an ansatz for the molecular distribution function.
4. Solutions to approximate ("model") Boltzmann equations.
5. Monte Carlo, or direct simulation, methods.

The chronology of these approaches generally follows the listed order above, with the relative accuracy of the approaches (for strong shock waves) also increasing in the same order. We will discuss the approaches by category, attempting to stress only the most important advances as the total body of work is very extensive.

1. Continuum Approaches

The earliest discussions of the shock problem centered primarily on the existence of shock-like solutions to the Euler (inviscid) or Navier-Stokes (viscous) flow equations of continuum fluid dynamics. The work of Earnshaw [1], Stokes [2], Rankine [3], Hugoniot [4], and others in the 19th century was unified finally by Rayleigh [5], and (independently and more concisely) by Taylor [6] in two papers submitted within days of each other in 1910 and appearing in the same issue of the Royal Society of London Proceedings.

This early work established that for a realistic wave to exist in the steady state, a non-adiabatic process must be involved and that therefore heat conduction is required. The necessary dissipation mechanism could furthermore be provided by viscosity. The second law of thermodynamics was shown to admit only compressive shocks and exclude rarefaction shocks. The conditions connecting the states on either side of the front were derived from the laws of conservation of mass, energy, and momentum and named after Rankine and Hugoniot.

Rayleigh applied his Navier-Stokes theory to the calculation of drag on a rifle bullet, assuming constant values for the coefficients of viscosity (μ) and heat conduction (κ). Taylor also studied the case of constant coefficients, obtained the solution for a weak shock and estimated

the thickness of stronger shocks. Taylor clearly recognized the important concept of a non-equilibrium distribution function within the shock.

The next advance was made by Becker [7] in 1922, who obtained a strong shock solution of the Navier-Stokes equations in a special case (for a Prandtl number of 3/4), again assuming constancy of μ and κ. The shock thicknesses predicted were so small that they not only implied failure of the Navier-Stokes assumptions (that a rapid change of state does not occur within a mean free path), but also violated even the Boltzmann equation assumptions (that the thickness not approach the average intermolecular distance).

An important paper by Thomas [8] in 1944 showed that it was vital to include the variation with temperature of μ and κ within the shock. He showed that although for strong shocks the Navier-Stokes assumptions may well be violated, the Boltzmann equations would always apply whatever the Mach number. He also included an estimate of the Burnett correction to the Navier-Stokes formulation, yielding a slight increase in shock thickness.

Later work on the shock problem consisted of successive refinements of the simple continuum theory, followed by more detailed applications of non-equilibrium kinetic theory. Calculations with the Navier-Stokes and Burnett equations, allowing very general variation of the viscosity and conductivity, have been made by Gilbarg and Paolucci [9], Schwartz and Hornig [10], and others. The overall conclusions from all the continuum work is that these approaches are accurate only for weak shocks ($M \lesssim 2$) and cannot be extended to higher M, where they consistently underpredict shock thicknesses.

2. Expansions about Equilibrium

This category partially overlaps category 1 as the Euler, Navier-Stokes, and Burnett continuum equations can be derived by the Chapman-Enskog method, which will be discussed here.

Wang-Chang [11] in 1948 made a thorough study of the shock problem with the Chapman-Enskog method up to third order, and showed that the resulting series solutions (involving powers of $M-1$) converged so slowly that they would not be of value above $M \sim 1.2$; for stronger shocks the implicit assumption of the Chapman-Enskog method, that the distribution function can be expanded about a local Maxwellian equilibrium function, becomes unsatisfactory.

A related difficulty was encountered by Grad [12] in 1952 when applying his own expansion method to the shock problem. Grad expanded the distribution function in an infinite series of Hermite polynomials in the velocity, with the local Maxwellian as weight function. He then set up a finite set of moment equations for the lower expansion coefficients, and by extending the set hoped to approach the solution of the Boltzmann equation as closely as desired. At the 13-moment stage, solutions ceased to exist for shocks with $M > 1.65$. In 1964 Holway [13] showed that beyond $M = 1.851$ (which corresponds to a temperature ratio $T_2/T_1 = 2$), the series cannot converge to the distribution function. This is because even near the cold side where $T = T_1$, there will always be a small number of "hot" (i.e., "shock-heated") molecules which have diffused back through the shock. Near the cold side, the weight function of the expansion becomes the local T_1 Maxwellian function and prevents a convergent representation of any Maxwellian component with $T_2 > 2T_1$.[†]

[†] For convergence in the least-squares sense, the approximated function must approach zero faster than the square root of the weight function as $c \to \infty$: this condition leads to the temperature inequality above.

We have once again seen that quasi-equilibrium theories are inadequate for the shock problem above shock strengths corresponding to $M \sim 2$.

3. Modelled Distribution Functions

This category of solutions is a very extensive one, as it contains most of the work done on the shock problem since 1950. This work began with the celebrated paper of Mott-Smith [14] in 1951, and most later authors draw upon his ideas. The principle common to all these approaches is to propose a form for the distribution function which contains a number of free parameters; equations for these parameters are then derived from the Boltzmann equation and solved to yield an approximate solution to that equation. Usually moments of the Boltzmann equation are used for this purpose (and the parameters are often moments themselves), and one obtains sets of ordinary differential equations for the parameters. Occasionally a minimum-error criterion is used instead of moment equations for the parameters.

The success of these methods depends mainly on the appropriateness of the ansatz chosen, and the number and form of the free parameters. The aim is always to avoid the errors of the quasi-equilibrium theories by including the essential non-equilibrium aspects of the problem. If the ansatz, parameters, or solution criteria are inconsistent or oversimplified, solutions will fail to exist for certain (or all) Mach numbers.

Because of its importance, both historically and as a source for certain ideas used in the present work, some details of the Mott-Smith method are given in Appendix C. The method's strengths are that it predicts strong shock thicknesses ($M \gtrsim 3$) in very good agreement with experiment and Monte Carlo results; that its simple ansatz provides a very good

physical picture of the non-equilibrium situation within the shock; and that it leads to a simple analytical formulation, involving numerical analysis only on the level of solving a differential equation. Later workers tried to retain as many of these features as possible, while correcting one or more of the weaknesses. These are:

a. Shock thicknesses at low Mach number agree poorly with the Navier-Stokes values, which are correct in this range.

b. Results (i.e., the value of B in Eqn. (C.5)) are very sensitive to the choice of the moment equation which is used to complete the solution, and no guide to this choice is offered by the theory. In fact, solutions fail to exist for the choice c_x^n for $n > 6$ [15].

c. The predicted density profile is symmetrical in form, and this is unsupported by experiment at high M.

In attempts to correct (a), while retaining the good results at high M, many workers have proposed modifications to the simple ansatz (C.2). Three or more Maxwellian components were included by Salwen [17], Krook [18,19], Macomber [20], and others. The hot Maxwellian $f_2^{(0)}$ in (C.2) was modified to an ellipsoidal Maxwellian by Holway [21]. Truncated expansions about f_{MS} or about $f_2^{(0)}$, avoiding the convergence difficulty of the Grad expansion, were used by Radin and Mintzer [22] and Muraoka et al. [23]. These methods permit at least two "free" moment equations. All succeed in improving (a) and (c), but usually not (b). However, along with improvements in these areas come some characteristic oddities, the most significant being the prediction by nearly all the methods of a "temperature overshoot" at high M. That is, near the hot side of the shock, the temperature reaches a maximum before settling out at its

equilibrium value T_2 at large positive x. This effect is not present in the Mott-Smith solution, although a numerical error in his original paper led him to state that it was; the correction to this point was given by Gustafson [24]. The best available evidence at the present time, due to Monte Carlo results, does not support the existence of such an overshoot.

To deal with weakness (b), two modified approaches are of interest. In the "Two-Fluid" method of Glansdorff [25], also used by Ziering et al. [26], the shock is treated as a two-component system governed by a pair of Boltzmann equations, one each for the cold and hot molecules. Collisions provide a small coupling term which converts cold molecules into hot molecules throughout the shock. Six unknown parameters appear initially and are evaluated using six moment equations which follow without arbitrariness from the two Boltzmann equations of the method. The solution turns out to be formally identical to the Mott-Smith solution (C.5), but with its own value of B. The resulting shock thicknesses at high M are similar to the Mott-Smith values. The main value of the approach lies in the physical arguments which lend support to the picture of a shock as a mixture of two coexisting components, each with its own temperature and mean velocity.

Very recently, Baganoff and Nathenson [27] avoided difficulty (b) in an original way. They closed a set of five moment equations (involving seven moments in all) by assuming two "constitutive relations" between certain of the moments, rather than by assuming an ansatz for the distribution function. They report shock thicknesses in excellent agreement with experiment.

4. Models of the Boltzmann Equation

The idea here is to substitute a simpler "model" for the Boltzmann equation and then solve this model equation. In 1954 Bhatnagar, Gross, and Krook [28] proposed the first "statistical model" (known by their initials as the BGK model), in which the collision operator J in (2.1) is replaced by a far simpler term. As the original J is a complicated fivefold nonlinear integral operator and forms the main obstacle to solution of the Boltzmann equation, the BGK model equation is a good deal easier (though still not simple) to solve. The detailed development of models is treated more fully in Chapter III, as these models form the basis for our own approach to the shock problem.

The first applications of the BGK model to the shock problem were made by Liepmann's group at Caltech [29,30,31] beginning in 1962, and by Anderson [32,33] at Harvard in 1963. Anderson's work was numerically superior and his solutions provide exact BGK predictions of shock structure for all M. The BGK shock thicknesses agree well with Navier-Stokes values for weak shocks but are appreciably smaller than the Mott-Smith and experimental values for strong shocks. In better accord with experiment are the BGK predictions of an asymmetric density profile and no temperature overshoot at high M.

In 1963, Holway [35,36] proposed an extension of the BGK model which he called the Ellipsoidal Statistical model, and obtained approximate ansatz-moments solutions for it [37] which indicated shock thicknesses in better agreement with the Mott-Smith values for strong shocks, together with a temperature overshoot. It was not clear, however, whether the overshoot was a property of the model itself or just a side effect of the

approximate moments method used for solution. At low M, the Navier-Stokes solutions were recovered.

Very recently, Giddens et al. [38,39] have reported numerical calculations by the discrete-ordinates method for both the BGK and Ellipsoidal models. Their BGK results agree with those of Anderson, but results for the Ellipsoidal model have not been published in detail. As will be seen in the later chapters of this work, the explicit calculation of a distribution function for models of this type is unnecessary.

A few final remarks can be added on a different sort of model, proposed in 1964 by Broadwell [40]. Here the gas itself is modelled physically, the molecules being idealized as moving with a single speed in one of the six Cartesian directions $(\pm x, \pm y, \pm z)$. The Boltzmann equation for such a system reduces to a coupled set of ordinary differential equations for the number of molecules in each direction. A shock solution is possible for the single case of infinite M, and has the Mott-Smith form (C.5) with a sensible value of thickness. Such a simple model is not of value for quantitative predictions, but is included here because of its suggestive idea of simulating the molecular motions directly in a model. This leads us naturally to the final category.

5. Monte Carlo Methods

The "Monte Carlo" approach is a very recent development which uses a large fast computer to perform a probabilistic numerical experiment. To date, three main variants exist, of which the third will be of especial interest to us.

The first method, that of Hicks et al. [41,42,43], simply attempts to estimate the fivefold Boltzmann collision integral by random sampling.

The method is not very efficient, but accurate results have been obtained with it.

The second ("test particle") method has been used by Haviland [44] and Perlmutter [45], and uses a successive linearization approach. A solution is assumed, leading to a distribution of target molecules. Test particles are then introduced and followed as they scatter in this background, but do not affect the background. When results have accumulated sufficiently, a new background of targets is generated which accounts for the results correctly, and the process reiterated. This again is not a very efficient method, but improvements are possible by input of physical insight.

The third ("direct simulation") method is due to Bird [46,47,48], and is both efficient and applicable to nonlinear and unsteady problems without difficulty. Its efficiency comes from a collision sampling method in which molecules are not followed deterministically but advantage is taken of the Boltzmann assumptions:

$$\text{Force range} \ll \text{molecular spacing} \ll \text{mean free path} .$$

The problem space is subdivided into small cells and collisions are generated randomly among molecules occupying the same cell. Collision probabilities are made proportional to a pair's relative velocity times the cross-section. The number of collisions sampled in a cell is made proportional to the local collision frequency by assigning each collision its correct relative collision time, and sampling until a suitable time step is exhausted. After each step all molecules are allowed to fly freely and collision sampling recommences with updated cell assignments.

Bird has shown the method to be equivalent in principle to the Boltzmann equation [49], and to be feasible in use with convenient choices for the cell volumes and the time step. Shock wave results of high accuracy have been obtained. In the only instance to date of a physical measurement having comparable accuracy (that of Schmidt [50], with a density profile in argon determined to within a few percent at Mach 8), the agreement between computed and measured density profiles is well within the experimental uncertainty. An inverse-12th power force law was assumed for this Monte Carlo run, consistent with the argon viscosity-temperature relation $\mu \sim T^{0.68}$ measured recently in the appropriate range by Matula [51]. Thus, as stated in the Introduction, the Bird method seems to provide the most convenient and reliable reference with which to compare approximate theories of shock structure.

D. Scope of the Present Work

Having surveyed the extensive approaches made by others to the shock problem, we will now outline our own approach, which falls into category 4 above. This approach allows economical yet accurate calculations of shock structure to be made without any assumptions or restrictions on the form of the distribution function.

In Chapter II we present the overall formulation of the shock problem, beginning with the Boltzmann equation. We then proceed to a general modelled form of this equation, transforming it finally into the equivalent system of moment equations used for solution.

In Chapter III we present details of the four statistical models used, including derivations of the two new models we have developed during the course of this work.

In Chapter IV we discuss the numerical methods used to calculate solutions to the various model equations, which are pairs of coupled nonlinear integral equations. We stress those methods which are either relatively new or which were developed by ourselves for the present work.

In Chapter V the results of the calculations are given and a discussion of their physical significance is presented. Comparisons with Monte Carlo results are made.

In Chapter VI we present a summary of the work and our conclusions.

CHAPTER II

FORMULATION OF THE PROBLEM

A. The Boltzmann Equation

The equation describing the behavior of a monatomic gas in steady one-dimensional flow is the Boltzmann equation for the molecular distribution function f:

$$c_x \frac{\partial f(\underline{c},x)}{\partial x} = \iiiint [f(\underline{c}')f(\underline{c}_1') - f(\underline{c})f(\underline{c}_1)]gbdbd\varepsilon d\underline{c}_1$$

$$\triangleq \mathcal{J}[f,f] - f\mathcal{L}[f] \qquad (2.1)$$

$$\triangleq J[f,f] \quad .$$

Here,

$f(\underline{c},x)dxd\underline{c}$ = the expected number of molecules in the space element dx about x with velocities in the range $d\underline{c}$ about $\underline{c}$.

$\underline{c}',\underline{c}_1'$ = the velocities before a binary collision of two molecules which after collision have respective velocities $\underline{c},\underline{c}_1$.

$g = |\underline{c}-\underline{c}_1| = |\underline{c}'-\underline{c}_1'|$, the relative speed of colliding molecules.

b = the collision parameter: the distance of closest approach of the molecule centers in the absence of a collision.

ε = the orientation angle in space of the plane of collision.

$\mathcal{J}[f,f] = \iiiint f(\underline{c}')f(\underline{c}_1')gbdbd\varepsilon d\underline{c}_1$, the Boltzmann "gain operator".

$\mathcal{L}[f] = \iiiint f(\underline{c}_1)gbdbd\varepsilon d\underline{c}_1$, the Boltzmann "loss operator".

The boundary conditions associated with (2.1) for the shock problem are:

$$\left.\begin{aligned} f(\underline{c},x = -\infty) &= f^{(0)}(n_1,u_1,T_1) \triangleq f_1^{(0)} \\ f(\underline{c},x = +\infty) &= f^{(0)}(n_2,u_2,T_2) \triangleq f_2^{(0)} \end{aligned}\right\} \qquad (2.1a)$$

where $f^{(0)}$ is the Maxwellian distribution function defined by:

$$f^{(0)}(n,\underline{u},T) = n(2\pi RT)^{-3/2}\exp[-(\underline{c}-\underline{u})^2/2RT] \quad , \qquad (2.2)$$

with parameters n, the density; $\underline{u}$, the flow velocity; and T, the temperature. In the case of a one-dimensional flow in the x direction, the velocity $\underline{u}$ will be understood to be in this direction and we shall write:

$$f^{(0)}(n,u,T) = n(2\pi RT)^{-3/2}\exp[-(\underline{c}-u\underline{i})^2/2RT] \quad , \qquad (2.2a)$$

where $\underline{i}$ is a unit vector in the x direction.

The upstream and downstream sets of parameters (n_1,u_1,T_1) and (n_2,u_2,T_2), respectively, are determined as follows. Two of the six parameters, n_2 and T_2, are fixed arbitrarily and a third is obtained by fixing the upstream Mach number M_1:

$$M_1 \triangleq u_1/(\gamma RT_1)^{1/2} \quad , \qquad (2.3)$$

where:

$$\gamma = c_p/c_v \qquad (= 5/3 \text{ for a perfect monatomic gas}) \quad , \qquad (2.4)$$

and c_p,c_v are the specific heats at constant pressure and volume, respectively. For convenience, we will drop the suffix 1 from M_1 from now on.

Three more relations, the well-known Rankine-Hugoniot relations, state the one-dimensional conservation of mass, momentum, and energy:

$$n_1 u_1 = n_2 u_2 \quad , \tag{2.5}$$

$$n_1(u_1^2 + RT_1) = n_2(u_2^2 + RT_2) \quad , \tag{2.6}$$

$$n_1 u_1(u_1^2 + 5RT_1) = n_2 u_2(u_2^2 + 5RT_2) \quad . \tag{2.7}$$

Algebraic manipulation of (2.3) - (2.7) yields the results:

$$u_2/u_1 = (M^2+3)/4M^2 \triangleq u_r(M) \quad , \tag{2.8}$$

$$T_2/T_1 = (M^2+3)(5M^2-1)/16M^2 \triangleq T_r(M) \quad , \tag{2.9}$$

$$n_2/n_1 = 4M^2/(M^2+3) \triangleq n_r(M) \quad . \tag{2.10}$$

Choosing the arbitrary values for n_2 and T_2 as:

$$n_2 = 1 \quad , \tag{2.11}$$

and:

$$RT_2 = 1 \quad , \tag{2.12}$$

we may finally write the expressions for the upstream and downstream boundary parameters in terms of the single dimensionless parameter M:

$$\left.\begin{aligned} n_1 &= 1/n_r(M) \quad , & n_2 &= 1 \\ u_1 &= M\sqrt{5/(3T_r(M))} \quad , & u_2 &= u_1 \cdot u_r(M) \\ T_1 &= 1/(RT_r(M)) \quad , & T_2 &= 1/R \quad . \end{aligned}\right\} \tag{2.13}$$

B. Model Boltzmann Equations

Equation (2.1) is formidable due to the very complicated nonlinear Boltzmann collision operator $J[f,f]$. This operator represents the net rate of increase of $f(\underline{c},x)$ in time due to molecular collisions; its complexity prevents exact solution of (2.1). The idea consequently emerged of replacing J by a simpler "model" operator which would allow solution of the resulting "model Boltzmann equation" while still giving a satisfactory account of the physical collision process. The details of choosing appropriate models for J will be discussed in Chapter III. To complete the present formulation we simply note that all the models we shall employ have the form:

$$J[f,f] \approx K(m_i) \cdot \{\Psi(\underline{c},m_i) - f\} \quad . \tag{2.14}$$

The function $K(m_i)$, which models the operator $\mathcal{L}[f]$, represents an average collision frequency and is assumed independent of $\underline{c}$. The function $\Psi(\underline{c},m_i)$ models $\mathcal{Q}[f,f]/\mathcal{L}[f]$ and is called the emission function as it describes the average distribution of molecules following a collision. The quantities m_i are velocity moments of f defined by:

$$m_i \triangleq \int \phi_i(\underline{c}) f(\underline{c}) d\underline{c} \quad ,$$

with the ϕ_i being a chosen set of functions of $\underline{c}$. Some of the interesting low-order moments are:

$$\left.\begin{aligned}
m_1 &= n \triangleq \int f d\underline{c} \quad , \\
\underline{m}_2 &= \underline{u} \triangleq \frac{1}{n} \int f \underline{c} d\underline{c} \quad , \\
m_3 &= T \triangleq \frac{1}{3Rn} \int f C^2 d\underline{c} \quad , \qquad \underline{C} = \underline{c} - \underline{u} \quad , \\
\underline{\underline{m}}_4 &= \underline{\underline{\tau}} \triangleq \frac{1}{n} \int f \underline{\underline{C^0C}} d\underline{c} \quad , \qquad \underline{\underline{C^0C}} = \underline{\underline{CC}} - \frac{1}{3} C^2 \underline{\underline{\delta}} \quad , \\
\underline{m}_5 &= \underline{q} \triangleq \frac{1}{2n} \int f \underline{C} C^2 d\underline{c} \quad .
\end{aligned}\right\} \tag{2.15}$$

These are physically the density n, the flow velocity $\underline{u}$, the temperature T, the stress tensor $\underline{\underline{\tau}}$, and the heat flux vector $\underline{q}$. It will be noted that all the hydrodynamical variables of common interest are included in the set m_i, $i = 1$ to 5, and in this work we restrict m_i to this set.

The major simplifying feature of all these models is their replacement of J by an operator on the moments of $f(\underline{c},x)$ rather than being a fivefold integral operator on f itself. This allows reduction of the model Boltzmann equation to equations for the moments, which are the quantities of physical interest, rather than for the distribution function f. Once the moments m_i are determined for a model equation, f can then be generated if desired.

C. Exact Moment Equations for the Models

A closed set of coupled nonlinear integral equations for the moments m_i is obtained as follows. For convenience, $K(m_i)$ is first absorbed into a new coordinate t, defined as:

$$\begin{aligned} dt &= K(x)dx \quad \underline{\text{or}}: \quad t = \int_{x_0}^{x} K(x)dx \ , \\ dx &= dt/K(t) \quad \text{or}: \quad x = \int_{t_0}^{t} dt/K(t) \ , \end{aligned} \tag{2.16}$$

where the dependence of K upon x or t is understood to be via the m_i. Here x_0 and t_0 are arbitrary reference origins. Apart from mere formal simplification, the use of the t frame has the advantage that in it shock profiles tend to an invariant form at high values of the Mach number, M. This will unify our present work, which deals with strong shocks falling into this range of M.

In the t-frame, Eqn. (2.1) with the model operator (2.14) becomes:

$$c_x \frac{\partial f(\underline{c},t)}{\partial t} + f(\underline{c},t) = \Psi(\underline{c},m_i(t)) \quad , \tag{2.17}$$

with the boundary conditions (2.1a) still applying. Formally integrating (2.17) over t, after division throughout by c_x, we now get an integral equation for f:

$$f(\underline{c},t) = \begin{cases} \displaystyle\int_{-\infty}^{t} dt' \frac{\Psi(\underline{c},m_i(t'))}{c_x} \exp \frac{-(t-t')}{c_x} \quad , & c_x > 0 \quad , \\ \displaystyle\int_{t}^{\infty} dt' \frac{\Psi(\underline{c},m_i(t'))}{(-c_x)} \exp \frac{-(t'-t)}{(-c_x)} \quad , & c_x < 0 \quad , \end{cases} \tag{2.18}$$

$$\triangleq \fint_{-\infty}^{\infty} dt' \frac{\Psi(\underline{c},m_i(t'))}{|c_x|} \exp -\left|\frac{t-t'}{c_x}\right| \quad ,$$

using the notation $\fint$ to indicate the split range of integration.

Taking velocity moments of equation (2.18), we obtain a set of moment equations:

$$m_i(t) = \iiint d\underline{c} \fint_{-\infty}^{\infty} dt' \phi_i(\underline{c}) \frac{\Psi(\underline{c},m_i(t'))}{|c_x|} \exp -\left|\frac{t-t'}{c_x}\right| \quad . \tag{2.19}$$

Without restricting the m_i, (2.19) would be an infinite set of equations, but with the restriction adopted in Section B that only the set m_i, $i = 1$ to 5, appears in Ψ, (2.19), for $i = 1$ to 5, becomes a closed set† of coupled integral equations for these m_i. For one-dimensional flows, the only five nonzero components of these moments are: n, u, T, τ_{xx}, and q_x, which correspond respectively to the five ϕ_i choices: 1, c_x/n, $C^2/3Rn$, $(C_x^2 - \frac{1}{3}C^2)/n$, and $C_x C^2/2n$.

† Note that because the set (2.19) is derived by taking moments of Eqn. (2.18) rather than of the Boltzmann equation (2.17), no "extra" moments are generated to prevent closure of the set.

Furthermore, if a related set of moment equations is substituted, these five components can be obtained by solving only a pair of coupled equations. Consider the moments μ_i corresponding to the choice $\phi_i^* = 1, c_x, c^2, c_x^2,$ and $c_x c^2$. These moments have the following relation to the five nonzero m_i of the preceding paragraph:

$$\begin{aligned}
\mu_1 &= n \ , \\
\mu_2 &= nu = \underline{\text{constant of flow}}^{\dagger} \ , \\
\mu_3 &= n(3RT + u^2) \ , \\
\mu_4 &= n(RT + u^2 + \tau_{xx}) = \underline{\text{constant of flow}}^{\dagger} \ , \\
\mu_5 &= nu(5RT + u^2 + 2\tau_{xx}) + 2nq_x = \underline{\text{constant of flow}}^{\dagger} \ .
\end{aligned} \tag{2.20}$$

Because μ_2, μ_4, and μ_5 are constants of the flow, and τ_{xx} and q_x both vanish at the endpoints, only equations for $\mu_1(t)$ and $\mu_3(t)$ are needed to determine all the μ_i, and hence all the nonzero $m_i(t)$, $i = 1$ to 5. These two moment equations are generated by putting $\phi_i^*(\underline{c}) = 1$ and c^2 into Eqn. (2.19), yielding:

$$\left.\begin{aligned}
\mu_1(t) &= \int_{-\infty}^{\infty} dc_x \int_0^{\infty} 2\pi c_t dc_t \oint_{-\infty}^{\infty} dt' \, \frac{\Psi(c_x, c_t, m_i(\mu_i(t')))}{|c_x|} \exp-\left|\frac{t-t'}{c_x}\right| \\
\mu_3(t) - \mu_4 &= \int_{-\infty}^{\infty} dc_x \int_0^{\infty} 2\pi c_t^3 dc_t \oint_{-\infty}^{\infty} dt' \, \frac{\Psi(c_x, c_t, m_i(\mu_i(t')))}{|c_x|} \exp-\left|\frac{t-t'}{c_x}\right|
\end{aligned}\right\} \tag{2.21}$$

where we have written the velocity $\underline{c}$ as (c_x, c_t), c_t being the component transverse to the x axis, and have used the relation $c^2 = c_x^2 + c_t^2$.

---

† Moments of the collision operator J taken with the collisional invariants $\psi_i^{col} \triangleq 1$, c_x and c^2 must vanish. By (2.1), the same moments of $c_x \frac{\partial f}{\partial x}$ must also vanish. Integrating this result over x, the moments of f taken with $c_x \psi_i^{col}$ must therefore be constants. These moments are μ_2, μ_4, and μ_5, respectively.

D. The H_n Kernel Functions

The kernels of Eqns. (2.21) are still inconvenient for computation as they involve double quadratures over the components of $\underline{c}$. For all the models to be studied, however, the emission function Ψ has the form of a Maxwellian function (or functions) multiplied by velocity polynomial(s). For this case the kernels can be expressed in terms of a well-studied [52,53] series of functions defined as:

$$H_n(p,q) \triangleq \frac{1}{\sqrt{2\pi}} \int_0^\infty y^{n-2} \exp - \left[\frac{1}{2}(y-p)^2 + q/y\right] dy \quad . \tag{2.22}$$

The $H_n(p,q)$ functions are conveniently computed using asymptotic or power series methods (as described in Ref. 53) for values of n from 1 to 3, and for all higher n use can be made of the recurrence relation:

$$H_n(p,q) = pH_{n-1} + (n-2)H_{n-2} + qH_{n-3} \quad . \tag{2.22a}$$

Another convenient method for computing $H_n(p,q)$, when H_n values for $n = 1$ to 3 are known at nearby p_0,q_0, is a bivariate N^{th}-order Taylor series of the form:

$$H_n(p_0+\delta p, q_0+\delta q) = H_n(p_0,q_0) + \sum_{i,j=1}^{(i+j)=N} \left(\frac{\partial^{i+j} H_n}{\partial^i p \partial^i q}\right)_{\substack{p=p_0 \\ q=q_0}} \frac{\delta p^i \delta q^j}{i!j!} \quad , \tag{2.22b}$$

where the partial differential coefficients are computed using the relations:

$$\frac{\partial H_n}{\partial p} = H_{n+1} - pH_n \quad , \tag{2.22c}$$

$$\frac{\partial H_n}{\partial q} = -H_{n-1} \quad . \tag{2.22d}$$

By substituting the emission function Ψ for each model into Eqn. (2.21), performing the c_t integration, and using (2.22) as shown in Appendix A, we find that each model can be cast into the same general form used for numerical solution:

$$\left.\begin{aligned} n(t) &= \int_{-\infty}^{\infty} n(t')\mathcal{K}_n(n(t'),T(t');t-t')dt' \quad , \\ n(t)T(t) &= \int_{-\infty}^{\infty} n(t')\mathcal{K}_T(n(t'),T(t');t-t')dt' + \frac{1}{3R}\left[\mu_4-\mu_2^2/n(t)\right] . \end{aligned}\right\} \quad (2.23)$$

The kernels $\mathcal{K}$ in Eqns. (2.23) for all the models are sums of low-order H_n functions; the actual kernels obtained for each model are given in Appendix A. All kernels $\mathcal{K}$ possess a logarithmic singularity at $t' = t$; as an example, we display the resulting kernels for the simplest of the models, the BGK model, for which the emission function $\Psi = f^{(0)}(n,u,T)$:

$$\mathcal{K}_n^{BGK} = [RT(t')]^{-\frac{1}{2}} H_1\left(\frac{\mu_2 \mathrm{sgn}(t-t')}{n(t')\sqrt{RT(t')}}, \frac{|t-t'|}{\sqrt{RT(t')}}\right) ,$$

$$\mathcal{K}_T^{BGK} = \frac{2}{3} T(t') \mathcal{K}_n^{BGK} .$$

CHAPTER III

DERIVATION OF THE MODELS

A. General Physical Considerations

Of the four kinetic models to be considered, two were developed by previous authors---the BGK [28] and Ellipsoidal [35] models---and two---the Polynomial and the Trimodal Gain Function (TGF) models---during the present work.†

The derivation of all kinetic models is subject to certain general physical conditions. These are:

CONDITION 1. Conservation of mass, momentum, and energy. Integrals of the collision operator J with the collisional invariants vanish:

$$\int J \cdot \{\psi_i(\underline{c})\}\, d\underline{c} = 0 \quad ; \quad \{\psi_i\} = \{1, \underline{c}, c^2\} \quad .$$

CONDITION 2. The collision operator acting on the equilibrium Maxwellian distribution function must produce a null result:

$$J[f^{(0)}, f^{(0)}] = 0 \quad .$$

CONDITION 3. J is rotationally invariant.

Within the scope of these conditions, a great deal of freedom remains for the exercise of physical intuition and inventiveness in the design of models. The basic intent is to replace the full Boltzmann collision

† Independently, a Russian author, E. M. Shakhov [54] recently published a version of the Polynomial model.

operator of (2.1) by a simple operator that retains as many of its properties as possible. To obtain the desired simplicity a number of restrictions is usually put on the models. In our work we make the four assumptions:

1. Model operators act only on a small number of moments $m_i[f]$, $i = 1$ to N, and not on f itself. The moments m_i, $i = 1$ to 5, are defined in Eqns. (2.15).
2. The form of the models is that of (2.14):

$$J_M = K(m_i) \cdot \{\Psi(\underline{c},m_i) - f\} \quad , \tag{3.1}$$

   where K is a collision frequency and Ψ the emission function.
3. The quantity K is independent of the molecular velocity $\underline{c}$, being only a function of the moments m_i. This is an exact property for Maxwellian molecules (repulsion proportional to the inverse fifth power of separation) and its adoption greatly simplifies the model equations. Models in which K is allowed to depend on $\underline{c}$ will be discussed in Chapter V and Appendix D.
4. The behavior of the model operators close to equilibrium should resemble that of the full Boltzmann linearized operator.

Although these conditions and assumptions form a basic framework for the construction of kinetic models, they specify very little when $f(\underline{c},x)$ is far from equilibrium. Because of the dependence of $J[f,f]$ on the distribution function, a generally valid yet simple model of the collision process is then hard to find. However, the design of a model specially suited to a particular class of non-equilibrium distribution functions is

easier to achieve. A special-purpose model for the plane shock problem, the TGF model, is developed in Section F.

Close to equilibrium it is possible to treat all the models in a unified manner. In the following two sections we derive some general results for this purpose. In the remaining sections of this chapter, the individual models will be discussed in more detail.

B. Linearized Models

We first proceed to relate the behavior of the model operators J_M to that of the Boltzmann operator J in the case of small disturbances from "absolute" equilibrium. Our treatment in both this section and the next will generally follow the elegant exposition by Uhlenbeck and Ford [55].

Define a dimensionless velocity:

$$\tilde{\underline{c}} \triangleq \underline{c}/\sqrt{2RT_0} \quad ,$$

and the absolute Maxwellian distribution function by:

$$f_0(\tilde{c}) \triangleq n_0(2\pi RT_0)^{-3/2} \exp-\tilde{c}^2 \quad .$$

For the rest of this section, the tilde on $\tilde{\underline{c}}$ will be omitted. We assume that:

$$f(\underline{c},\underline{r}) \rightarrow f_0\{1 + \phi(\underline{c},r)\} \quad ,$$

where the dimensionless quantity ϕ is small. Inserting this into equation (2.1) and neglecting second and higher order terms in ϕ, we obtain the linearized form of the Boltzmann collision operator:

$$J[f,f] \rightarrow f_0 J(\phi) = f_0 \iiiint f_0(\underline{c}_1)[\phi(\underline{c}') + \phi(\underline{c}_1') - \phi(\underline{c}) - \phi(\underline{c}_1)] \cdot \cdot \tag{3.2}$$

$$\cdot (2RT_0)^{3/2} \, d\underline{c}_1 g b db d\varepsilon \quad .$$

For any intermolecular force law, as shown by Chapman and Cowling [56], $J(\phi)$ may also be written:

$$J(\phi) = -\sigma(c)\phi(\underline{c}) + \iiint f_0(\underline{c}_1) K(\underline{c},\underline{c}_1)\phi(\underline{c}_1) d\underline{c}_1 \quad , \tag{3.2a}$$

with:

$$\sigma(c) = \iiiint f_0(\underline{c}_1) \cdot (2RT_0)^{3/2} \, d\underline{c}_1 g b db d\varepsilon \quad .$$

This operator has the property:

1. Whatever the molecular force law, there exist five zero eigenvalues of the equation:

$$J(\psi_i) = \lambda_i \psi_i \quad , \tag{3.3}$$

corresponding to the five collisional invariants:

$$\{\psi_i\} = \{1, c_x, c_y, c_z, c^2\} \quad .$$

All other eigenvalues are negative and real. Furthermore, for Maxwell molecules, Wang-Chang and Uhlenbeck [57] showed:

2. The full series of eigenfunctions of (3.3) forms a complete orthogonal set with respect to the weight function f_0, and in polar coordinates this set can be written:

$$\psi_{r\ell m} = N_{r\ell m} Y_{\ell m}(\theta,\phi) c^{\ell} S^{(r)}_{\ell+1/2}(c^2) \quad ,$$

where the $Y_{\ell m}$ are spherical harmonics, the $S^{(r)}_{\ell+1/2}$ are Sonine polynomials (i.e., associated Laguerre polynomials), and the $N_{r\ell m}$ are normalization factors.

3. The collision frequency $\sigma(c)$ in Eqn. (3.2a) is a constant, K_0, for Maxwell molecules, and the eigenvalues $\lambda_{r\ell}$ converge to $-K_0$ for large r and ℓ; however, K_0 is infinite unless some cutoff is assumed for the Maxwell force law. This assumption is usually made. The "constant collision frequency" for the Maxwell case is a consequence of the result that for Maxwell molecules the quantity $gbdb$ in the $J[f,f]$ integral is independent of g.

The linearized Maxwell molecule Boltzmann operator can be written in the manner of Gross and Jackson [58]:

$$\begin{aligned} f_0 J(\phi) &= f_0 K_0 \{ \sum_{i=1}^{\infty} (\lambda_i^B + 1) a_i \psi_i(\underline{c}) - \phi \} \\ &= f_0 K_0 \sum_{i=1}^{\infty} \lambda_i^B a_i \psi_i(\underline{c}) \quad , \end{aligned} \tag{3.4}$$

with:

$$\begin{aligned} a_i &= \pi^{-3/2} \int e^{-c^2} \phi \psi_i(\underline{c}) d\underline{c} \\ &= \frac{(2RT_0)^{3/2}}{n_0} \int f_0 \phi \psi_i(\underline{c}) d\underline{c} \quad . \end{aligned}$$

The Gross-Jackson models are obtained by truncating the series in (3.4) at some finite N.

In (3.4) and what follows, we have replaced the index pair r,ℓ by the single index i. The set of degenerate eigenfunctions $\psi_{r\ell m}$

(with fixed r and ℓ) is then fashioned into a tensor of rank ℓ in a standard way and denoted by ψ_i as shown in Table 1.

Having summarized the necessary results for the exact Boltzmann operator $J(\phi)$, we now turn to the linearization of the model operators, J_M. The model operators depend only on the moments of f, $m_i[f] \triangleq \int f\phi_i d\underline{c}$, where the ϕ_i are chosen functions of $\underline{c}$. Thus, if:

$$f \to f_0 + \delta f \quad \text{with:} \quad \delta f \triangleq f_0\phi(\underline{c},\underline{r}) \ ,$$

then:

$$m_i[f] \to m_{i,0} + \delta m_i \quad \text{with:} \quad \delta m_i = \int \delta f \phi_i d\underline{c}$$

and:

$$J_M \to \cancel{J_{M,0}} + \sum_{i=1}^{N} \left(\frac{\partial J_M}{\partial m_i}\right)_{f=f_0} \delta m_i \triangleq f_0 J_M(\phi) \ . \tag{3.5}$$

Using (3.1) in (3.5) we get:

$$f_0 J_M(\phi) = K(m_{i,0})\left\{\sum_{i=1}^{N} \left(\frac{\partial \Psi}{\partial m_i}\right)_{f=f_0} \delta m_i - f_0\phi\right\} + \cancel{(\Psi(m_{i,0})-f_0)} \sum_{i=1}^{N} \left(\frac{\partial K}{\partial m_i}\right)_{f=f_0} \delta m_i$$

or:

$$f_0 J_M(\phi) = K_0\left\{\sum_{i=1}^{N} \left(\frac{\partial \Psi}{\partial m_i}\right)_0 \delta m_i - f_0\phi\right\} \ . \tag{3.5a}$$

To assist comparison of (3.5a) with the Maxwell molecule form (3.4), we can choose the functions ϕ_i in m_i to be the normalized Maxwell eigenfunctions $\psi_i(\underline{c})$ of Table I; this leads to the result $\delta m_i = a_i$.

Equation (3.5a) may now be written:

TABLE 1

THE LOWER EIGENFUNCTIONS AND EIGENVALUES OF THE MAXWELL OPERATOR $J(\phi)/K_0$

i	r	ℓ	m	λ_i^B	$\psi_i(\underline{c})$	a_i	A_i †
1	0	0	0	0	1	$\frac{n-n_0}{n_0}$	0
2	0	1	0,±1	0	$\sqrt{2}\underline{c}$	$\sqrt{2}\underline{u}/(2RT_0)^{1/2}$	0
3	1	0	0	0	$\sqrt{\frac{2}{3}}(\frac{3}{2} - c^2)$	$-\sqrt{\frac{3}{2}}\frac{T-T_0}{T_0}$	0
4	0	2	0,±1,±2	-3/5	$\sqrt{2}(\underline{\underline{cc}} - \frac{1}{3}\underline{\underline{\delta}}c^2) \triangleq \sqrt{2}\underline{\underline{c^0 c}}$	$\sqrt{2}\underline{\underline{\tau}}/2RT_0$	$\sqrt{2}\underline{\underline{\tau}}/2RT$
5	1	1	0,±1	-2/5	$\sqrt{\frac{4}{5}}\underline{c}(\frac{5}{2} - c^2)$	$-2\sqrt{\frac{4}{5}}\underline{q}/(2RT_0)^{3/2}$	$-2\sqrt{\frac{4}{5}}\underline{q}/(2RT)^{3/2}$

† The quantities A_i will be defined and used in Section C.

$$f_0 J_M(\phi) = K_0 \left\{ \sum_{i=1}^{N} \left(\frac{\partial \Psi}{\partial a_i} \right)_0 a_i - f_0 \phi \right\} , \qquad (3.5b)$$

and for this to be a Gross-Jackson model we must have:

$$\left(\frac{\partial \Psi}{\partial a_i} \right)_0 = f_0 (\lambda_i^B + 1) \psi_i(\underline{c}) \quad , \quad i = 1 \text{ to } N \ . \qquad (3.6)$$

All the models used in this work satisfy (3.6) for values of N between 3 and 5, except that for some models $\lambda_4 \neq \lambda_4^B$ and/or $\lambda_5 \neq \lambda_5^B$. Thus the linearized form of all our model operators is the Gross-Jackson form:

$$f_0 J_M(\phi) = f_0 K_0 \left\{ \sum_{i=1}^{N} (\lambda_i + 1) a_i \psi_i(\underline{c}) - \phi \right\} \ . \qquad (3.7)$$

C. The Chapman-Enskog Treatment

The Chapman-Enskog treatment of the Boltzmann equation involves a "local" linearization which differs from the "absolute" linearization of the previous section.

The Boltzmann equation is to be solved for flows in which the distribution function f is always close to the local equilibrium form $f^{(0)}(n,\underline{u},T)$, where the parameters of this Maxwellian are the local macroscopic density, velocity, and temperature. Small deviations of f from $f^{(0)}$ are produced by the streaming operator, while the collision operator drives f back towards $f^{(0)}$.

The distribution function is thus assumed to be of the form:

$$f(\underline{c},\underline{r},t) = f^{(0)}(n,\underline{u},T) \cdot \{1 + \Phi(\underline{c},\underline{r},t)\} \ , \qquad (3.8)$$

where Φ is a dimensionless quantity $<< 1$. Because the parameters of $f^{(0)}$ are the moments of f, m_i, $i = 1$ to 3, Φ must obey the conditions:

$$\int f^{(0)}\Phi \begin{Bmatrix} 1 \\ \underline{c} \\ c^2 \end{Bmatrix} d\underline{c} = 0 \quad . \tag{3.9}$$

Equation (3.8) can now be substituted into the Boltzmann equation. In the first-order Chapman-Enskog approximation for Φ, to which we confine ourselves here, only zeroth-order contributions to the streaming term are retained [46] and we have an inhomogeneous, linear integral equation, with the only term containing Φ being the linearized collision term $f^{(0)}J(\Phi)$. Here J is the same linearized operator as in the previous section.† For a solution to such an equation to exist, the inhomogeneous term must be orthogonal to any solutions of the homogeneous equation. In our case, this equation, $f^{(0)}J(\Phi) = 0$ has the five solutions $\{\psi_i\}$, the collisional invariants of (3.3), whatever collision law is assumed. We must therefore impose the solubility conditions:

$$\int (\text{Streaming terms of Boltzmann equation}) \cdot \{\psi_i\} d\underline{c} = 0 \quad . \tag{3.10}$$

In the first approximation, these solubility conditions turn out to be the Euler macroscopic equations for n, $\underline{u}$, and T, with the scalar pressure equal to nkT. Their use allows the removal of explicit time dependence of the streaming term, and the first-order equation for Φ becomes:

† Due to the use of local, not absolute, Maxwellian parameters, the eigenfunctions of $J(\Phi)$ are $\psi_i(\tilde{\underline{C}})$, with $\tilde{\underline{C}} \triangleq (\underline{c}-\underline{u})/(2RT)^{1/2}$.

$$[2\underline{\underline{D}}:\underline{\underline{\overset{o}{\tilde{C}}\,C}} + \underline{\nabla}\,\ell n\ T \cdot \underline{C}(\tilde{C}^2 - \tfrac{5}{2})]f^{(0)} = f^{(0)}J(\Phi) \quad , \qquad (3.11).$$

where:

$$\underline{\underline{D}} \triangleq \frac{1}{2}\left\{\frac{\partial u_i}{\partial x_j} + \frac{\partial u_j}{\partial x_i}\right\} ,$$

$$\underline{\nabla}\,\ell n\ T \triangleq \frac{1}{T}\frac{\partial T}{\partial x_i} \quad ,$$

$$\underline{\tilde{C}} \triangleq \underline{C}/(2RT)^{1/2} = (\underline{c}-\underline{u})/(2RT)^{1/2} \quad .$$

For the model operators:

$$f^{(0)}J_M(\Phi) = f^{(0)}K\left\{\sum_{i=1}^{N}(\lambda_i+1)A_i\psi_i(\tilde{\underline{C}}) - \Phi\right\} \quad , \qquad (3.12)$$

where the A_i are defined as $\frac{1}{n}\int f^{(0)}\Phi\psi_i(\tilde{\underline{C}})d\underline{C}$, and are given in Table 1.

We can now perform a unified Chapman-Enskog treatment for all the models. Using the definitions of ψ_i from Table 1, we can rewrite (3.11) with the collision term (3.12) as:

$$[\sqrt{2}\underline{\underline{D}}:\underline{\underline{\psi}}_4(\tilde{\underline{C}}) + \sqrt{\frac{5R}{2T}}\,\underline{\nabla}T \cdot \underline{\psi}_5(\tilde{\underline{C}})]f^{(0)} = f^{(0)}K\left\{\sum_{i=1}^{N}(\lambda_i+1)A_i\psi_i(\tilde{\underline{C}})-\Phi\right\} \qquad (3.11a)$$

and the associated conditions (3.9) can be rewritten as:

$$A_i = 0 \quad , \quad i = 1 \text{ to } 3 \quad . \qquad (3.9a)$$

The solution for Φ satisfying (3.11a) and (3.9a) is:

$$\Phi = \underline{\underline{A}}_4:\underline{\underline{\psi}}_4(\tilde{\underline{C}}) + \underline{A}_5 \cdot \underline{\psi}_5(\tilde{\underline{C}}) \quad , \qquad (3.13)$$

using which, after algebraic manipulation of (3.11a), we obtain Newton's relation:

$$\underline{\underline{\tau}} = -\frac{2\mu}{\rho}\underline{\underline{D}} \quad ; \qquad \mu \triangleq \text{viscosity} \quad , \tag{3.14}$$

Fourier's relation:

$$\underline{q} = -\frac{\kappa}{\rho}\underline{\nabla T} \quad ; \qquad \kappa \triangleq \text{heat conductivity} \quad , \tag{3.15}$$

and the further result:

$$K = (p/\mu)/|\lambda_4| = \left(\frac{5Rp}{2\kappa}\right)/|\lambda_5| \quad , \tag{3.16}$$

where $p = \rho RT$ is the scalar pressure, and $\rho = mn$ is the mass density.

Using the definition of the Prandtl number $Pr = \frac{5R\mu}{2\kappa}$, we also obtain

$$Pr = \lambda_5/\lambda_4 \quad . \tag{3.17}$$

To summarize the results of this section: we have applied the first-order Chapman-Enskog method to the general form of model Boltzmann equation used in this work, and have obtained approximate relations (3.16-17) for the model collision frequency K and Prandtl number Pr in terms of the model parameters λ_4 and λ_5 and the quantities p, the pressure, and μ, the viscosity.

D. The BGK and Ellipsoidal Models

We are now ready to discuss the development and properties of the four models used in this work. In this section we consider the two models developed by previous authors.

The BGK model of Krook et al. [28], developed in 1954,[†] adds a further idea to the basic framework outlined in Section A. This idea is

[†] The BGK model was independently developed by Welander [60], also in 1954.

suggested by a property of hard-sphere molecules. Scattering between two hard spheres is isotropic in the center-of-mass system. This suggests that for a general molecular distribution the emission of scattered molecules should be approximately isotropic in the flow frame, or that the emission function Ψ should be a function of the thermal speed C. The simplest choice for $\Psi(C)$ subject to the conditions of Section A and this assumption of isotropy is the BGK choice:

$$\Psi^{BGK}(C,m_i) = f^{(0)}(n,\underline{u},T) = n(2\pi RT)^{-3/2}\exp[-C^2/2RT] \quad , \quad (3.18)$$

with $\underline{C} \triangleq \underline{c} - \underline{u}$. Thus, the BGK model is:

$$J^{BGK} = K^{BGK}\{f^{(0)}(n,\underline{u},T) - f\} \quad . \quad (3.19)$$

The linearized form, applying equation (3.5), is:

$$f_0 J^{BGK}(\phi) = f_0 K_0 \left\{ \left(\frac{n-n_0}{n_0}\right) + 2\tilde{\underline{c}}\cdot\tilde{\underline{u}} + (\tilde{c}^2 - 3/2)\left(\frac{T-T_0}{T_0}\right) - \phi \right\} \quad , \quad (3.20)$$

with $\tilde{\underline{u}} \triangleq \underline{u}/(2RT_0)^{1/2}$. This is just the Gross-Jackson form (3.7) with N = 3, the minimum allowable N. All eigenvalues λ_i, $i > 3$ of the BGK model are equal to -1. Using the Chapman-Enskog results (3.16) and (3.17), we can write

$$K^{BGK} = (p/\mu) \quad ; \quad p = nkT = \rho RT \quad , \quad (3.21)$$

and

$$Pr^{BGK} = 1 \quad . \quad (3.22)$$

The value of unity given by (3.22) for the BGK Prandtl number is in poor agreement with the correct perfect gas value of close to 2/3.

The Ellipsoidal Model, developed by Holway [35] in 1963,† was an attempt to improve the BGK model, particularly the value of Prandtl number, by relaxing the BGK assumption of an isotropic emission function. The emission function was generalized to the bivariate Gaussian (or "ellipsoidal Maxwellian") form:

$$\Psi^E(\underline{c}) \approx \exp - \frac{1}{2} \sum_{i,j} \varepsilon_{ij}(c_i-b_i)(c_j-b_j) \quad ,$$

where ε_{ij} and b_i are parameters to be determined and where i and j sum over the three Cartesian directions x, y, and z. Application of the conservation Condition 1 yields:

$$\Psi^E(\underline{C},m_i) = n(2\pi)^{-3/2} (\det \underline{\underline{\varepsilon}})^{1/2} \exp - \frac{1}{2} \underline{\underline{\varepsilon}}:\underline{C}\underline{C} \quad , \qquad (3.23)$$

with

$$\underline{\underline{\varepsilon}} = (\lambda\underline{\underline{\tau}} + RT\underline{\underline{\delta}})^{-1} \quad ,$$

$$\underline{\underline{\tau}} = \underline{\underline{m}}_4 \text{ of (2.15)} \quad ,$$

$$\lambda = \text{an adjustable parameter} \quad ,$$

$$\underline{\underline{\delta}} = \text{the unit tensor} \quad ,$$

$$\underline{C} = \underline{c} - \underline{u} \quad .$$

The main advance over the BGK model is the presence of the adjustable parameter λ, which can be chosen so that the Prandtl number will be 2/3. The linearized form of the Ellipsoidal model operator $J^E = K^E\{\Psi^E - f\}$ is of the Gross-Jackson form (3.7) with $N = 4$. In this model, the

† The Ellipsoidal model was later independently derived by Cercignani and Tironi [61].

eigenvalue λ_4 turns out to equal $(\lambda-1)$. Using the Chapman-Enskog result (3.17), we obtain $Pr = 1/(1-\lambda)$, which suggests the choice $\lambda = -1/2$ to yield:

$$Pr^E = 2/3 \quad , \tag{3.24}$$

$$K^E = \frac{2}{3}(p/\mu) \quad ; \quad p = nkT \quad . \tag{3.25}$$

Although Pr is improved by this choice of $\lambda = -1/2$, the resulting value of $\lambda_4 = -3/2$ is even further from the correct Maxwell molecule value of $-2/3$ than was the BGK value of -1. Furthermore, as we shall see later, the anisotropy of the emission function in the Ellipsoidal model is in the opposite direction to that expected in the shock problem, and this is related to the choice of λ. However, the choice of positive values of λ, leading to better values of λ_4 and more appropriate emission functions, leads also to outsize (or infinite) values of the Prandtl number.

E. The Polynomial Model

The first of the two new models developed during the course of this work will now be described. It represents an attempt to extend the BGK model in a more systematic way than the Ellipsoidal model, but still in a general manner, unrelated to any particular problem. The main idea is to develop a nonlinear hierarchy of models related in form to the well-known Gross-Jackson hierarchy of linearized models [58]. The requirements demanded of the scheme are:

1. To satisfy the basic framework of Section A.
2. To possess the Gross-Jackson linearized form (3.7).
3. To have a Prandtl number of $2/3$.

There are many ways to satisfy these requirements, but a simple solution is obtained as follows: by generalizing the domain of Eqn. (3.6) away from the linearized range $f \approx f_0$, we are led to suggest a "delinearized equation" for the emission function Ψ:

$$\frac{\partial \Psi(\underline{c},a_i)}{\partial a_i} = (\lambda_i+1)\psi_i(\tilde{\underline{c}})F(\underline{c},a_i) \quad , \quad i = 1 \text{ to } N \quad , \tag{3.26}$$

where the function F must satisfy the condition:

$$F(\underline{c},a_i)\Big)_{f=f_0} = f_0 \quad . \tag{3.26a}$$

Of course the choice for F is all-important. Two simple possibilities are $F = f^{(0)}(n,\underline{u},T)$ and $F = \Psi$. The second choice leads to emission functions of the type $\Psi \approx \exp[\sum_i(\lambda_i+1)A_i\psi_i(\tilde{C})]$, the type suggested by Cercignani and Tironi [61] as extensions of the BGK model. However, this becomes physically unreasonable when powers of c greater than 3 appear in the exponential. The mixed choice

$$\left.\begin{aligned} N &= 4 \quad , \\ F(\underline{c},a_i) &= f^{(0)}(n,\underline{u},T) \quad , \quad i = 1,2,3 \\ &= \Psi(\underline{c},a_i) \quad , \quad i = 4 \end{aligned}\right\}$$

leads to the Ellipsoidal model. These examples show the generality of (3.26) as a source of nonlinear models.

We retain the very simple choice;

$$F(\underline{c},a_i) = f^{(0)}(n,\underline{u},T) \quad , \quad \text{all } i \quad , \tag{3.27}$$

which leads to what we have called the Polynomial model, with emission function:

$$\Psi^{Pol}(\underline{C},m_i) = f^{(0)}(n,\underline{u},T)\left\{1 + \sum_{i=4}^{N} (\lambda_i+1)A_i\psi_i(\tilde{\underline{C}})\right\} \quad . \qquad (3.28)$$

The quantities A_i and ψ_i are those of Table 1, and again $\underline{C} = \underline{c} - \underline{u}$ and $\tilde{\underline{C}} = \underline{C}/(2RT)^{1/2}$. It is easily verified that $J^{Pol} = K^{Pol}\{\Psi^{Pol} - f\}$ satisfies requirements 1 and 2 for all N. In this work we apply the model with N = 5. To achieve requirement 3 we fix the ratio $\lambda_5/\lambda_4 = 2/3$. The Chapman-Enskog results (3.16-17) for the model are:

$$Pr^{Pol} = 2/3 \quad , \qquad (3.29)$$

and

$$K^{Pol} = (p/\mu)/|\lambda_4| \quad . \qquad (3.30)$$

With N = 5 and the ratio λ_5/λ_4 fixed, the Polynomial model has a single adjustable parameter λ_4. A main advantage of the model, over the other models we use here, is the ability to vary λ_4 while leaving Pr unaffected. The effect of an adjustment of λ_4 upon the emission function Ψ^{Pol} is clearly displayed by equation (3.28), in contrast with its very indirect effect in the Ellipsoidal model.

F. The Trimodal Gain Function (TGF) Model

For a model to give a satisfactory description of a physical flow, its emission function Ψ must closely represent the physical emission process within that flow. Furthermore, for the shock problem, the model should possess a value of $|\lambda_4|$ such that the scale length in the shock, which is roughly proportional to this parameter, is of the correct order.

All three models discussed so far have allowed only small deviations of Ψ from isotropic emission in the flow frame. This does not adequately

represent the physical emission process inside a shock. The emission function in a shock can be rather well estimated because the distribution function is known to resemble the Mott-Smith bimodal form (C.2). Since collisions tend to smooth the distribution, the emission function should have a shape intermediate between the Mott-Smith and Maxwellian forms, i.e., a smoothed bimodal shape.

Evidence for the bimodal form of the distribution function in a shock wave is provided not only by the success of the Mott-Smith theory, but by Monte Carlo [46,48] and model [31] calculations in which the distribution function has been evaluated. It should be stressed that even a BGK shock calculation will predict a bimodal distribution function, which is physically inconsistent with an assumed isotropic form of Ψ.

We have developed a new model for this work which allows Ψ to follow closely the form found physically in the shock problem. For reasons which will become clear, the model is called the Trimodal Gain Function or TGF model.

The detailed requirements for the model to satisfy are set out as follows:

1. The emission function Ψ must be a good fit to the emission function calculated on the basis that the distribution function is of Mott-Smith form and that the collision frequency K is velocity-independent.
2. The model emission function should have a simple analytical form, preferably one similar to the other models to facilitate the numerical analysis.
3. The model must obey Conditions 1-3 of Section A.
4. The linearized model operator should have a sensible value of λ_4.

We now discuss how requirements 1-4 are satisfied and lead to development of the TGF model.

Requirement 1

Referring to Chapter II, we recall from Eqns. (2.1) and (2.14) that Ψ is a model for $\mathcal{J}[f,f]/\mathcal{L}[f]$, and that K is a model for $\mathcal{L}[f]$. If f is assumed to be the Mott-Smith form discussed in Appendix C:

$$f = f_{MS} \triangleq (1-\nu(x))f_1^{(0)} + \nu(x)f_2^{(0)} \quad , \tag{3.31}$$

where $\nu(x)$ is:

$$\nu(x) = \frac{n(x)-n_1}{n_2-n_1} \quad , \tag{3.32}$$

then the functions $\mathcal{J}_{MS}[f_{MS},f_{MS}]$ and $\mathcal{L}_{MS}[f_{MS}]$ may be calculated in closed form for the case of quasi-Maxwell molecules, appropriate for a model in which K is finite but independent of c. By "quasi-Maxwell" here, we mean molecules which scatter isotropically like hard spheres, but with diameters inversely proportional to the relative collision speed g. In a Maxwellian distribution this leads to a constant mean collision frequency, rather than a constant mean free path as for hard spheres. It also leads to a viscosity coefficient proportional to the temperature, rather than to the square root of the temperature. Deshpande and Narasimha [62] first performed such a calculation for the case of hard-sphere molecules, and in Appendix B we give our related calculation. The form of $\mathcal{J}_{MS}$ and $\mathcal{L}_{MS}$ is:

$$\begin{aligned} \mathcal{J}_{MS} &= (1-\nu)^2\mathcal{J}_{11} + \nu^2\mathcal{J}_{22} + 2\nu(1-\nu)\mathcal{J}_{12} \\ \mathcal{L}_{MS} &= (1-\nu)\mathcal{L}_1 + \nu\mathcal{L}_2 \quad , \end{aligned} \tag{3.33}$$

where, for quasi-Maxwell molecules†:

$$\mathcal{L}_i = 2\pi\sigma^2 n_i \quad ,$$

$$\mathcal{J}_{ii} = \mathcal{L}_i f_i^{(0)} \quad , \tag{3.34}$$

$$\mathcal{J}_{12} = \frac{2\pi^{5/2}\sigma^2 f_1^{(0)} f_2^{(0)}}{(\beta_1\beta_2)^{1/2}(\beta_1^{1/2}+\beta_2^{1/2})} \cdot e^{Q} \cdot \frac{\sinh R}{R} \quad ,$$

with:

$$Q \triangleq \frac{1}{2}(\mathcal{C}_1^2+\mathcal{C}_2^2) \quad ,$$

$$R^2 \triangleq \frac{1}{4}(\mathcal{C}_1^2-\mathcal{C}_2^2) + |\underline{\mathcal{C}}_1 \times \underline{\mathcal{C}}_2|^2 = Q^2 - (\underline{\mathcal{C}}_1 \cdot \underline{\mathcal{C}}_2)^2 \quad ,$$

$$\underline{\mathcal{C}}_i \triangleq \beta_i^{1/2}(\underline{c}-\underline{u}_i) \quad ,$$

$$\beta_i \triangleq 1/(2RT_i) \quad ,$$

and $i = 1$ or 2.

The quantity σ^2 is a normalizing constant with units of a cross-section. In deriving Eqn. (3.34) we have assumed isotropic scattering in the center-of-mass system (as is the case for hard spheres) but a collision frequency independent of relative speed (the Maxwell molecule result). The model appears to retain most of the features of Maxwell molecules.

---

† For hard spheres, the corresponding results are:

$$\mathcal{L}_i = 2\pi^2\sigma^2\beta_i^{-2} f_i^{(0)} \Phi(2,\tfrac{3}{2},\mathcal{C}_i^2) \quad ,$$

$$\mathcal{J}_{ii} = \mathcal{L}_i f_i^{(0)} \quad , \tag{3.34a}$$

$$\mathcal{J}_{12} = \frac{\pi^2\sigma^2 f_1^{(0)} f_2^{(0)}}{2\beta_1\beta_2 R}\left[\Phi(1,\tfrac{1}{2},Q+R) - \Phi(1,\tfrac{1}{2},Q-R)\right] \quad ,$$

where Φ is the confluent hypergeometric function and σ is the sphere diameter.

Thus, in order to satisfy requirement 1, Ψ^{TGF} must approximate the function $\Psi_{MS} \triangleq \mathcal{G}_{MS}/\mathcal{L}_{MS}$, with $\mathcal{G}_{MS}$ and $\mathcal{L}_{MS}$ given by (3.33-4). Ψ_{MS} is a function of $\underline{c}$, of the Mach number M, and of the "reduced density" $\nu(x)$. Figure 1 shows a plot of $\Psi_{MS}(c_x, c_t = 0)$ for a typical case, $\nu = 0.2$ and $M = 10$, together with the corresponding values of Ψ for the BGK, Ellipsoidal and Polynomial $(\lambda_4 = -1)$ models. Figure 1 confirms the fact that all the emission functions for these models are poor approximations to Ψ_{MS}. In particular, the Polynomial model's anisotropic correction, while in the correct direction, is far too small. The anisotropy of the Ellipsoidal model is also small but is physically different from that of Ψ_{MS}. Rather than the correct bimodal departure from isotropy, Ψ^{E} predicts less emission in the x direction for large $|C_x|$ and more transverse emission near $C_x = 0$ (this is not visible in Figure 1).

The dominant features of Ψ_{MS} are separate "hot" and "cold" components. These components are associated with important streams of molecules in the shock, the former with high-speed molecules returning from the hot $(T = T_2)$ side, and the latter with the highly collimated beam penetrating from the cold $(T = T_1)$ side. In all the previous models, only the local temperature $T(x)$ appears in Ψ, preventing the description of these components with any accuracy. This difficulty is aggravated by the fact that near either end of the shock, the principal perturbation to a BGK-type emission function is the penetration of the component from the other end.

Figure 1: EMISSION FUNCTION $\Psi(c_t = 0)$ vs. c_x

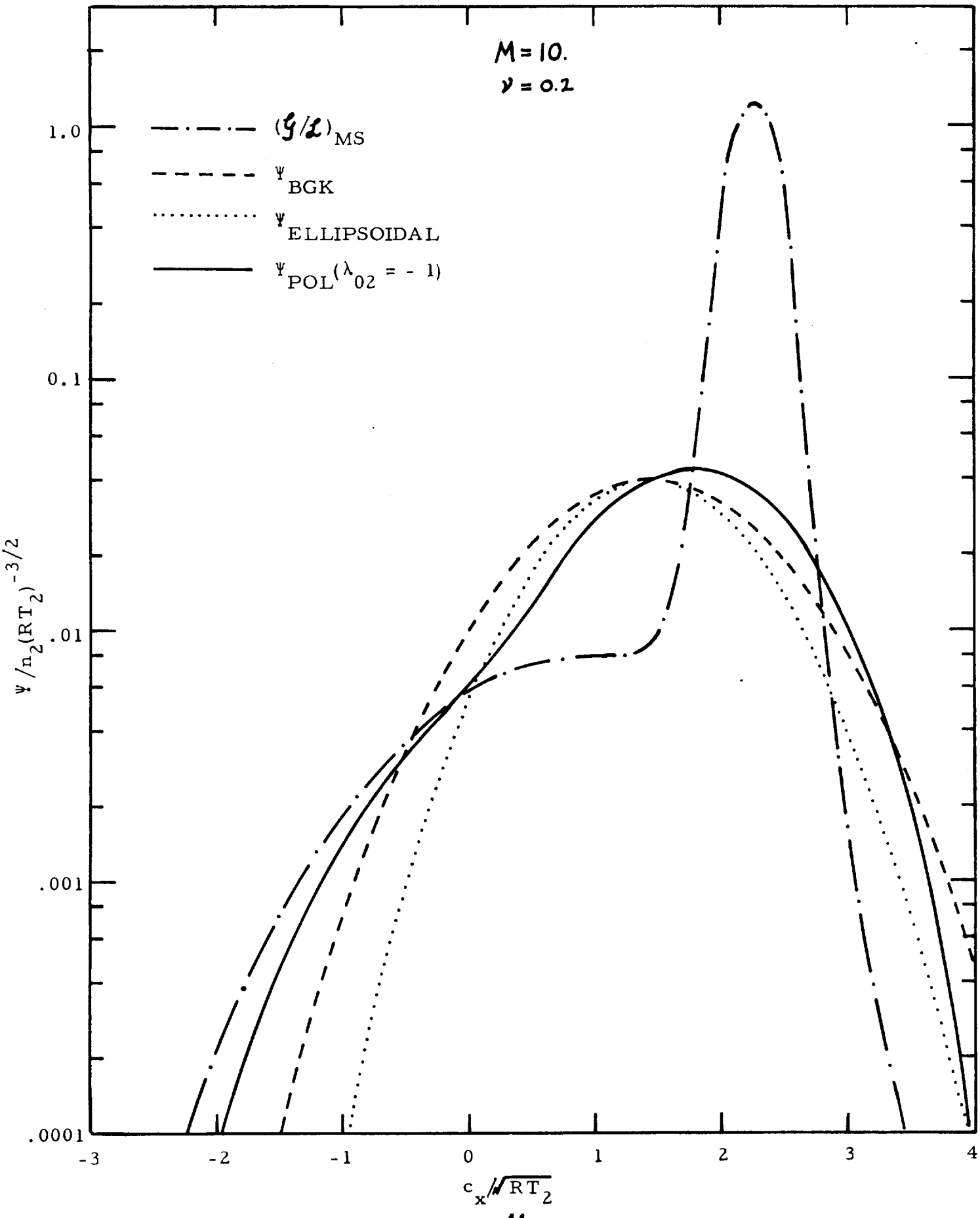

Requirement 2

This requirement is best satisfied if we express Ψ^{TGF} as a sum of Maxwellian functions; the H_n kernel functions used for the earlier models will then reappear. Requirement 1 suggests that two of these Maxwellian functions should be $f_1^{(0)}$ and $f_2^{(0)}$, with coefficients smaller than their respective values $(1-\nu)$ and ν in f_{MS}. Thus we anticipate:

$$\Psi^{TGF} \approx k_1(x) \cdot (1-\nu)f_1^{(0)} + k_2(x) \cdot \nu f_2^{(0)} + \ldots \quad , \qquad (3.35a)$$

with $k_1, k_2 \leq 1$, to be determined later.

Requirement 3

A natural, and probably the simplest, function that may be included in the ansatz (3.35a) is a third Maxwellian $f_3^{(0)}$ with parameters $n_3(x)$, $u_3(x)$, and $T_3(x)$ chosen to assure conservation. However, to be physically reasonable for the shock problem, these parameters must satisfy the conditions: $n_3(x) \geq 0$; $u_2 \leq u_3(x) \leq u_1$; $T_1 \leq T_3(x) \leq T_2$.† This is because $f_3^{(0)}$ plays the part in Ψ^{TGF} of the smoothed component of the distribution after collision, intermediate between $f_1^{(0)}$ and $f_2^{(0)}$. A simple way to satisfy these conditions is to set $k_1 = k_2 = k(x)$ in (3.35a). The terms in $f_1^{(0)}$ and $f_2^{(0)}$ then reduce to kf_{MS} and a trimodal ansatz for Ψ^{TGF} is suggested:

$$\Psi^{TGF} = k(x)f_{MS} + (1-k(x))f_3^{(0)}(n_3,u_3,T_3) \quad . \qquad (3.35b)$$

It is easily verified, using equations (3.35b), (C.3), and (C.4a-c), that conservation requires:

† In case the temperature overshoots near the hot side, i.e., $T > T_2$, the condition $T_3 \leq T_2$ can be relaxed,

$$n_3(x) = n(x) \; ; \quad u_3(x) = u(x) \; ; \quad T_3(x) = \frac{T(x)-k(x)\cdot T_{MS}(x)}{(1-k(x))} \; ,$$

which will satisfy the conditions in all cases. The form (3.35b) also satisfies Conditions 2-3 of Section A, as Ψ^{TGF} reduces to $f^{(0)}$ when $f \to f^{(0)}$, and it is rotationally invariant.

Requirement 4

To obtain a suitable λ_4 in the simplest way, we now make the restriction that $\Psi^{TGF}(\underline{c},m_i)$ as given by (3.35b) should depend only on the lowest moments m_i, $i = 1$ to 3. This can be shown† to ensure that the model will linearize to the BGK form (3.20). Accordingly, we choose as the final form of the TGF emission function:

$$\Psi^{TGF} = k(\nu)f_{MS} + (1-k(\nu))f_3^{(0)} \; , \qquad (3.35)$$

where:

$$f_3^{(0)} = f^{(0)}(n,u,T_3) \; ,$$

$$T_3 = (T-k(\nu)T_{MS})/(1-k(\nu)) \; ,$$

T_{MS} is defined by equation (C.4c) ,

and where $k(\nu)$ is an adjustable function, less than unity, to be discussed below.

---

† To linearize the TGF model we require a weak shock so that $f \to f_0(1+\phi)$; Ψ^{TGF} becomes a linear combination of Maxwellian functions, with parameters which differ from (n_0,u_0,T_0) by first-order quantities related to the a_i, $i = 1,2,3$. The linearized conservation relations are equivalent to:

$$\left(\frac{\partial \Psi^{TGF}}{\partial a_i}\right)_0 = \left(\frac{\partial f^{(0)}}{\partial a_i}\right)_0 \; , \quad i = 1,2,3 \; ,$$

in the notation of Section B, which by (3.5b) ensures that the TGF and BGK linearized forms are identical.

Due to its linearization to the BGK form, the model has $\lambda_i = -1$ for all $i > 3$, and consequently the Chapman-Enskog results (3.16-17) are:

$$K^{TGF} = (p/\mu) \quad , \tag{3.36}$$

and:

$$Pr^{TGF} = 1 \quad . \tag{3.37}$$

Modified versions of the TGF model could easily be constructed with different values of λ_i, Pr, etc., by modifying the $f_3^{(0)}$ term in the Polynomial or Ellipsoidal manner, for example. An important advantage of the simple form adopted is that the eigenvalues λ_i are independent of the function $k(\nu)$.

The choice of $k(\nu)$ is crucial for the success of the model. As stated above, Ψ^{TGF} must fit the "hot" and "cold" components of Ψ_{MS} within the shock, particularly where each of these components represents the principal perturbation to local equilibrium, i.e., on the <u>cold</u> and <u>hot</u> sides of the shock, respectively.

A fit $k_h(\nu)$ to the hot component of Ψ_{MS} is easily made; since, as $c \to \infty$, the hot component dominates, we have:

$$\lim_{c \to \infty} \Psi^{TGF} = k(\nu)\nu f_2^{(0)} \quad ,$$

and using (3.33-4):

$$\lim_{c \to \infty} \Psi_{MS} = \nu^2 \mathcal{G}_{22}/[(1-\nu)\mathcal{L}_1 + \nu\mathcal{L}_2] \quad .$$

In the second limit we have used the result that $\mathcal{G}_{12} \sim \mathcal{G}_{22}/c^2$ as $c \to \infty$ and have therefore omitted the term in $\mathcal{G}_{12}$. Equating the two limits, we obtain:

$$k_h(\nu) = \nu\mathcal{L}_2/[(1-\nu)\mathcal{L}_1 + \nu\mathcal{L}_2] = \nu n_2/n \quad , \tag{3.38}$$

where we have used the results from (3.34) that $\mathcal{L}_1/\mathcal{L}_2 = n_1/n_2$ and $\mathcal{J}_{22} = \mathcal{L}_2 f_2^{(0)}$.

A fit to the cold component of Ψ_{MS} is made by matching the cold peaks corresponding to the T_1 Maxwellian components of Ψ_{MS} and Ψ^{TGF}. The two functions are equated at the peak itself, i.e., at $c_x = u_1$, $c_t = 0$. Thus the cold fit $k_c(\nu)$, for fixed Mach number M, is the solution of the nonlinear equation:

$$k_c(\nu)f_{MS} + (1-k_c(\nu))f^{(0)}\left(n,u,\frac{T-k_c(\nu)T_{MS}}{1-k_c(\nu)}\right) = \frac{(1-\nu)^2\mathcal{J}_{11}+\nu^2\mathcal{J}_{22}+2\nu(1-\nu)\mathcal{J}_{12}}{(1-\nu)\mathcal{L}_1 + \nu\mathcal{L}_2} \quad , \tag{3.39}$$

where all the coefficients $\mathcal{J}$ and $\mathcal{L}$ are evaluated at $\underline{c} = (u_1,0)$. The solution of (3.39) must be found numerically. Only one physically appropriate solution exists and is easily found in practice.

The function $k(\nu)$ can now be chosen. We must apply $k_h(\nu)$ for $\nu \to 0$ and $k_c(\nu)$ for $\nu \to 1$ to achieve the desired behavior specified above. In Figure 2 both k_h and k_c are plotted for a typical Mach number of 10, over the full range of ν. The fits are different, though not as inconsistent as Figure 2 may suggest; the largest differences occur at the endpoints, where f_{MS} and $f_3^{(0)}$ approach each other, reducing the sensitivity of Ψ^{TGF} to $k(\nu)$.

The best simple choice for $k(\nu)$ is thus:

$$k(\nu) = \min(k_h,k_c) \quad . \tag{3.40}$$

This choice assures correct treatment of the hot component near the cold side and vice versa, as required.

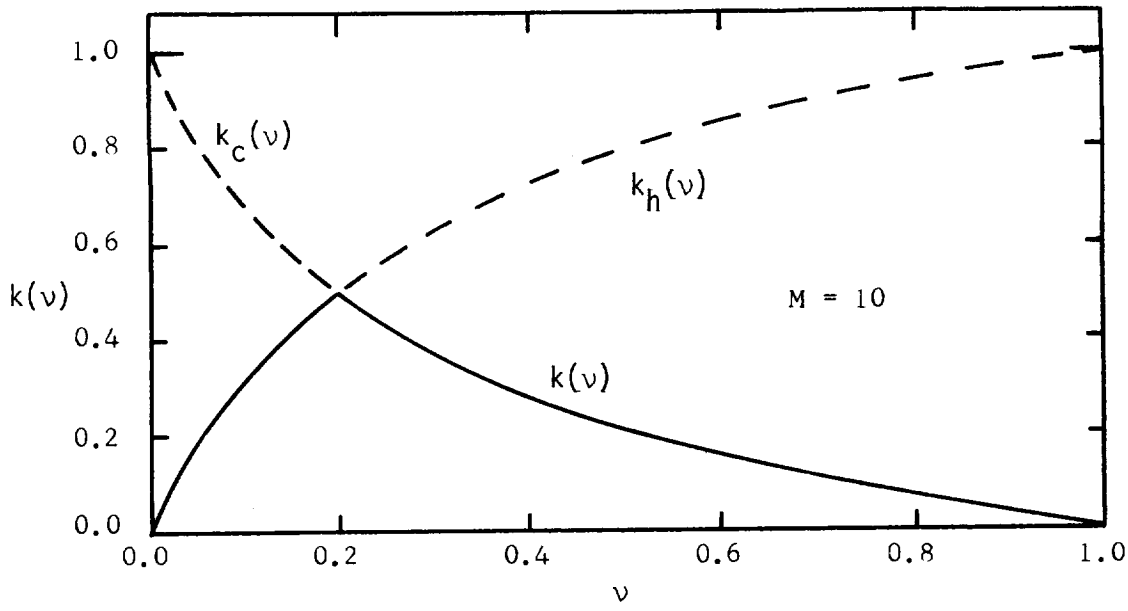

Fig. 2. Choice of $k(\nu)$ for the TGF Model.

Applied at all values of ν within the shock, (3.40) is found to give a very satisfactory fit of Ψ^{TGF} to Ψ_{MS}. Figure 3 shows a typical plot of this fit under the same conditions used for Figure 1, from which it is seen that the previous shortcomings in matching emission functions to Ψ_{MS} have been largely overcome.

Figure 3: EMISSION FUNCTION $\Psi(c_t = 0)$ vs. c_x

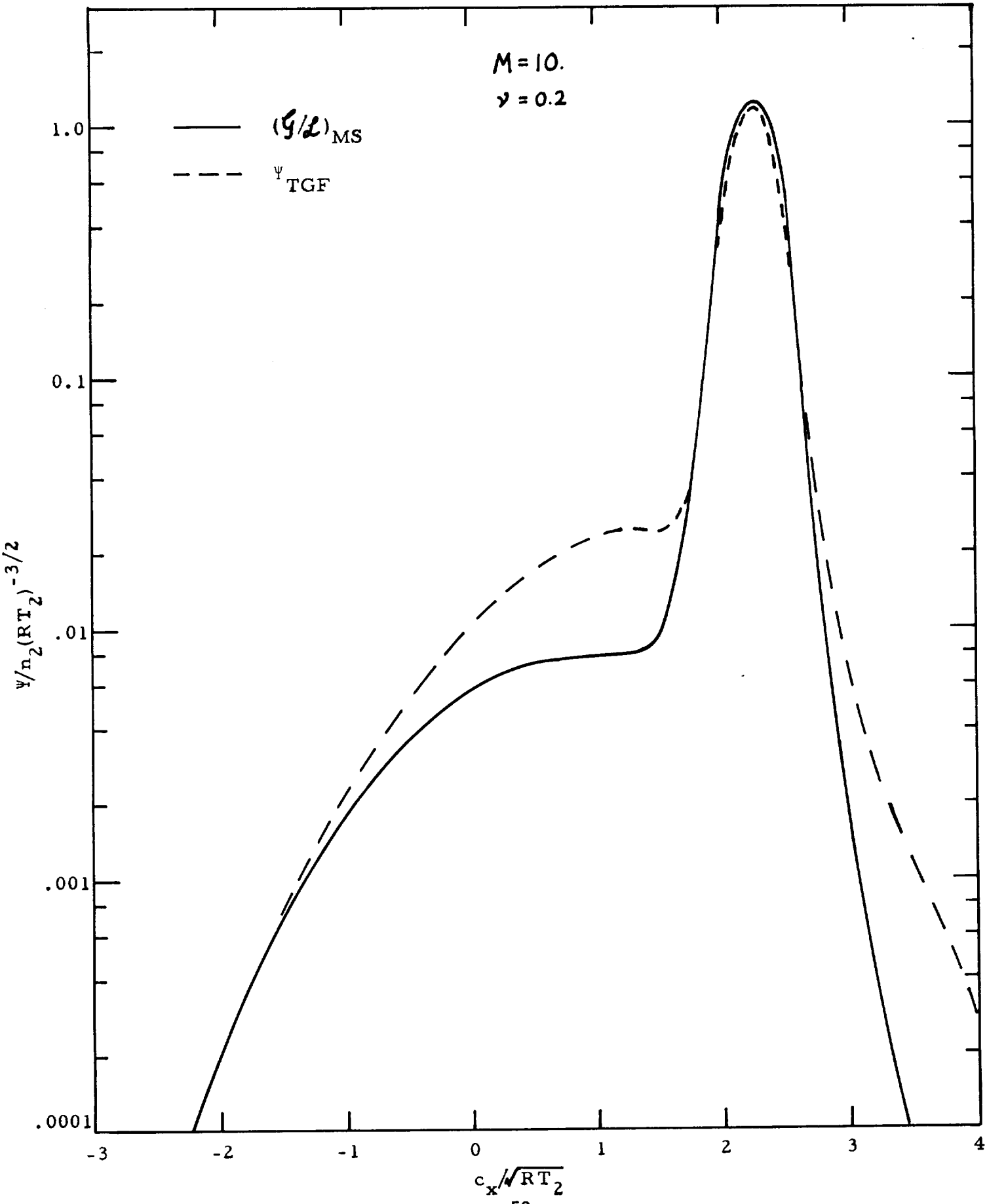

CHAPTER IV

NUMERICAL METHODS

A. Discrete Form of the Model Equations

For each model considered we must solve a coupled pair of nonlinear integral equations of the form (2.23) with logarithmically singular kernels $\mathcal{K}$. The independent variable t is first discretized; that is, Eqn. (2.23) is enforced only at selected t values t_i, $i = 1$ to N, and an interpolation formula is used for each dependent variable n (or u) and T at all intermediate values of t. The integral operator in each equation is replaced by a quadrature formula. The solutions for $n(t)$ and $T(t)$ are then obtained by iteration techniques to be described in the next section.

The particular methods used for discretization, interpolation and quadrature are carefully chosen for their efficiency applied to the present problems. They are based on the experience of Anderson [32,33,34], whose work on the BGK problem since 1963 is the most thorough and accurate available. However, Anderson's published work does not include several recent improvements made by him while overcoming certain numerical difficulties which he reported in his original study of the problem. These improvements were made available to us privately by Anderson and will be described here, as they remain unpublished.

1. Discretization and Interpolation Schemes

Both the discretization and interpolation schemes are based on the use of an analytical "backbone" profile for increased accuracy. This

backbone is a known approximate solution of the problem and its use allows the selection of the mesh points t_i and the interpolation to be improved accordingly. The points are placed initially so that differences of n (or u) between successive points are approximately constant in the backbone. Later, points may be moved or added optionally, to deal with special profile features in particular cases, such as a temperature overshoot. Interpolation is done, not directly on the profiles themselves, but on the small differences between the computed and backbone profiles; this is a more accurate procedure as long as the backbone remains a reasonable approximation to the model solution, which is the case in practice. By these means N, the number of t points required (which directly influences the running time), is kept to a minimum of about 20-30 points, and additionally a very rapid low-degree ("cubic spline") interpolation formula can be used. Spline interpolation is the mathematical analog of a draftsman's fairing between fixed points on a drawing using flexible "splines" of thin wood. Mathematically, the spline is a fit by piecewise cubics between points. The coefficients are obtained by imposing continuity of first and second derivatives at the mesh points and minimizing the integral of the square of the second derivative over the full range of the fit. The very convenient recurrence relations which govern the coefficients of such a fit are given in Chapter 2 of the textbook by Ahlberg et al. [63].

In his original published work, Anderson used simpler but less effective methods. The infinite t interval $-\infty < t < \infty$ was mapped into a finite z interval $-1 < z < 1$ by the simple transformation pair suggested by Taylor's weak shock solution:

$$t \rightarrow \frac{\delta}{2} \ell n \frac{1+z}{1-z} \quad ; \qquad z \rightarrow \tanh(t/\delta) \quad ,$$

where δ is a suitable scaling constant. This transformation pair was coupled with Chebyshev interpolation in z with placement of the mesh points z_i at the extrema of the highest degree polynomial used. However, the symmetry of this scheme was found by Anderson to interfere with a procedure (discussed in the next section) necessary to correct unwanted translational shifts during solution. The new "backbone" method, beside being more flexible and accurate, involves an asymmetrical transformation from the infinite to a finite interval, which reduces the problem with the shift correction.

The backbone profile selected is an accurate analytical approximation to the BGK shock solution developed by Macomber [20], and given in Appendix A.2 of Ref. 20. We simply note that it is of the form:

$$t = \mathcal{T}(u_b) \quad ; \qquad u_b = \text{backbone velocity profile} \quad , \tag{4.1}$$

with the inverse transformation:

$$\begin{aligned} u_b &= \mathcal{T}^{-1}(t) \quad ; \\ n_b &= \text{const.}/u_b \quad . \end{aligned} \tag{4.2}$$

This inverse transformation is not as convenient as before, involving the numerical solution of a nonlinear equation ($\mathcal{T}$ is an awkward sum of logarithmic and algebraic functions). However, as shown in Section C, this disadvantage can be overcome. The Macomber solution also yields a temperature backbone T_b very simply in terms of u_b.

2. Quadrature Scheme

The quadrature scheme chosen is a compound Gaussian, tailored to the shape of the kernels $\mathcal{K}$ of Eqns. (2.23). The formula is centered at $t' = t$, where each $\mathcal{K}$ has a logarithmic singularity, and the upstream $(t' < t)$ and downstream $(t' > t)$ regions are separated; each region is further split up into three zones. Thus, if the integrals in Eqn. (2.23) are written as $\int_{-\infty}^{\infty} \mathcal{J}(t';|t-t'|)dt'$, the transition to the quadrature formula may be represented as follows, writing $\tau^+ \equiv t' - t$ and $\tau^- \equiv t - t'$:

$$\int_{-\infty}^{\infty} \mathcal{J}(t';|t-t'|)dt' = \int_0^{\infty} \mathcal{J}(t+\tau^+;\tau^+)d\tau^+ + \int_0^{\infty} \mathcal{J}(t-\tau^-;\tau^-)d\tau^-$$

$$= \left\{ \int_0^{\tau_1^+} \mathcal{J}\cdot d\tau^+ + \int_{\tau_1^+}^{\tau_2^+} \mathcal{J}\cdot d\tau^+ + \int_{\tau_2^+}^{\infty} \mathcal{J}\cdot d\tau^+ \right\} + \left\{ \int_0^{\tau_1^-} \mathcal{J}\cdot d\tau^- + \int_{\tau_1^-}^{\tau_2^-} \mathcal{J}\cdot d\tau^- + \int_{\tau_2^-}^{\infty} \mathcal{J}\cdot d\tau^- \right\}$$

$$\rightarrow \sum_{k=1}^{3} \sum_{j=1}^{L_z^+} \mathcal{J}(a_{jk}^+)w_{jk}^+ + \sum_{k=1}^{3} \sum_{j=1}^{L_z^-} \mathcal{J}(a_{jk}^-)w_{jk}^- ,$$

where the signs + and - denote the downstream and upstream regions, respectively, the k index (1,2,3) refers to the zone number, and $w_{jk}^{\pm}$ and $a_{jk}^{\pm}$ are the Gaussian weights and abscissas. The values of $\mathcal{J}$ at these abscissas are found using the interpolation formula. Each Gaussian formula is adapted to its particular τ interval and requires $L_k^{\pm}$ points in all. As the treatment of the two regions is identical in manner, we can discuss the details of the scheme simply by zone, as follows.

Zone 1

This zone contains the singularity at $\tau = 0$, an imperfect treatment of which will lead to profile inaccuracies, particularly on the downstream side [31]. The interval $(0,\tau_1)$ is mapped onto $(0,1)$ and the singular and nonsingular parts of $\mathcal{J}$ are separated:

$$\mathcal{J} = a(\tau) + b(\tau)\ell n\,\tau \quad ; \quad \tau = \tau_1 y$$

$$\therefore \int_0^{\tau_1} \mathcal{J}\cdot d\tau = \tau_1 \int_0^1 a(\tau_1 y)dy + \tau_1 \int_0^1 (\ell n\, y + \ell n\, \tau_1)b(\tau_1 y)dy$$

$$= \tau_1 \int_0^1 [a(\tau_1 y) + \ell n\, \tau_1 \cdot b(\tau_1 y)]dy + \tau_1 \int_0^1 \ell n\, y \cdot b(\tau_1 y)dy \ .$$

The first integral is replaced by a half-range Gauss-Legendre formula of L_1^{ℓ} points and the second by a special Gaussian formula of L_1^{s} points, adapted to the singularity, for which the weights and abscissas are given in Refs. 64 and 65. Thus in each region, the number of zone 1 points used is:

$$L_1 = L_1^{\ell} + L_1^{s} \ . \tag{4.3}$$

Zone 2

This zone covers the intermediate interval (τ_1,τ_2) and is treated by compound Gauss-Legendre quadrature; J subintervals of equal extent $(\tau_2-\tau_1)/J$ are each mapped onto $(-1,1)$ and treated by a K^{th}-order Legendre formula. Thus in each region the number of points used is:

$$L_2 = J \cdot K \ . \tag{4.4}$$

Zone 3

The final zone covers the interval (τ_2,∞), over which the integrand decays like $\exp(-\tau/\delta)$. The interval is thus mapped onto $(0,\infty)$ and an I^{th}-order Gauss-Laguerre formula is used:

$$\int_0^\infty \mathcal{J}(\tau)dt = \delta \int_0^\infty \mathcal{J}(y\delta)dy \quad ; \quad y = \tau/\delta$$

$$\simeq \delta \sum_{i=1}^{I} \mathcal{J}(a_i\delta)w_i e^{a_i} \quad ,$$

where w_i, a_i are Laguerre weights and abscissas on $(0,\infty)$. In each region the number of points used is:

$$L_3 = I \quad . \tag{4.5}$$

Thus for the complete quadrature, using (4.3-5), the total number of points used is:

$$\begin{aligned} L &= L_1^+ + L_2^+ + L_3^+ + L_1^- + L_2^- + L_3^- \\ &= 2 \cdot \left[(L_1^\ell + L_1^s) + J \cdot K + I \right] \quad , \end{aligned} \tag{4.6}$$

where in the second expression we have assumed that both ranges are treated with the same number of points, as is usually the case.

The choices of τ_1, τ_2, δ, I, J, K, L_1^ℓ, L_1^s in (4.6) are adjusted by trial to preserve adequate accuracy while minimizing L. Typical values are:

$$\tau_1 = .05$$

$$\tau_2 = 9.$$

$$\delta = 1.5$$

$$I = 6\text{-}12$$

$$J = 8\text{-}15$$

$$K = 5$$

$$L_1^{\ell} = L_1^{S} = 3\text{-}5 \quad ,$$

which lead to values of L in (4.6) within the range 104-194. Normally a value close to the smaller of these is achieved, i.e., $L \approx 100$ in practice.

B. Iteration Schemes

The solution of the discretized form of (2.23) must now be obtained by iteration. Representing the dependent variables $n(t_i)$ and $T(t_i)$ as a single vector $\underline{z}$ of dimension $2N$, Eqn. (2.23) can be written as:

$$G\underline{z} = \underline{z} \quad ,$$

where G is a suitably chosen (nonlinear) iteration operator. An iteration cycle is then denoted by:

$$\underline{z}^{\ell+1} = G\underline{z}^{\ell} \quad , \qquad (4.7)$$

where ℓ is the iteration counter.

Special forms of G of particular interest are:

1. A Gauss-Jacobi operator G_J defined by:

$$\underline{z}^{\ell+1} = G_J\underline{z}^{\ell} \quad ,$$

where all the values used on the right side are the unchanged components of the previous iterate.

2. A relaxed Jacobi iteration defined by:

$$\underline{z}^{\ell+1} = [\theta^{\ell}G_J + (1-\theta^{\ell})I]\underline{z}^{\ell} \quad ,$$

where I is the identity operator and θ^{ℓ} is a parameter of order 1.

3. A Gauss-Seidel operator G_S defined by:

$$\underline{z}^{\ell+1} = G_S\underline{z}^{\ell} \triangleq G_J\underline{z}^{\ell'} \quad ,$$

where the values $\underline{z}^{\ell'}$ on the right side are the latest available data, i.e.,

$$z_i^{\ell'} \equiv z_k^{\ell+1} \quad , \qquad k < i \quad ,$$

$$\equiv z_k^{\ell} \quad , \qquad k > i \quad .$$

4. A relaxed Gauss-Seidel iteration defined by:

$$\underline{z}^{\ell+1} = [\theta^{\ell}G_S + (1-\theta^{\ell})I]\underline{z}^{\ell} \quad .$$

Higher-degree iterations are also possible, in which combinations of iterates from past cycles $(\ell-j)$, $j = 0,1,2,\ldots,D$ are used during the $(\ell+1)^{th}$ iteration cycle, in order to accelerate the convergence.

Anderson [66] made an extensive empirical study of Jacobi-type iteration methods for the BGK problem and concluded that the simple Jacobi iteration (1), with or without relaxation (2), was uneconomical, as 50 or more iterations were required for convergence. He then developed a higher-degree iteration 3-5 times as effective as (1), based on a 2N-dimensional generalization of the secant method for nonlinear root-finding. This "Extrapolation Algorithm" of Anderson is fully described in Ref. 66; it takes the form of a quasi-linear combination of pairs of Jacobi iterates:

$$\underline{z}^{\ell+1} = \text{linear comb.}\{\underline{z}^{\ell},\underline{y}^{\ell};\underline{z}^{\ell-1},\underline{y}^{\ell-1}; \ \ldots \ ;\underline{z}^{\ell-D},\underline{y}^{\ell-D}\} \quad ,$$

with:

$$\underline{y}^{\ell} = G_J \underline{z}^{\ell} \quad ,$$

and

$$D = \text{degree of process} \approx 1\text{-}4 \text{ in practice.}$$

The particular linear combination chosen is given in Ref. 66; it is quite complicated in form. Because the coefficients of this combination depend nonlinearly on the $\underline{z}^{\ell-j}$, the resulting form is only quasi-linear.

Anderson's method was found by him to require only 10-12 iterations to converge the BGK problem, and similar results were found by us for all the four models considered. However, the Anderson iteration is complicated and conceptually difficult to understand. A simpler alternative was felt to be desirable and we investigated the Gauss-Seidel approach. Anderson did not consider such iterations in his work, possibly on account of the so-called "shift" phenomenon, which will now be discussed.

Because there exists no natural coordinate origin in the shock problem, the solution is spatially invariant: if $\underline{z}(t)$ is a solution then so is $\underline{z}(t-t_0)$. An awkward consequence is that any iteration operator G can induce a translation by t_0 as well as a shape change. The actual size of t_0 depends on the discretization scheme, the operator G, and the current iterate $\underline{z}^{\ell}$. Whereas, in an analytical approach, the value of t_0 would very likely approach zero as convergence occurred, in the discrete case the minimum-error solution to the problem is likely to have a small but finite t_0 associated with it; if this is not accounted for, the convergence of the solution will appear very much poorer than it is, or divergence may be induced if an acceleration scheme is being used.

This shift phenomenon can be dealt with fairly simply in the case of a Jacobi iteration: after each complete sweep the new iterate is shifted to a standard reference point before any comparisons or combinations are made with previous iterates. In practice, the point with average velocity $\bar{u} = (u_1+u_2)/2$ is moved to $t = 0$. After reshifting, residuals can be calculated, convergence estimated, and linear combinations formed for any extrapolation scheme which may be in use. This was the technique used successfully by Anderson and ourselves in conjunction with his iteration method; as mentioned in the preceding section, suitable discretization and interpolation schemes must also be adopted to ensure the effectiveness of the shift correction.

In the case of a Gauss-Seidel iteration, the situation is more complex. The particular iteration G_S that we developed involves a sweep over the points t_i from the cold to the hot side of the shock, in which the two components n and T of $\underline{z}^{\ell+1}$ are computed simultaneously at each given t_i and then incorporated into the data $\underline{z}^{\ell'}$ for the rest of that sweep. This is the third form defined on page 58. Clearly, if no account is taken of possible shifts during this type of sweep, the shift can accumulate and instability will result.

The situation is illustrated in Fig. 4. The upper plot is of the simpler Jacobi case, where a shift by t_0 (measured at the point where $u = \bar{u}$) has been produced by the sweep $\underline{z}^{\ell+1} = G_J\underline{z}^{\ell}$. The shift is seen to produce errors of $\delta u(t;t_0)$ in the u profile and to similar errors (not shown) of $\delta n(t;t_0)$ and $\delta T(t;t_0)$ in the n and T profiles. The scheme adopted for shift correction in the Gauss-Seidel case is illustrated in the lower plot. Before starting the full sweep from the point t_1,

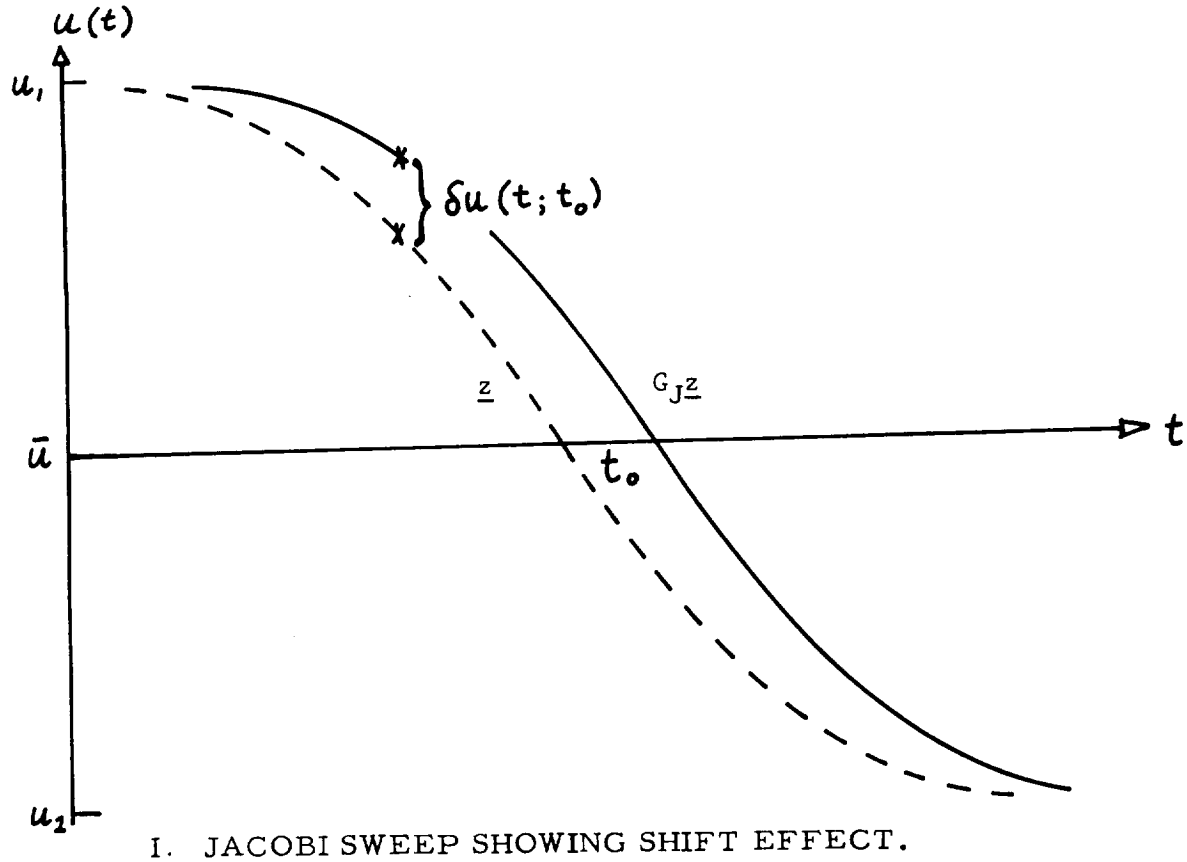

I. JACOBI SWEEP SHOWING SHIFT EFFECT.

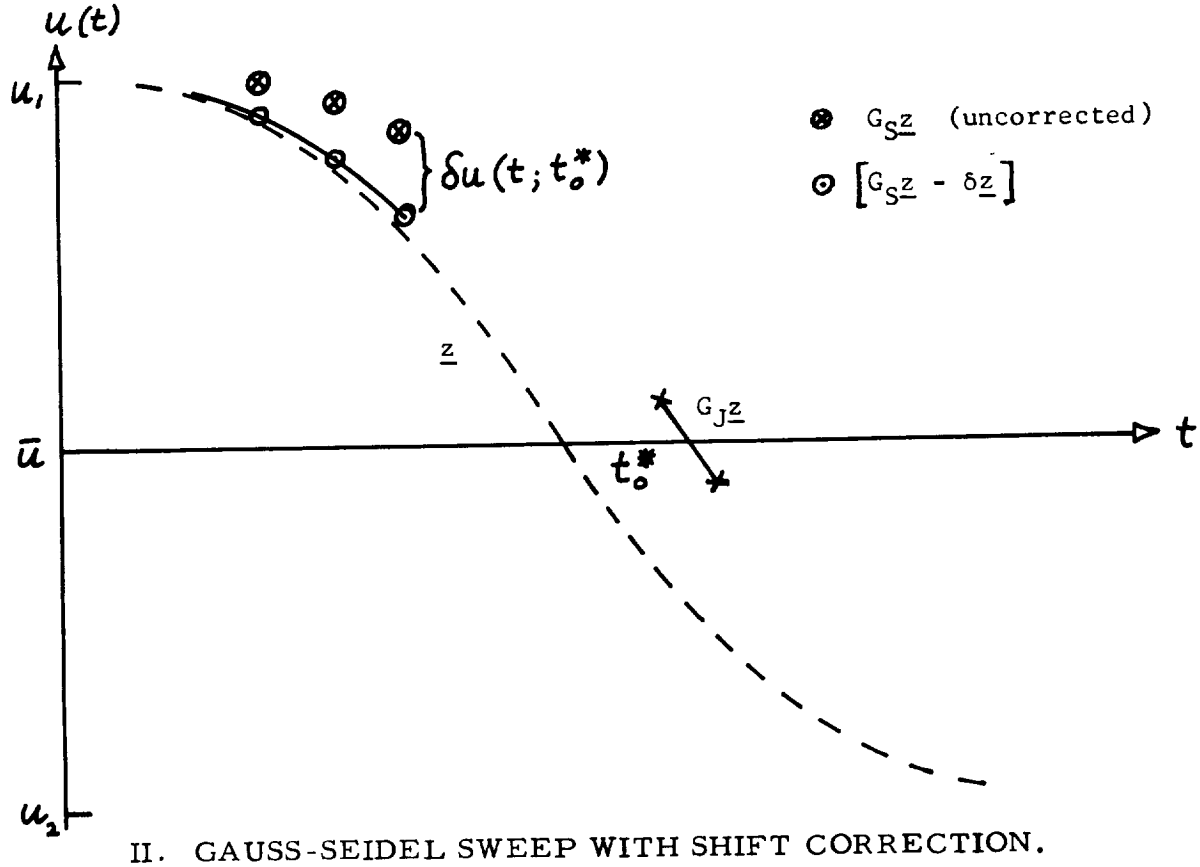

II. GAUSS-SEIDEL SWEEP WITH SHIFT CORRECTION.

Figure 4.

sample Jacobi calculations are made at the two t_i points which straddle the value $u = \bar{u}$, allowing a rapid estimate to be made of the t_0 value which would be found after a full Jacobi sweep. Denoting this estimate by t_0^*, the corresponding values of $\delta n(t_i;t_0^*)$ and $\delta T(t_i;t_0^*)$ can then be calculated and stored for all i, using the undisturbed $\underline{z}^\ell$ profile as a basis. The full Gauss-Seidel sweep is then performed, the values of $\delta n(t_i;t_0^*)$ and $\delta T(t_i;t_0^*)$ being subtracted from each new $n(t_i)$ and $T(t_i)$ before these are incorporated into $\underline{z}^{\ell+1}$ and the data $\underline{z}^{\ell'}$. Additionally, a point relaxation scheme is incorporated so that the actual replacement made at the i^{th} point is:

$$z^{\ell+1}(t_i) \rightarrow (1-\theta^\ell) \cdot z^\ell(t_i) + \theta^\ell\left[G_J z^{\ell'}(t_i) - \delta z^\ell(t_i;t_0^*)\right] \quad . \quad (4.8)$$

This procedure results in a stable iteration in the problems studied. The optimum value of θ^ℓ is found empirically to decline from a value of $\approx$ 1.2 (over-relaxation) far from convergence, to $\approx$ 0.8 (under-relaxation) in the final stages, with about 8-12 iterations necessary to achieve convergence.

In all the work, convergence was defined as follows. Iterations were continued until all monotonic trends in convergence had been eliminated by the acceleration schemes. The remaining changes between iterates were random in nature, due to rounding, etc. Statistical estimates showed that good graphical accuracy was achieved in the work for both n and T profiles (i.e., values determined to within $\approx$ 0.5%).

C. Programming Considerations

As shown in Section A, the discretized problem has $L \times N$ nodes, at each of which the kernels $\mathcal{K}$ must be evaluated once per iteration.

Here L is the number of quadrature points ($\sim$ 100-200) and N is the number of t_i points ($\sim$ 20-30), resulting in values of $L \times N$ between $\sim$ 2000-6000. In practice, the lower figure of 2000 nodes usually proves sufficient, and this will be assumed for the rest of the discussion. Thus a 1-msec. operation within the main "node loop" of the program will require 2 seconds of execution time per iteration, or about 20 seconds for a full problem of 10 iterations.

An economical calculation must obviously minimize the number of operations carried out at each node. This is achieved by:

1. Removing all possible parts of the kernel calculation from within the node loop by careful setup of the program.
2. Optimizing all calculations left within the node loop, particularly the H_n function evaluations.

Some details of these methods are now given. All timings referred to are for an IBM 360/67 computer.

1. Program Setup

To remove operations from within the node loop, we precalculate and store all major items which do not change between iterations. Typical of such items are:

--- The value of the backbone velocity u_b at each node, involving the nonlinear inversion (4.2). Each such value requires 2 msec. (or 4 seconds per iteration), but remains fixed unless the t_i or quadrature points change. The u_b values are therefore calculated on the first iteration of a problem and stored for all later iterations; they can also be used for other problems with matching mesh and quadrature points.

--- For a TGF model problem, two major items can be calculated and stored before the first iteration. First are the values at each node of

$$H_1\left(\frac{u_1^\sigma}{r_1}, \frac{|t-t'|}{r_1}\right) \quad \text{and} \quad H_1\left(\frac{u_2^\sigma}{r_2}, \frac{|t-t'|}{r_2}\right)$$

appearing in the kernels (Case 4 of Appendix A). Second are the coefficients $\mathcal{J}_{11}$, $\mathcal{J}_{22}$, $\mathcal{J}_{12}$, $\mathcal{L}_1$ and $\mathcal{L}_2$ which appear in the nonlinear fit (3.39) for $k_c(\nu)$.

2. H_n Function Evaluation

In each model there exists one set of H_n functions in the kernel with arguments which depend on the current state of the iteration as well as on the node. As convergence proceeds these arguments also converge at each node, and we can use the Taylor series expansion (2.22b) about the latest nodal value rather than a direct evaluation of each H_n. This expansion takes about 4 msec. per node rather than about 20 msec. for the direct evaluation; these times are for calculations of H_n, n = 1 to 3, from which all other H_n are rapidly derived by recursion relations. (The case in which only H_1 is needed is discussed at the end of this section.)

Values of H_n, n = 1 to 3, together with the argument values p and q, are stored for each node.† These H_n values are obtained by direct evaluation on the first iteration of a problem, or read in from a suitable dump if available. On all later iterations the new nodal values of p and q are first compared with the stored values (p_0 and q_0) at that node. If the differences $\delta p = p - p_0$ and $\delta q = q - q_0$ are

† Nodes in quadrature Zone 1 are an exception, as here a splitting of H_n into singular and nonsingular parts is made and Taylor coefficients are unavailable. For this reason, L_1 in (4.3) must be kept to a minimum to reduce the number of direct H_n calculations required in Zone 1.

suitably small, a third-order Taylor expansion ($N = 3$ in Eqn. (2.22b)) is used to calculate $H_n(p,q)$, $n = 1$ to 3. Only if the third-order terms are unacceptably large, or δp or δq are too big at the start, is a new direct H_n calculation made, and in this case the store is updated at that node.

This procedure is found to reduce the iteration time after 2-3 iterations by a factor of about 4-5 from the nominal value of 40 seconds. This, of course, reflects the substitution of a 4-msec. for a 20-msec. process at most nodes. The necessary core storage is correspondingly increased by $5 \times L \times N \sim 10{,}000$ words. At the end of a problem or run, this H_n store can be dumped to disk or tape and used to restart later runs.

The procedure is worthwhile even when only the H_1 functions are needed by a model. (In fact, only the Polynomial model requires H_n values for $n > 1$.) Use of the Taylor expansion requires H_n, $n = 1$ to 3, to be available, as H_n functions for a wide range of n appear in the coefficients of (2.22b). Direct evaluation of H_1 only; omitting H_2 and H_3, requires about 10 msec.; thus 10 iterations without the Taylor method will require about 200 seconds, with 20 additional seconds for each possible extra (or test) iteration. A problem with the Taylor method requires about 40 seconds for the first iteration, a total of about 40 seconds for the next three iterations, and then only 8-10 seconds per additional iteration, making about 140 seconds for 10 iterations. Besides this saving, all extra (or test) iterations, including those on other problems with matching mesh schemes, can take advantage of the dump of H_n functions now available and thus require only about 8-10 seconds per iteration.

CHAPTER V

RESULTS AND DISCUSSION

A. Results of the Model Calculations

The basic results of the model calculations are density and temperature profiles in the t frame, for high Mach number. For all the models studied, these profiles were found to be independent of M above $M \approx 5$. The results shown in Fig. 5 are for $M = 10$. The reduced density, $\nu = (n-n_1)/(n_2-n_1)$ and reduced temperature, $\hat{T} = (T-T_1)/(T_2-T_1)$ are given, with both profiles positioned so that $\nu = 0.5$ at $t = 0$.

The models studied are listed below, together with some comments on the results:

1. BGK Model

These results agree exactly with those of Anderson [33], confirming the accuracy of our numerical methods.

2. Ellipsoidal Model

These are the first exact calculations reported for the Ellipsoidal model, so no comparison results are available. The density profile is steeper than the BGK version and the temperature profile overshoots by 1% at the hot side. The temperature crosses the asymptote near $t = 1$.

3. Polynomial Model ($\lambda_4 = -3/2$)

This model has the same linearized form as the Ellipsoidal model, although a very different nonlinear form. Interestingly, the results are practically indistinguishable from the Ellipsoidal model, and are not plotted for this reason.

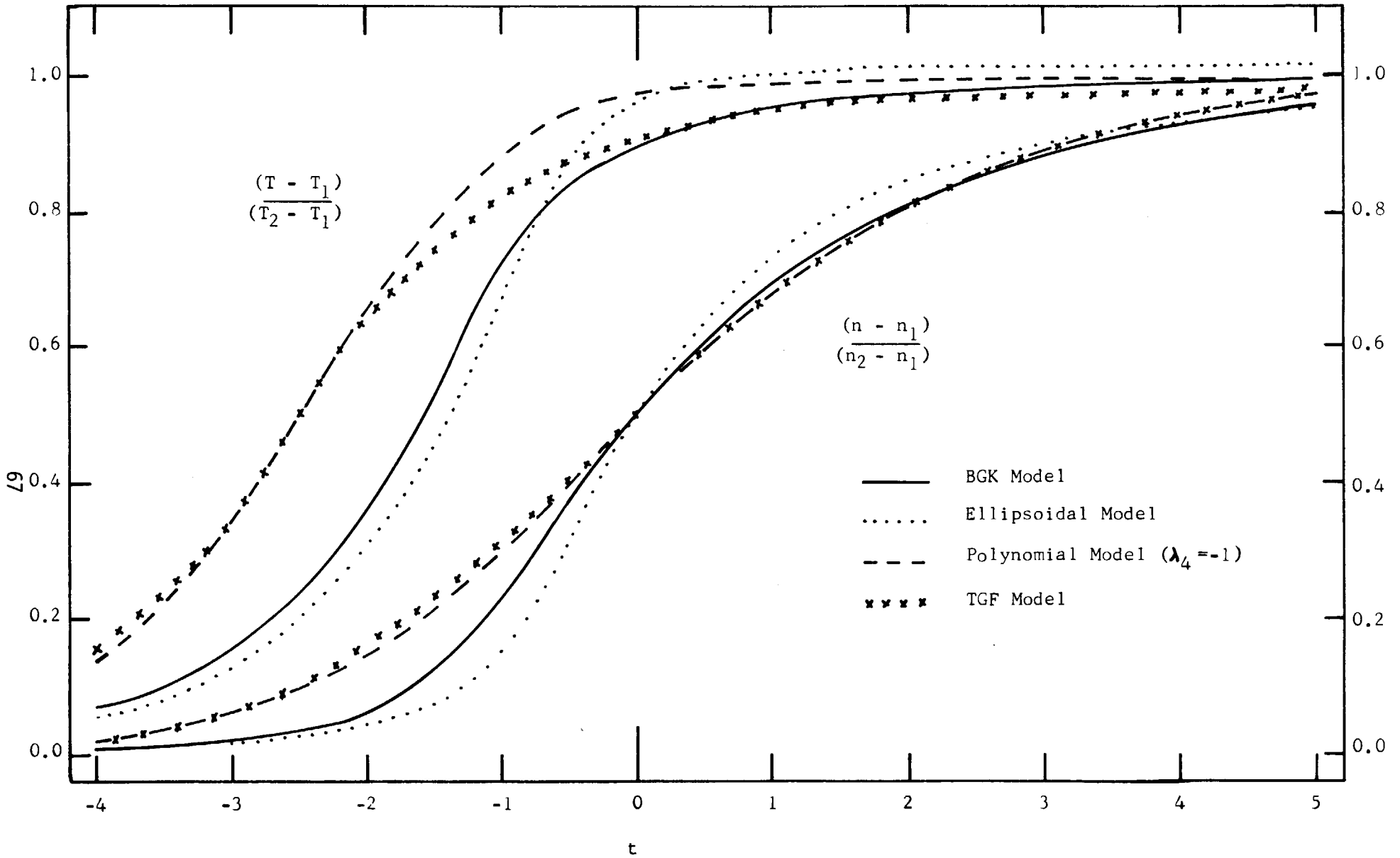

Figure 5: Reduced density and temperature profiles vs. t

4. Polynomial Model ($\lambda_4 = -3/5$)

This model has the same linearization as the exact Maxwell operator, up to $N = 5$. However, the results are disappointing. Downstream, a small overshoot of the density appears ($\sim 3\%$ in ν) beyond $t = 4$, and the reduced temperature, which reaches 0.97 at $t = 0$, dips to 0.94 at around $t = 3$ before recovering to unity at high t. Upstream, both density and temperature are unreasonably high. A plot is omitted from Fig. 5 as these results seem of little interest; however, a plot for this case is given in the next section, where it aids the discussion.

5. Polynomial Model ($\lambda_4 = -1$)

This model has the same λ_4 as the BGK model, but $\lambda_5 = -2/3$ and $Pr = 2/3$. The density profile is shallower and the temperature rises earlier than the BGK version. No overshoot exists in either profile, and the results are physically reasonable.

6. TGF Model

The density profile is very close to that of the previous case. The temperature profile is close to the previous case upstream, but approaches the BGK temperature profile for positive t. Again, no overshoots occur and the results are reasonable.

B. Comparisons with Monte Carlo Results

Monte Carlo results have been selected from several sources for these comparisons, as no single source is sufficiently comprehensive. Two groups of comparisons are made, one using the physical distance x as the independent variable and the other using the reduced density ν.

1. Profiles versus x/Λ_1

For all these comparisons the model results must be transformed from the t frame into a physical x frame using Eqn. (2.16). We follow all previous authors and use a "reduced" x frame, x/Λ_1, where Λ_1 is an upstream mean free path for hard-sphere molecules, expressed in terms of the upstream viscosity as:

$$\Lambda_1^{-1} = \frac{1}{2}\rho_1\bar{c}_1/\mu_1 \quad ; \quad \begin{matrix}\rho_1 = mn_1 \\ \mu_1 = \mu(T_1)\end{matrix} \quad , \tag{5.1}$$

with $\bar{c}_1$ defined as:

$$\bar{c}_1 = \frac{2}{\sqrt{\pi}}(2RT_1)^{1/2} \quad . \tag{5.1a}$$

As μ is proportional to $T^{1/2}$ for hard spheres, Λ_1 is independent of T_1 and is simply a convenient scale factor.

In order to use Eqn. (2.16), a form for $K(m_i)$ must be adopted. Close to local equilibrium, the Chapman-Enskog result (3.16) is appropriate:

$$K(m_i(t)) = K(T) = \frac{\rho RT}{\mu(T)}\Big/|\lambda_4| \quad , \tag{5.2}$$

together with the first-order Chapman-Enskog result [56] for $\mu(T)$ for molecules with repulsion proportional to the inverse r^{th} power of the separation:

$$\mu(T) = \mu_1 \cdot \left(\frac{T}{T_1}\right)^{\left[\frac{1}{2} + \frac{2}{r-1}\right]} \quad . \tag{5.3}$$

Although only the Maxwell molecule case ($r = 5$) is consistent with our basic assumption $K \neq K(c)$, we will for the moment follow earlier authors and apply Eqn. (5.3) for all r. Results can thereby be generated for all monatomic gases via their viscosity-temperature laws. We will

furthermore apply Eqns. (5.2-3) for all t, not just for regions of the shock in which the gas is close to local equilibrium. Again this follows the practice of earlier authors, and is another definite extrapolation. These extrapolations have received little attention in the past, although they are fundamental to the use of model equations of this type. A fuller discussion of their effects upon our results is presented in the next section. In the remainder of this section we simply display the results and comment on their general appearance.

The $t \to x/\Lambda_1$ transformation adopted, using Eqns. (5.1-3), is:

$$x/\Lambda_1 = \frac{|\lambda_4|\rho_1\bar{c}_1}{2\mu_1}\int_{t_0}^{t}\frac{\mu(t)\cdot dt}{\rho(t)RT(t)}$$

$$= |\lambda_4|\sqrt{\frac{2}{\pi RT_1}}\int_{t_0}^{t}\left(\frac{n_1}{n(t)}\right)\left(\frac{T(t)}{T_1}\right)^{\left[\frac{2}{r-1}-\frac{1}{2}\right]}dt \quad . \tag{5.4}$$

Figure 6 shows the model results for Mach 10 and $r = 5$, compared with the Mach 10 Maxwell molecule Monte Carlo results of Bird [48] for density and Perlmutter [45] for temperature. The latter was used in the absence of a published Maxwell molecule density profile by Bird. Although Perlmutter, unlike Bird, assumes an approximate target molecule distribution, his temperature profile is very close to recent provisional Maxwell molecule results of Deiwert [67], who used a version of the Bird program; Perlmutter's density profile also agrees very closely with Bird's density. The Bird results of Ref. 48 were calculated at Mach 8, so a relation given by Bird: $(\text{shock scale length})/\Lambda_1 \propto M^{4/(r-1)}$ was used to convert those results to Mach 10, i.e., a 25% scale increase was applied to the Bird Maxwell profiles and a 9% increase to the argon ($r = 12$) profiles referred to in the next paragraph. The BGK density profile rises too late

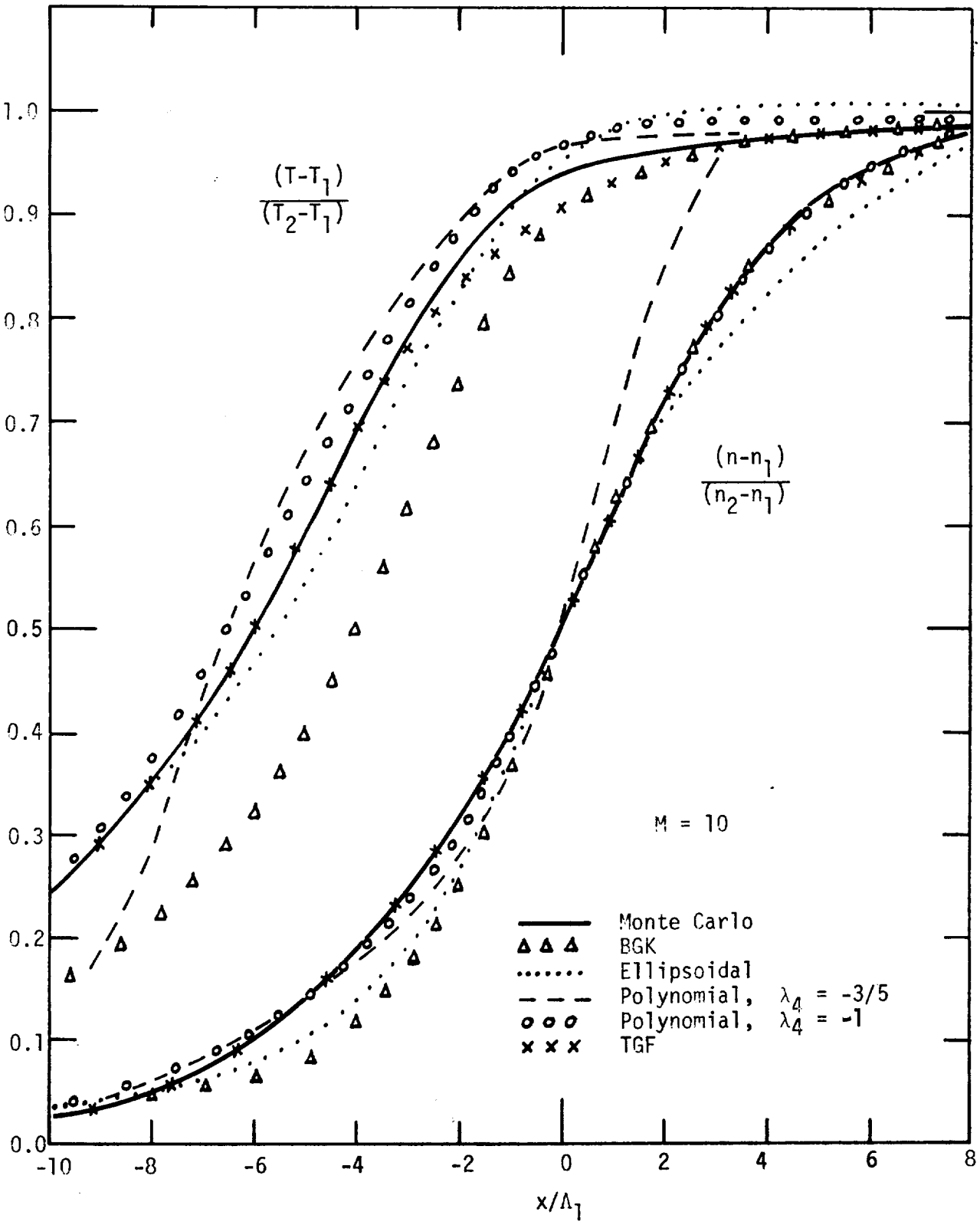

Figure 6. Reduced density and temperature profiles vs. x/Λ_1 for Maxwell molecules.

upstream but agrees well with Monte Carlo results downstream; the BGK temperature profile is displaced by $\sim \Lambda_1$ in the downstream direction. The Ellipsoidal model corrects the temperature displacement but shows density discrepancies both upstream and downstream; furthermore, a 1% temperature overshoot appears upstream for this model. The Polynomial ($\lambda_4 = -3/5$) model agrees poorly with the Monte Carlo results; this case is included here to aid the discussion in Section C. Both the TGF and Polynomial ($\lambda_4 = -1$) models show excellent agreement with both density and temperature Monte Carlo profiles.

Figures 7 and 8 show the model results assuming $r = 12$ and $r = \infty$, respectively; the former corresponds to argon molecules [50] and the latter to hard-sphere molecules. The accompanying Mach 10 Monte Carlo results are due to Bird [48] for $r = 12$,† and Hicks [43] and Bird [48] for $r = \infty$. Both sets of comparisons show the same trends: all the models predict steeper density profiles than Monte Carlo, and temperature profiles which are displaced in the downstream direction. The BGK model shows the poorest agreement with Monte Carlo, the TGF and Polynomial ($\lambda_4 = -1$) models show the best agreement, and the Ellipsoidal model shows intermediate agreement.

2. Profiles versus ν

Plotting profiles against ν avoids the need for a $t \to x$ transformation, and also reduces the influence of Mach number and molecular force law variations, allowing a wider range of Monte Carlo results to be included.

† The argon profiles were Mach 8 results, rescaled by 9%, as already noted.

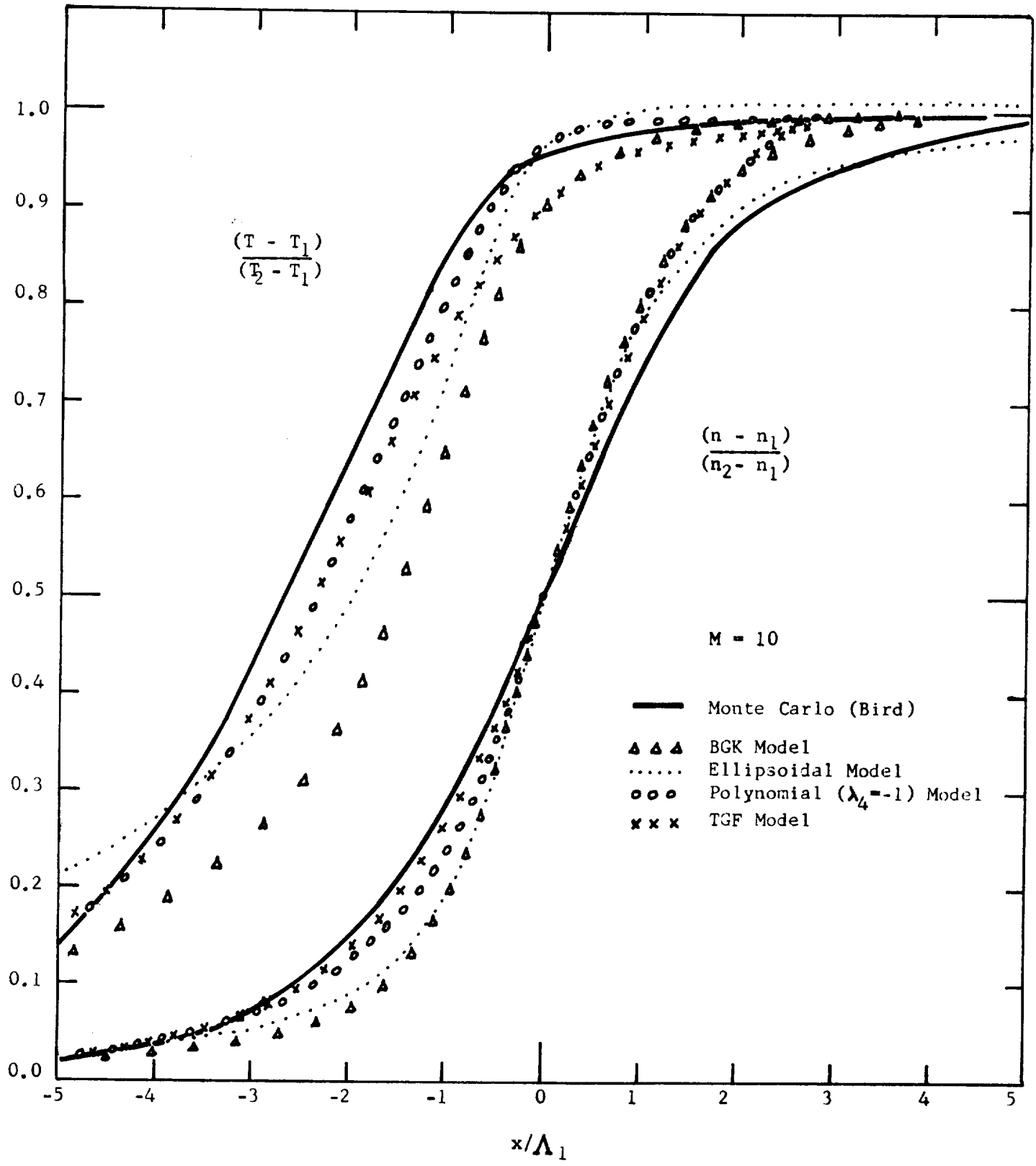

Figure 7: Reduced density and temperature profiles vs. x/Λ_1 for argon (r=12) molecules.

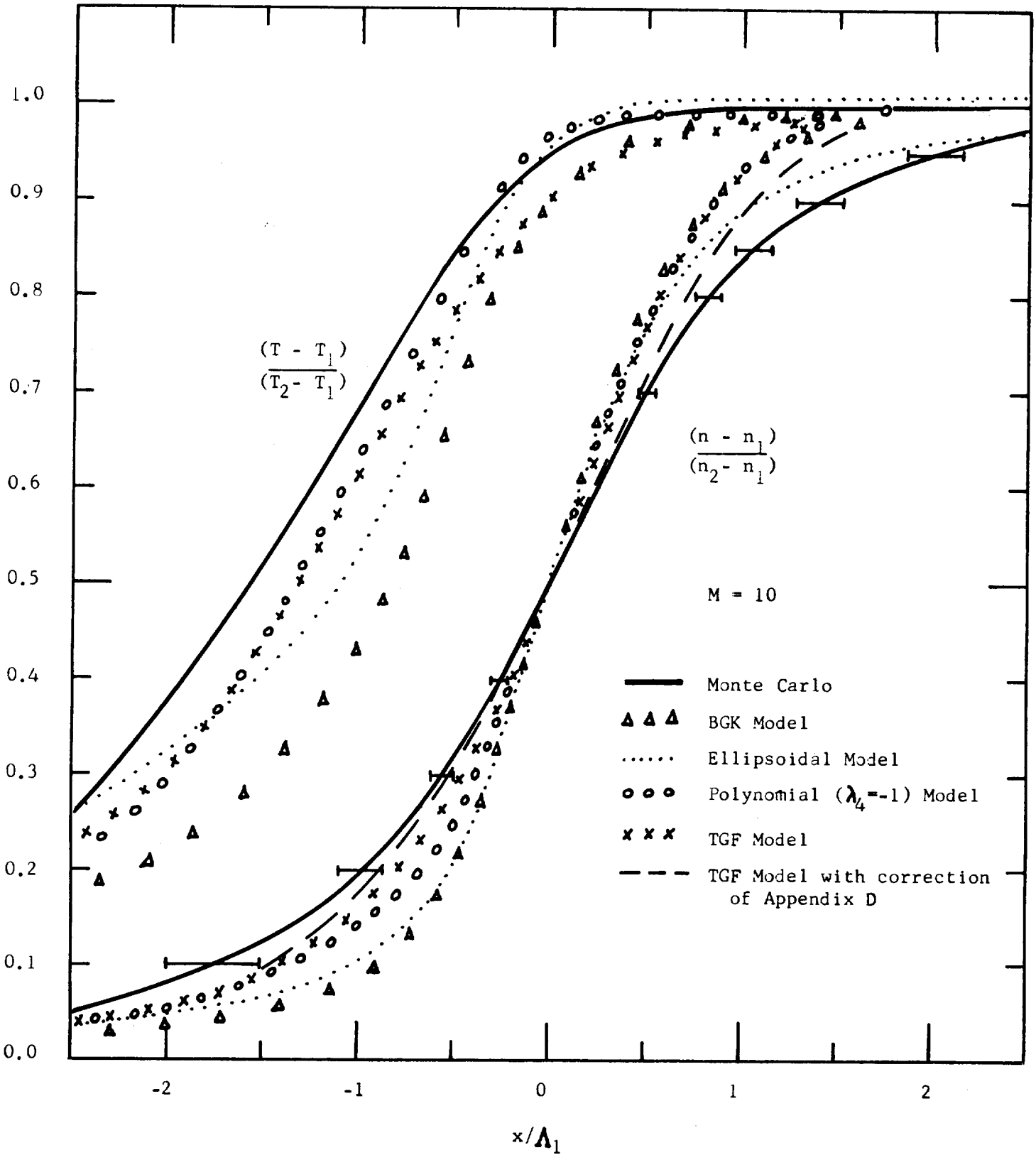

Figure 8: Reduced Density and Temperature Profiles vs. x/Λ_1 for Hard Sphere Molecules

Figure 9 shows the reduced temperature $\hat{T} = (T-T_1)/(T_2-T_1)$ for the models compared with Monte Carlo calculations using hard spheres [43] and Maxwell molecules [45] at Mach 10. All results coincide upstream, below about $\nu = 0.2$ and $\hat{T} = 0.7$. Further downstream, the Ellipsoidal and Polynomial $(\lambda_4 = -1)$ models show close agreement with Monte Carlo results while the TGF and BGK models predict $\hat{T}$ values about 5% lower.

Figures 10 and 11 show the results for viscous stress τ_{xx} and heat flux q_x, respectively. The most appropriate published Monte Carlo results were chosen, namely those at Mach 8 for $r = 12$ by Bird [48]. The figures for both τ_{xx} and q_x show that, as for $\hat{T}$, the Ellipsoidal and Polynomial $(\lambda_4 = -1)$ results form one closely related pair, while the TGF and BGK results form another. All the model results fall within about 10% of each other in all significant ranges of τ_{xx} or q_x, and the peaks occur at the same values of ν for all models. However, the models show definite disagreement in peak size and position with the $r = 12$ Monte Carlo results. Some provisional results by Deiwert [67] for $r = 5$ at Mach 10 have very recently become available, and these show significant differences from the Bird $r = 12$ results and closer agreement with the models; in fact, they coincide almost exactly with the Ellipsoidal/Polynomial pair of results.

Figure 12 shows the ratios $|\tau_{xx}/p|$ and $H_0/H_{0,1}$ which are related to the departure from equilibrium within the shock. The first ratio is zero and the second is unity at equilibrium. H_0 is the total (or stagnation) enthalpy, equal to $(5RT + u^2)/2$, and $H_{0,1}$ is the equilibrium upstream value of H_0. The Monte Carlo results are from Mach 10 hard sphere calculations by Hicks [43], and Mach 8 $r = 12$ calculations by

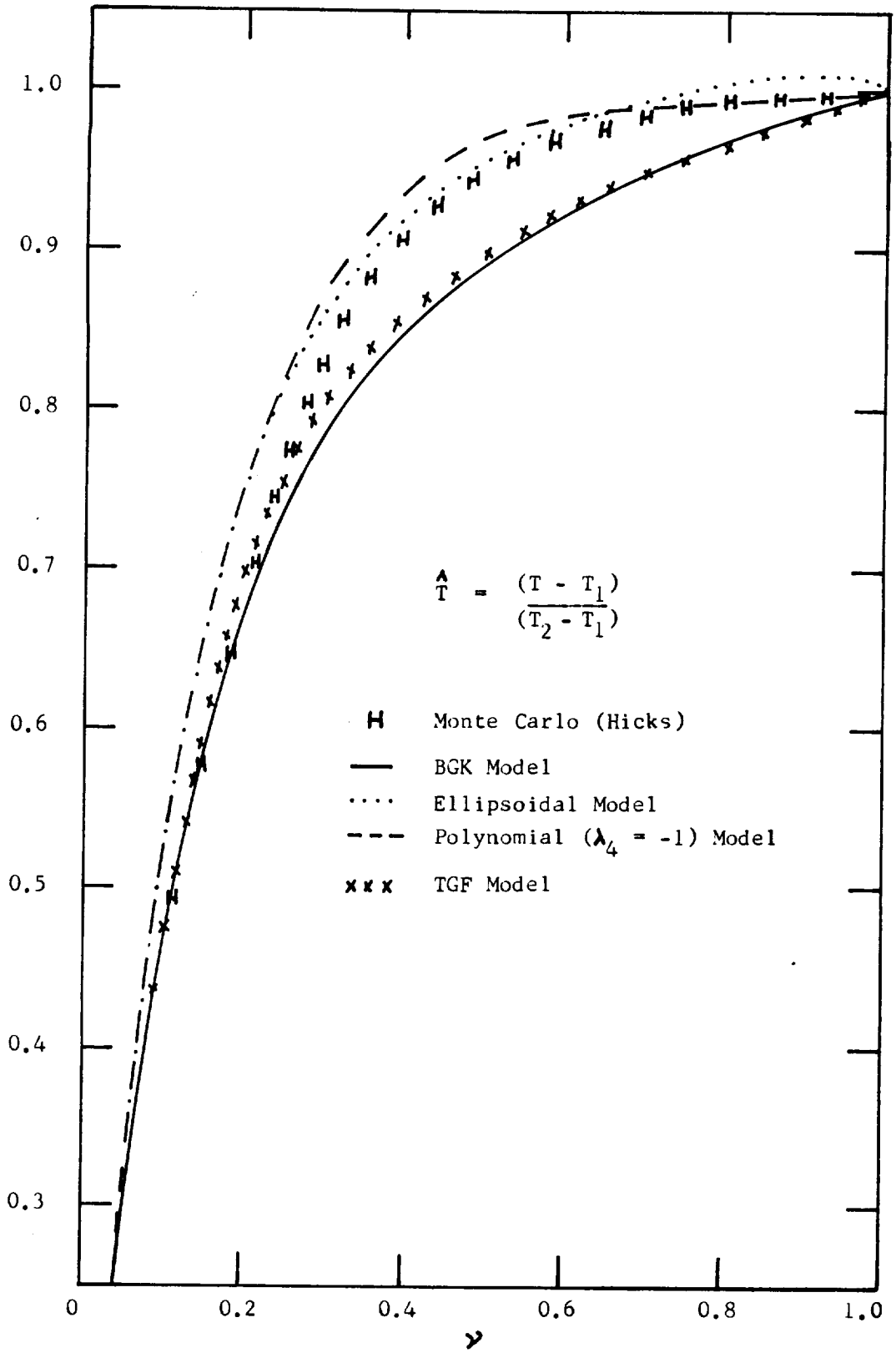

Figure 9: Reduced temperature $\hat{T}$ vs. reduced density ν.

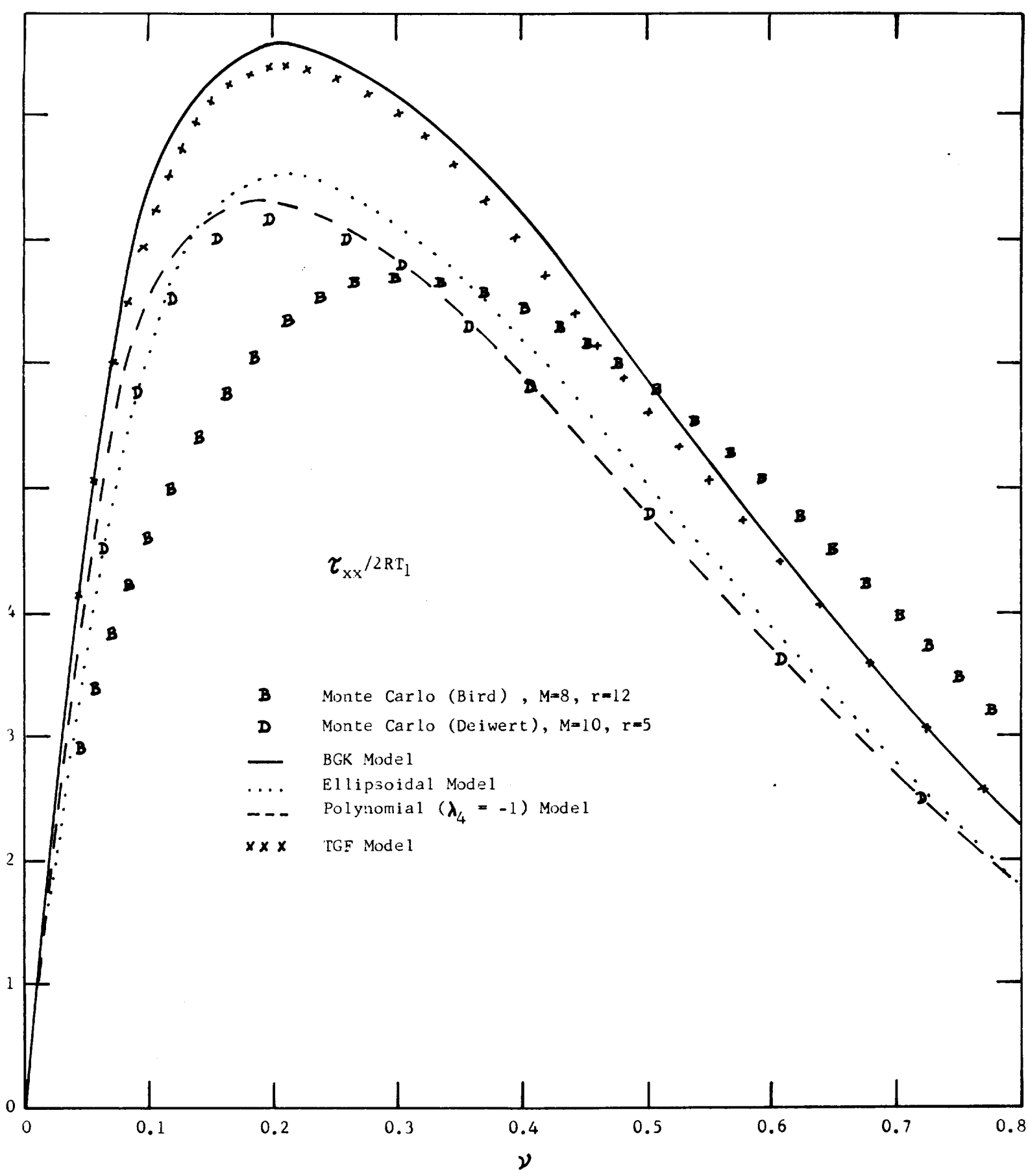

Figure 10: Normalized viscous stress $\tau_{xx}/2RT_1$ vs. reduced density ν.

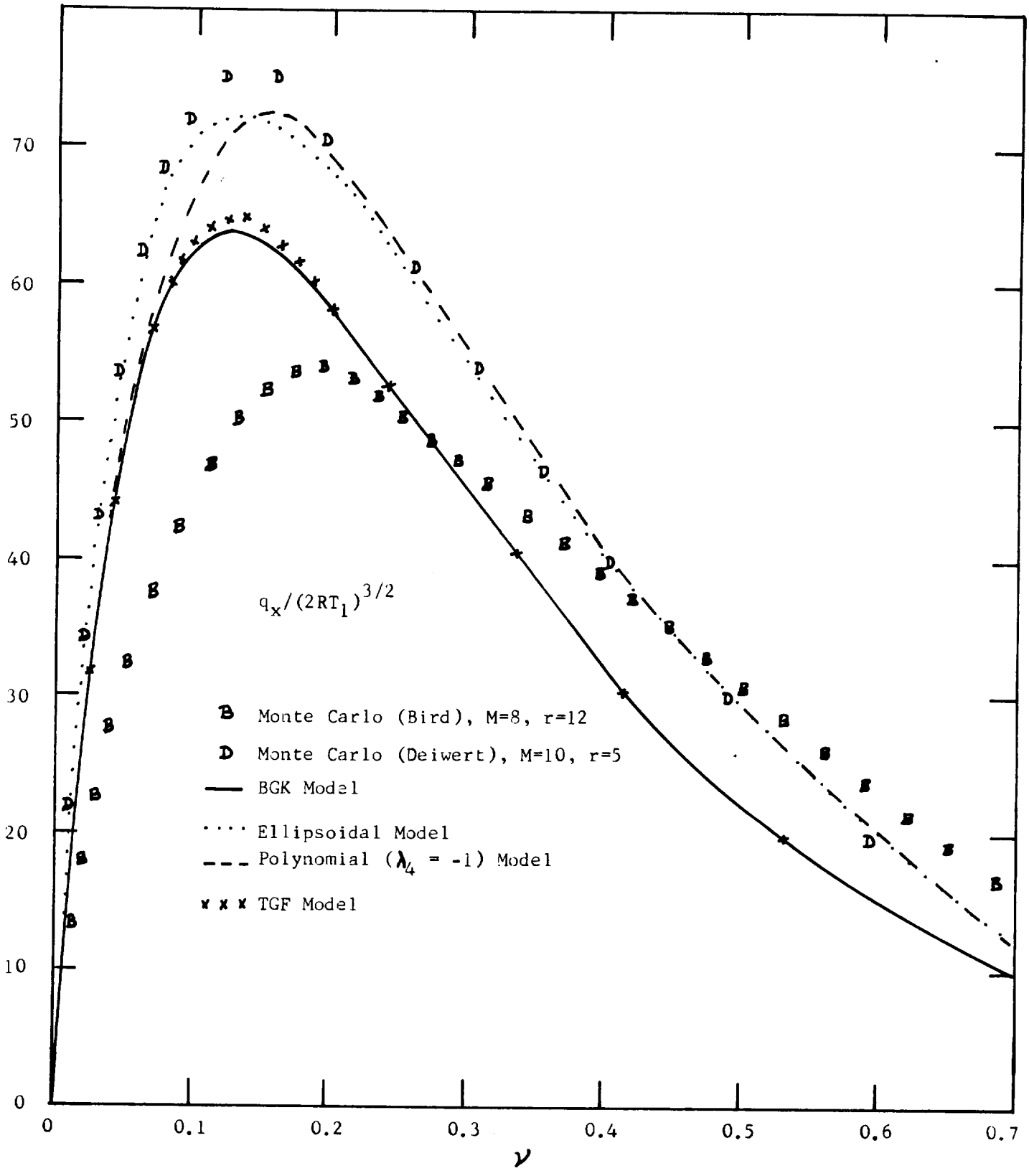

Figure 11: Normalized heat flux $q_x/(2RT_1)^{3/2}$ vs. reduced density ν.

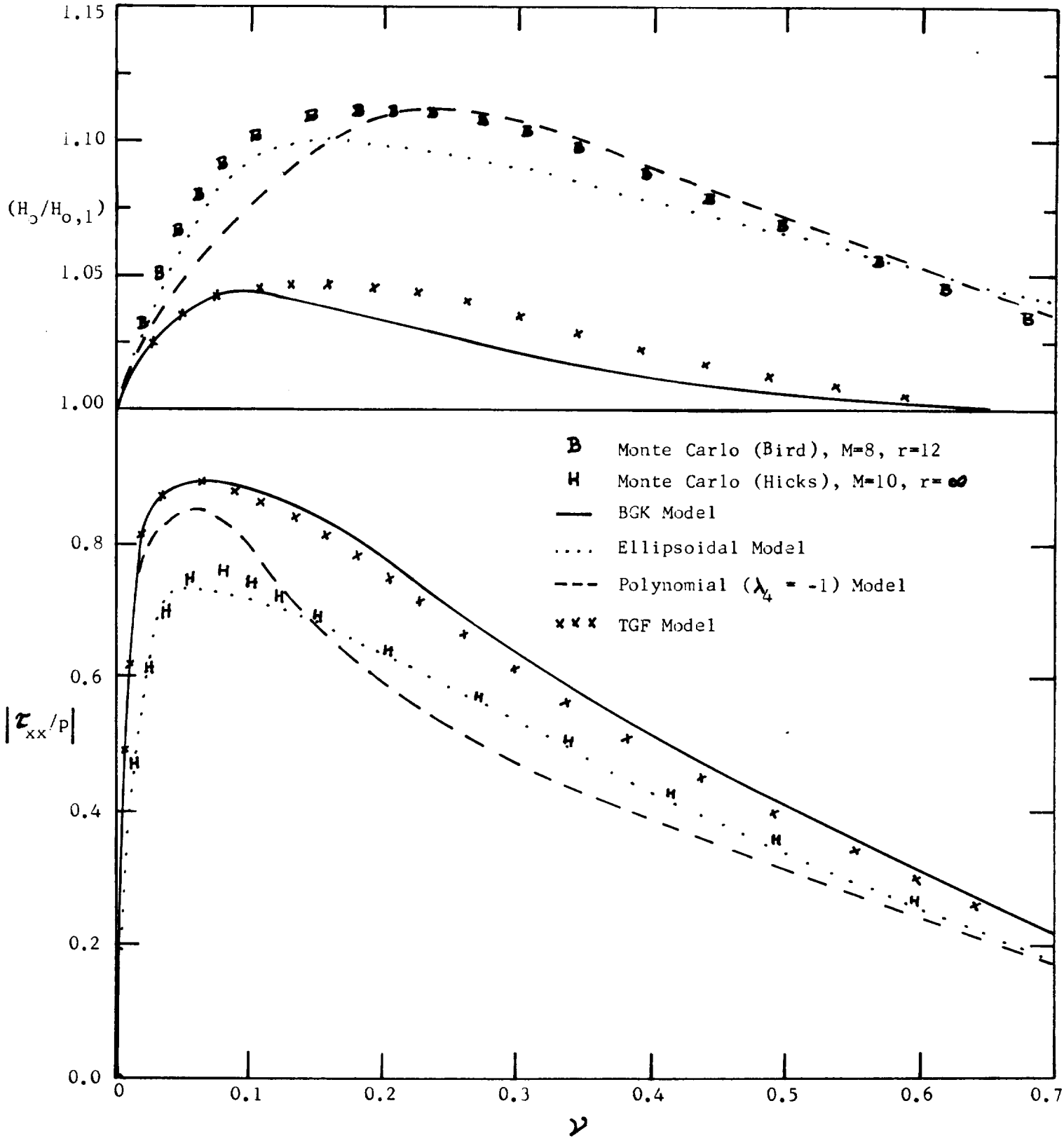

Figure 12: Ratios $H_o/H_{0,1}$ and $|\tau_{xx}/p|$ vs. reduced density ν.

Bird [48], respectively. In this case both Monte Carlo results are confirmed by Deiwert's provisional Mach 10 $r = 5$ results. The model results again split into the same two pairs, the splitting being slight for $|\tau_{xx}/p|$ but stronger for $H_0/H_{0,1}$ with the Ellipsoidal/Polynomial pair again in closer agreement with the Monte Carlo results.

C. Discussion

Four main aspects of the results warrant further discussion:

1. Validity of the $t \rightarrow x/\Lambda_1$ Transformation

The derivation of the $t \rightarrow x/\Lambda_1$ transformation (5.4) included two extrapolations, noted as they were introduced: the retention far from equilibrium of a Chapman-Enskog relation for K in terms of n, T and μ, and the inconsistent use for non-Maxwell molecules of a K that depends on temperature but not on molecular velocity.

A very strong argument exists, however, to support the use of this transformation (5.4). Both extrapolations are expected to be weakest at high Mach number, but it will now be shown that at high M the use of (5.4) leads to shock thicknesses, for all the models, which are proportional to $M^{4/(r-1)}$, in agreement with Monte Carlo [48] and Mott-Smith [16] predictions. Eqn. (5.4) can be written:

$$\begin{aligned} x/\Lambda_1 &= \frac{(\text{constant})}{\sqrt{RT_1}} \int_{t_0}^{t} \frac{u(t)}{u_1} \left(\frac{T(t)}{T_1}\right)^{s-1} dt \\ &= (\text{constant}) \frac{(RT_1)^{(1-2s)/2}}{u_1} \int_{t_0}^{t} u T^{s-1} dt \quad , \end{aligned} \tag{5.5}$$

with:

$$s \equiv \frac{1}{2} + \frac{2}{r-1} \quad .$$

At high M, by the Rankine-Hugoniot relations (2.13), $RT_1 \to 16/5M^2$ and $u_1 \to 4/\sqrt{3}$; further, all the model profiles versus t are found to become independent of M. The shock thickness is therefore proportional only to the factor multiplying the integral on the right hand side of Eqn. (5.5). Thus, by (5.5), the shock thickness can be seen to reduce to a constant times M^{2s-1}, i.e., to a constant times $M^{4/(r-1)}$.

For Maxwell molecules, the transformation (5.4) is now determined up to a constant scale factor set for each model by the parameter $|\lambda_4|$ in Eqn. (5.4). As discussed in Chapter III, Section F, during the derivation of the TGF model, the value of λ_4 depends on the form of the emission function chosen for a model. The BGK model (and the TGF model by deliberate choice) have $|\lambda_4|$ set at unity; the Ellipsoidal model has $|\lambda_4|$ set at 3/2; and the Polynomial model has λ_4 freely adjustable. The effects of these scale factors can be seen in Fig. 6: the Ellipsoidal model, which has the largest scale factor but an incorrect emission function, shows distorted profiles with an over-stretched appearance. The Polynomial model with the smallest value of $|\lambda_4| = 3/5$ shows the effects of an over-contraction in scale. The BGK model with $|\lambda_4| = 1$ suffers from an incorrect emission function, not a scaling defect, as shown by its agreement with Monte Carlo results downstream but not upstream. The TGF and Polynomial models with the same value of $|\lambda_4| = 1$ seem to be appropriately scaled for their emission functions.

For non-Maxwell molecules, we expect the results to worsen progressively as r departs from 5, due to the use of a velocity-independent collision frequency. This is in fact seen in the results for argon ($r = 12$, Fig. 7) and for hard spheres ($r = \infty$, Fig. 8). By comparison

with Monte Carlo, the models predict thinner density profiles, and temperatures which rise too late upstream. For argon, the error in maximum density-slope thickness is under 20% for the two best models (TGF and Polynomial with $\lambda_4 = -1$), with about a 20% contraction of scale evident in the downstream density wing and negligible errors upstream. For hard spheres and the same models, the thickness error is 25% and a scale contraction of up to 20% exists in the upstream density wing, and up to 50% in the downstream wing. Although the accuracy of the Monte Carlo density profile is poorest in the wings, these discrepancies are almost certainly due to shortcomings in the models, as they considerably exceed the Monte Carlo uncertainties.†

The divergence between the Maxwell molecule and hard-sphere results indicates that the deficiency is most probably related to the use of a velocity-independent collision frequency. Since, as will be shown later, model calculations with a velocity-dependent K are difficult, and since the Mott-Smith method is fairly accurate at high Mach number, this hypothesis was tested by the latter method (see Appendix D). Mott-Smith calculations were made for hard spheres and for a model similar to ours, i.e., one in which the correct K(c) was replaced by the K(n,T) of the models. The results show that this replacement leads to shock thicknesses contracted by about 15% (at Mach 10), and to small density and temperature discrepancies upstream and larger density errors upstream, of exactly the type found in our results. The quantitative effect is of course approximate, being less than the observed effect, but the qualitative effect shown

† The Monte Carlo error bars shown in Fig. 8 are based on the spread reported by Bird between Mach 25 and Mach 100 hard-sphere density profiles, which both should agree with a Mach 10 profile.

is very convincing as can be seen from Fig. 8, where a corrected TGF density profile is included, based on the method of Appendix D.

An even simpler qualitative explanation of the effect of the collision frequency upon shock thickness can be given as follows. Regarding the shock as a diffusion process involving hot and cold components, the shock scale at any point will be inversely proportional to some average of the collision frequencies for cold-hot (1-2) and hot-cold (2-1) encounters. Assuming a bimodal-Maxwellian distribution function of the form (C.2), the mean collision frequency for (1-2) collisions, per cold molecule, is $\bar{K}_{12}(\nu) = \frac{\nu}{n_1} \int f_1^{(0)} \mathscr{L}_2(\underline{c}) d\underline{c}$ and the result for (2-1) collisions, per hot molecule, is $\bar{K}_{21}(\nu) = \frac{(1-\nu)}{n_2} \int f_2^{(0)} \mathscr{L}_1(\underline{c}) d\underline{c}$. Here $\mathscr{L}_1$ and $\mathscr{L}_2$ are the loss functions defined in Eqn. (3.34a). At Mach 10, setting $n_2 = RT_2 = 1$ as usual, these mean frequencies are: $\bar{K}_{12}(\nu) \doteq 6.8\ \nu$ and $\bar{K}_{21}(\nu) \doteq 1.2(1-\nu)$. The effective average collision frequency at any point in the shock is then $\bar{K}(\nu) = [(1-\nu)n_1 K_{12} + \nu n_2 K_{21}]/n \doteq \frac{3.0\nu(1-\nu)}{n(\nu)}$, using $n_1 = 0.257$. According to the models, however, the same collision frequency per colliding pair, $\bar{K}(T)$, is assigned to both (1-2) and (2-1) collisions, i.e., $\bar{K}_{12} = \nu n_2 \bar{K}(T)$ and $\bar{K}_{21} = (1-\nu)n_1 \bar{K}(T)$. The value of $\bar{K}(T)$ is chosen so that the correct hard sphere viscosity is obtained at local equilibrium, which in turn requires that $\bar{K}(T) = \frac{1}{n^2} \int f^{(0)} \mathscr{L}^{(0)}(\underline{c}) d\underline{c}$, where $\mathscr{L}^{(0)}(\underline{c})$ is the usual loss function defined with local Maxwellian parameters n, u, T. This yields $\bar{K}(T) = 4\sqrt{\pi RT} = 7.1\ \sqrt{RT}$, whence $\bar{K}_{12}(\nu) \doteq 7.1\ \sqrt{RT}\nu$ and $\bar{K}_{21}(\nu) \doteq 1.8\ \sqrt{RT}(1-\nu)$. Averaging as before, we now get $\bar{K}(\nu) \doteq 3.6\ \sqrt{RT}\nu(1-\nu)/n(\nu)$. At the center of the shock we have $\nu = 0.5$, $\sqrt{RT} = 0.94$, and thus we estimate that the model collision frequency is $3.4/(4n)$ while the more exact result is $3.0/(4n)$, which would lead to a model shock thickness $\sim 13\%$ smaller than the correct result.

This result is gratifyingly close to the previous estimate of a 15% effect, though both results are approximate and fall short of the observed 25% effect. Like the previous method, this method also predicts the same qualitative behavior of the correction through the shock: the greatest discrepancies occur downstream where RT is large; in fact the model and exact profiles should have roughly the same scales when $\sqrt{RT}$ falls to $\sim 3.0/3.6$, or $RT \sim 0.7$, which occurs at $\nu \sim 0.2$. This behavior is seen qualitatively in Fig. 8. However, we must add a cautionary remark here: to be more consistent when using the TGF model to predict hard-sphere profiles, we should modify the fitting function $k(\nu)$ of Fig. 2 to match Ψ^{TGF} to the hard-sphere emission function of Eqn. (3.34a) rather than the Maxwell molecule function (3.34). The former has a cold peak only about one-third as pronounced as the latter, leading to smaller $k(\nu)$ values, particularly in the region near $\nu = 0.2$. This case was calculated and shifted the TGF hard-sphere profiles of Fig. 8 approximately half-way toward the BGK hard-sphere profiles, thereby producing a marked dip in the upstream density profile near $\nu = 0.2$. Though this modification applies only to the TGF profiles (i.e., it does not affect the very similar Polynomial $(\lambda_4 = -1)$ profiles), it somewhat weakens our ability to account in detail for all the hard-sphere profile discrepancies using the present simple estimates.

2. The Effect of the Prandtl Number

The splitting into two pairs of all the model results plotted versus ν (Figs. 9-12) seems to be significant. This effect is strongest for the higher moments τ_{xx} and q_x, particularly in combinations such as $H_0/H_{0,1}$, which are sensitive to the relative peak positions of τ_{xx} and

q_x.[†] Because of the sensitivity of these results (particularly Monte Carlo) to calculational inaccuracies, our conclusion must be a tentative one, but it appears that the models split into pairs according to their values of Prandtl number. Of the two pairs, the Polynomial/Ellipsoidal pair with the correct $Pr = 2/3$ always agrees better with the most reliable of the Monte Carlo results (especially those of Deiwert [67]). The TGF/BGK pair with $Pr = 1$ shows higher $|\tau_{xx}|$ values and lower $|q_x|$ values than the first pair, which is the trend expected from the relation $Pr \propto \frac{\mu}{\kappa} \propto |\tau_{xx}|/|q_x|$.

The incorrect value of Pr in the TGF model may also be responsible for the poor agreement with Monte Carlo of the TGF temperature in the region $x/\Lambda_1 \sim 0$ in Fig. 6. As shown by Fig. 9, models with $Pr = 1$ have lower temperatures in this region than models with $Pr = 2/3$. As has already been noted in Section F of Chapter III, a TGF model with a correct value of Pr could be constructed quite easily by modifying the $f_3^{(0)}$ term of Eqn. (3.35) to either the Polynomial, Ellipsoidal, or other suitable form. This would very likely be at the expense of making the eigenvalues λ_i, $i > 3$, depend on ν, but this is not a great complication; such an extension is recommended in Chapter VI.

3. Temperature Overshoot

Although not an important effect, a good deal of interest has been shown (see Chapter I) in the existence or absence of a temperature overshoot in the shock problem. As Holway has shown [68], such an effect is more likely to occur for softer molecular force laws: the contribution of

[†] The quantity $(H_0/H_{1,0}-1)$ is proportional to $(\tau_{xx}u-q_x)$.

a molecule to the temperature depends on the difference of its velocity from the mean flow velocity; thus the farther back upstream that a hot molecule can penetrate, the more likely an overshoot effect. Accurate Monte Carlo results by Hicks [43] and Bird [46,48] show no evidence of overshoot for $r = \infty$ or 12, and the approximate results of Perlmutter [45] show none for $r = 5$. Additional evidence for the absence of overshoot at $r = 5$ is given by the provisional results of Deiwert [67]. This Monte Carlo evidence may not be accurate enough to rule out the existence of small overshoots of the order of 1% in $\hat{T}$. However, Hicks [43] claimed average probable errors of under 1% in his $\hat{T}$ versus density profiles, and he specifically examined $d\hat{T}/dv$ for evidence of overshoot at high Mach number. Deiwert's results [67] had a similarly small statistical scatter, and a least-squares fit performed for $\hat{T}(x)$ was monotonic and did not reach unity within the downstream range studied (25 units of Λ_1 beyond $x = 0$).

The absence of temperature overshoot found in both the TGF and Polynomial ($\lambda_4 = -1$) models therefore lends some further support to their accuracy.

4. The Predicted Departure from Equilibrium

The comparisons of Fig. 12 show that all the models predict the stress ratio $|\tau_{xx}/p|$ very well. As discussed by Liepmann [29], and Baganoff and Nathenson [27], this is an important parameter in determining shock structure. The other sensitive parameter $H_0/H_{0,1}$ is assumed to be unity in the approximate theories of Becker [7] and Baganoff and Nathenson [27]. In Fig. 12 it is seen to reach 1.11 at Mach 10 according to Monte Carlo

results and the Polynomial/Ellipsoidal pair of models, and 1.05 according to the TGF/BGK pair.

These results appear to confirm that the models are capable of describing the departure from equilibrium rather well within the shock.

CHAPTER VI

SUMMARY AND CONCLUSIONS

A. Summary

The structure of strong plane shock waves in a perfect monatomic gas was studied using four nonlinear models of the Boltzmann equation. The models involved the use of a simplified collision operator with velocity-independent collision frequency, in place of the complicated Boltzmann collision operator. The models employed were the BGK and Ellipsoidal models developed by earlier authors, and the Polynomial and Trimodal Gain Function (TGF) models developed during the work. An exact set of moment equations was derived for the density, velocity, temperature, viscous stress, and heat flux within the shock. This set was reduced to a pair of coupled nonlinear integral equations and solved using specially adapted numerical techniques. A new and simple Gauss-Seidel iteration was developed during the work and found to be as efficient as the best earlier iteration methods. Extensive comparisons were made of the model results with Monte Carlo solutions, and significant aspects of the comparisons were discussed.

B. Conclusions

Four main conclusions were drawn from the work:

1. The use of models allows rapid calculations of shock structure, and solutions are obtainable for all Mach numbers above unity. In the most interesting range of high Mach number the models are especially convenient, as a single calculation provides the results for all M except for a scaling quadrature.

2. The model shock profiles, particularly those for the newly developed Polynomial and TGF models, compare extremely well with Maxwell molecule Monte Carlo results but less well for non-Maxwell molecules. This latter deficiency is traced to the assumption of a velocity-independent collision frequency for all the models. A correction for this effect was developed and applied to the hard-sphere model results, greatly improving the agreement with Monte Carlo.
3. Both new models are very adaptable. By two simple parameter choices in the Polynomial model the profiles of both the earlier models can be reproduced, and a third choice gives profiles in very close agreement with Maxwell molecule Monte Carlo results. Alternatively, as shown by the TGF example, improved models can be constructed by incorporating more physical data. In the TGF case, by physically accounting for the bimodal features of the emission function, but otherwise retaining the features of a BGK model, shock profiles greatly superior to the BGK results are obtained.
4. For practical applications, models appear to be of greatest value when used in conjunction with Monte Carlo methods. The relatively expensive Monte Carlo method can provide benchmarks and ideas for improvement for the models, which then can offer reliability, accuracy, and great gains in economy.

C. Possible Extensions

Three possible extensions can be suggested:

1. A relatively simple extension would be the development of a modified TGF model with a Prandtl number of 2/3, as suggested in Section F of Chapter III. This would allow a check to be made on the tentative

conclusion of Chapter V that T, τ_{xx}, and q_x are sensitive to Prandtl number.

2. An extension to problems in more than one space dimension, such as the oblique shock problem. Of particular value here would be a method of extending the fit of the TGF emission function to more than one dimension. Another valuable feature would be a procedure to combine model solutions obtained in the shock zones with simpler hydrodynamic solutions in outer zones.

3. A rigorous extension to models with velocity-dependent collision frequency $K(c)$. This would involve discarding the present formulation in terms of t and the inclusion of more moments than at present, both of which would lead to considerable loss of economy. The extra moments could possibly be dealt with by the method of constitutive relations [27], referred to in Chapter I. More detailed notes on this possible extension are given in Appendix E.

Appendix A

Derivation of the Kernel Functions $\mathcal{K}_n$ and $\mathcal{K}_T$ for the Models

For each model we insert the emission function Ψ into Eqns. (2.21) and perform the c_t integrations using the relation:

$$\int_0^\infty x^{2n+1} e^{-px^2} dx = \frac{n!}{2p^{n+1}} \tag{A.1}$$

The c_x integrations are carried out formally using Eqn. (2.22a) to express $\mathcal{K}_n$ and $\mathcal{K}_T$ in terms of the H_n functions. For this step we use the relation:

$$\int_{-\infty}^{\infty} dt' \int_{-\infty}^{\infty} dc_x F(c_x) \triangleq \int_{-\infty}^{t} dt' \int_0^\infty dc_x F(c_x) + \int_t^\infty dt' \int_{-\infty}^{0} dc_x F(c_x)$$

$$= \int_{-\infty}^{\infty} dt' \int_0^\infty d|c_x| F(c_x) \quad .$$

The integrands of Eqn. (2.21) have the function $F(c_x)$ equal to $\Psi(c_x) \frac{1}{|c_x|} \exp - \frac{|t-t'|}{|c_x|}$, resulting in the form:

$$\int_{-\infty}^{\infty} dt' \int_{-\infty}^{\infty} dc_x F(c_x) = \int_{-\infty}^{\infty} dt' \int_0^\infty \frac{dy}{y} \Psi(y \, \mathrm{sgn}(t-t')) \exp - \frac{|t-t'|}{y}, \tag{A.2}$$

where we have written y for $|c_x|$.

Case 1. BGK Model

For this model $\Psi(\underline{c},m_i) = f^{(0)}(n,u,T) = n(2\pi RT)^{-3/2} \exp - \left[\frac{(c_x-u)^2+c_t^2}{2RT}\right]$.

Write $\sqrt{RT(t')} \equiv r$ and use (2.21) and (A.2):

$$\mathcal{K}_n^{BGK} = \int_0^\infty 2\pi c_t dc_t e^{-c_t^2/2r^2} \int_0^\infty \frac{dy}{(2\pi)^{3/2} r^3 y} \exp - \left[\frac{1}{2}\left(\frac{y \, \mathrm{sgn}(t-t')}{r} - \frac{u(t')}{r}\right)^2 + \frac{|t-t'|}{y}\right],$$

$$\mathcal{K}_T^{BGK} = \int_0^\infty \frac{2}{3R} c_t^3 dc_t \exp(-c_t^2/2r^2) \quad x\{\text{same y integral}\} \quad .$$

C-2

The result follows immediately using (A.1) and (2.22) in the form:

$$H_n(p,\frac{q}{r}) = \frac{r^{1-n}}{\sqrt{2\pi}} \int_0^\infty y^{n-2} \exp-\left[\frac{1}{2}\left(\frac{y}{r} - p\right)^2 + \frac{q}{y}\right] dy \quad .$$

We obtain:

$$\mathcal{K}_n^{BGK} = \frac{1}{r} H_1\left(\frac{u(t')\mathrm{sgn}(t-t')}{r}, \left|\frac{t-t'}{r}\right|\right)$$

$$\mathcal{K}_T^{BGK} = \frac{2r^2}{3R} \cdot \mathcal{K}_n^{BGK} \quad .$$

Case 2. Ellipsoidal Model

For this model, $\Psi(\underline{c},m_i) = n(2\pi R)^{-3/2} T_t^{-1} T_x^{-1/2} \exp-\left[\frac{(c_x-u)^2}{2RT_x} + \frac{c_t^2}{2RT_t}\right]$

Write: $\sqrt{RT_x(t')} \equiv r_x$ and: $\sqrt{RT_t(t')} \equiv r_t$, and follow an essentially identical procedure as for the BGK model to obtain:

$$\mathcal{K}_n^{ELL} = \frac{1}{r_x} H_1\left(\frac{u(t')\mathrm{sgn}(t-t')}{r_x}, \left|\frac{t-t'}{r_x}\right|\right) .$$

$$\mathcal{K}_T^{ELL} = \frac{2r_t^2}{3R} \cdot \mathcal{K}_n^{ELL} \quad .$$

Case 3. Polynomial Model

For this model, $\Psi(\underline{c},m_i) = f^{(0)}(n,u,T)\cdot\{1+\eta_1\tau_{xx}\beta^2(c_x^2-\frac{1}{3}C^2)+\eta_2 q_x\beta^2 C_x \cdot (\frac{5}{2} - \beta C^2)\}$, with $\beta = 1/2RT$ and: $\underline{C} \equiv \underline{c} - u\underline{i}$.

The constants η_1 and η_2 are abbreviations for $2(1+\lambda_4)$ and $-\frac{8}{5}(1+\lambda_5)$, respectively. Writing $\sqrt{RT(t')} \equiv r$, we obtain first:

$$\Psi(c_x,c_t) = f^{(0)}(n,u,T)\{1 + \frac{\eta_1\tau_{xx}}{4r^4} \cdot \frac{1}{3}(2c_x^2 - 4uc_x + 2u^2 - c_t^2) + \frac{\eta_2 q_x}{8r^6} \cdot (-c_x^3 + 3uc_x^2 + c_x[5RT-3u^2-c_t^2] + u[-5RT+u^2+c_t^2])\} .$$

Again, following the procedure outlined above, and writing $\sigma \triangleq \text{sgn}(t-t')$ and understanding that u stands for $u(t')$, we obtain the kernels:

$$\mathcal{K}_n^{POL} = \frac{1}{r}\{H_1 + \frac{\eta_1\tau_{xx}}{6r^2}[H_3 - \frac{2\sigma u}{r}H_2 + \left(\frac{u^2}{r^2} - 1\right)H_1] + \frac{\eta_2 q_x}{8r^3}[-\sigma H_4 + \frac{3u}{r}H_3 - 3\sigma\left(\frac{u^2}{r^2} - 1\right)H_2 + \frac{u}{r}\left(\frac{u^2}{r^2} - 3\right)H_1]\}$$

$$\mathcal{K}_T^{POL} = \frac{2r}{3R}\{H_1 + \frac{\eta_1\tau_{xx}}{6r^2}[H_3 - \frac{2\sigma u}{r}H_2 + \left(\frac{u^2}{r^2} - 2\right)H_1] + \frac{\eta_2 q_x}{8r^3}[-\sigma H_4 + \frac{3u}{r}H_3 - \sigma\left(\frac{3u^2}{r^2} - 1\right)H_2 + \frac{u}{r}\left(\frac{u^2}{r^2} - 1\right)H_1]\}$$

The arguments of all H_n functions for the Polynomial Model are the same as for the BGK model.

Case 4. The TGF Model

For this model, $\Psi(\underline{c},m_i) = k(\nu)\cdot\left[(1-\nu)f_1^{(0)}+\nu f_2^{(0)}\right]+(1-k(\nu))f_3^{(0)}(n,u,T_3)$. Write:

$$\sqrt{RT_1} \equiv r_1 \ ,$$

$$\sqrt{RT_2} \equiv r_2 \ ,$$

$$\sqrt{RT_3(t')} \equiv r_3 \ ,$$

and:

$$a_1 \equiv (1-\nu)k(\nu) \ ,$$

$$a_2 \equiv \nu k(\nu) \ ,$$

$$a_3 \equiv 1 - k(\nu) \ .$$

Each Maxwellian function $f_i^{(0)}$, $i = 1,2,3$, leads to a BGK-type kernel contribution. Thus the TGF kernels can be written down simply by reference to the BGK case:

$$\mathcal{K}_n^{TGF} = \frac{a_1}{r_1} H_1\left(\frac{u_1\sigma}{r_1}, \frac{|t-t'|}{r_1}\right) + \frac{a_2}{r_2} H_1\left(\frac{u_2\sigma}{r_2}, \frac{|t-t'|}{r_2}\right) + \frac{a_3}{r_3} H_1\left(\frac{u(t')\sigma}{r_3}, \frac{|t-t'|}{r_3}\right)$$

$$\mathcal{K}_T^{TGF} = \frac{2a_1r_1}{3R} H_1\left(\frac{u_1\sigma}{r_1}, \frac{|t-t'|}{r_1}\right) + \frac{2a_2r_2}{3R} H_1\left(\frac{u_2\sigma}{r_2}, \frac{|t-t'|}{r_2}\right) + \frac{2a_3r_3}{3R} H_1\left(\frac{u(t')\sigma}{r_3}, \frac{|t-t'|}{r_3}\right) .$$

Appendix B

Evaluation of the Bimodal Gain and Loss Operators for Quasi-Maxwell Molecules

We follow the treatment and notation of Deshpande and Narasimha [62] (DN), making modifications where necessary to substitute a quasi-Maxwell force law for their hard-sphere law. Their procedure applies to both cases up to and including their equation (2.12), which is:

$$\mathcal{J}_{ij} = \frac{8\pi^2}{\beta_i^2} F_i F_j \int dg\, bdb \exp(-\gamma^2 g^2) \cdot \cdot \sum_{m=0}^{\infty} \{ i_m(2\chi g) g^{\rho-1} \cdot \frac{B^{2m}}{m!\chi^m} \cdot {}_2F_1(-m,-m;1;\Psi) \} \quad , \tag{B.1}$$

where ${}_2F_1$ is the hypergeometric function, i_m is a Bessel function defined for all integers m by:

$$i_m(z) \triangleq \frac{\sqrt{\pi}}{2} (z/2)^{-1/2} I_{m+1/2}(z) \quad , \tag{B.1a}$$

and with:

$$\gamma^2 \triangleq \cos^2\psi + \beta_{ji}\sin^2\psi \; ; \quad \beta_{ji} \triangleq \beta_j/\beta_i \; ;$$

$$\chi \triangleq C\cos^2\psi + \beta_{ji}c_j\cos\alpha \; ; \; \underline{C} \triangleq \underline{c}_i - \beta_{ji}\underline{c}_j \; ; \; \underline{c}_i \triangleq \underline{c} - \underline{u}_i \; ;$$

$$\Psi \triangleq (C \sin 2\alpha/2B)^2 \; ; \quad B \triangleq \beta_{ji}c_j \sin\alpha \; ;$$

$$F_i \triangleq f^{(0)}(n_i, \underline{u}_i, T_i) \; ; \quad \alpha \triangleq \text{angle between } \underline{C} \text{ and } \underline{c}_j \; .$$

However, instead of now making the hard-sphere assumption, $b = \sigma \sin\psi$, we make the quasi-Maxwell substitution:

$$b = \frac{\beta_i^{1/2}}{g} \sigma \sin\psi \quad , \tag{B.2}$$

remembering that all velocities including g in DN have been non-dimensionalized with respect to $\beta_i^{-1/2}$.

We now make use of the corrected[†] relation:

$$\int g^{\rho-1}\exp(-\gamma^2 g^2) i_m(\alpha g)\,dg = \frac{\sqrt{\pi}}{4}\left(\frac{\alpha}{2\gamma}\right)^m \gamma^{-\rho}\,\frac{\Gamma\left(\frac{m+\rho}{2}\right)}{\Gamma(m+3/2)} \cdot \Phi\left(\frac{m+\rho}{2};\ m+3/2;\ (\alpha/2\gamma)^2\right) \quad . \tag{B.3}$$

Here Φ is the confluent hypergeometric function.

We first perform the g integral in (B.1), noting that the value of ρ in the quasi-Maxwell case becomes $(m+3)$ rather than $(m+4)$ for hard spheres. Thus instead of the hard-sphere result of DN:

$$\frac{\sqrt{\pi}}{4}\left(\frac{\chi}{\gamma^2}\right)^m \gamma^{-4}\,\frac{\Gamma(m+2)}{\Gamma(m+3/2)} \cdot \Phi(m+2;\ m+3/2;\ \chi^2/\gamma^2) \quad ,$$

we get the result[††]:

$$\beta_i^{1/2}\,\frac{\sqrt{\pi}}{4}\left(\frac{\chi}{\gamma^2}\right)^m \gamma^{-3}\exp(\chi^2/\gamma^2) \tag{B.4}$$

for the g integral in (B.1).

Now use of the identity quoted in DN:

$${}_2F_1(-m;-m;1;\Psi) = \frac{1}{2\pi}\int_0^{2\pi} (1 + \Psi + 2\Psi^{1/2}\cos\theta)^m d\theta \quad ,$$

together with the summation formula:

$$\frac{\Gamma(a)}{\Gamma(b)}\,\Phi(a;b;x+y) = \sum_{m=0}^{\infty} \frac{\Gamma(m+a)}{\Gamma(m+b)}\,\frac{y^m}{m!}\,\Phi(m+a;m+b;x)$$

[†] The proof of the corrected version that we use is given in the Addendum to this Appendix.

[††] Note that $\Phi(a,a,z) = \exp(z)$.

allows Eqn. (B.1) to be transformed to:

$$\mathcal{G}_{ij}^{MM} = \left(\frac{\pi}{\beta_i}\right)^{3/2} \sigma^2 F_i F_j \int \gamma^{-3} \sin 2\psi d\psi \int_0^{\pi} \exp(A'(\theta,\psi)) d\theta \quad , (B.5)$$

instead of the hard-sphere result of DN:

$$\mathcal{G}_{ij} = 2\pi\beta_i^{-2}\sigma^2 F_i F_j \int \gamma^{-4} \sin 2\psi d\psi \int_0^{\pi} \Phi(2,\tfrac{3}{2},A'(\theta,\psi)) d\theta \quad ,$$

with:

$$A'(\theta,\psi) \triangleq [\chi + B^2(1 + \Psi + \Psi^{1/2}\cos\theta)]/\gamma^2 \quad .$$

We now apply the ζ-transformation, equation (2.14) in DN:

$$\zeta = (1+\beta_{ji}\tan^2\psi)^{-1} = \frac{\cos^2\psi}{\gamma^2} = 1 - \frac{\beta_{ji}\sin^2\psi}{\gamma^2} \quad ,$$

$$d\zeta = -\beta_{ji}\gamma^{-4}\sin 2\psi d\psi \quad .$$

In the present case we find an extra factor of $\gamma = \left[\zeta + \frac{(1-\zeta)}{\beta_{ji}}\right]^{-1/2}$

in the expression, compared to the hard-sphere case; we obtain:

$$\mathcal{G}_{ij}^{MM} = \frac{\sqrt{\pi}}{2}\beta_i^{1/2}\frac{2\pi\sigma^2 F_i F_j}{\beta_i\beta_j}\int_0^{\pi} d\theta \int_0^{1} d\zeta \left[\zeta + \frac{(1-\zeta)}{\beta_{ji}}\right]^{-1} \exp(A(\theta,\zeta)) \quad , (B.6)$$

with:

$$A(\theta,\zeta) \triangleq \zeta\mathcal{E}_i^2 + (1-\zeta)\mathcal{E}_j^2 + 2\zeta^{1/2}(1-\zeta)^{1/2}|\underline{\mathcal{E}}_i \times \underline{\mathcal{E}}_j|\cos\theta \quad .$$

The transformations of DN's Appendix can now be applied, with the same arguments leading to the conclusion that only the $n = 0$ term of the spherical harmonic decomposition of $\exp(Q + R\cos\theta)$ will survive. Thus in our case:

$$\int_0^{\pi} \exp(Q + R\cos\theta)d\theta \;\rightarrow\; \pi i_0(R)\exp Q$$

$$= \pi\, e^{Q}\,\frac{\sinh R}{R} \quad ,$$

and the ζ-integral in Eqn. (B.6) can be easily performed:

$$\int_0^1 \left[\zeta + \frac{(1-\zeta)}{\beta_{ji}}\right]^{-1/2} d\zeta \;=\; \frac{2\beta_{ji}^{1/2}}{(\beta_{ji}-1)}\,(\beta_{ji}^{1/2}-1) \;=\; 2\beta_{ji}^{1/2}/(1+\beta_{ji}^{1/2}) \quad .$$

Thus we find:

$$\mathcal{G}_{ij}^{MM} \;=\; \frac{2\pi^{5/2}\sigma^2 F_i F_j}{(\beta_i\beta_j)^{1/2}(\beta_i^{1/2}+\beta_j^{1/2})}\, e^{Q}\,\frac{\sinh R}{R} \quad , \qquad (B.7)$$

and, letting i tend to j, $\mathcal{G}_{ii} \rightarrow F_i\mathcal{L}_i$, $R \rightarrow 0$ and $Q \rightarrow \zeta_i^2$, we also find:

$$\mathcal{L}_i^{MM} \;=\; 2\pi\sigma^2 n_i \quad . \qquad (B.8)$$

Addendum: Proof of the corrected relation (B.3):

Gradshteyn and Ryzhik (GR), p. 720, Eqn. 6.643, No. 2, give the integral:

$$\int_0^{\infty} x^{\mu-1/2}\, e^{-\alpha x} I_{2\nu}(2\beta\sqrt{x})dx \;=\; \frac{\Gamma(\mu+\nu+\frac{1}{2})e^{\beta^2/2\alpha}}{\Gamma(2\nu+1)\beta}\,\alpha^{-\mu} M_{-\mu,\nu}(\beta^2/\alpha) \quad . \qquad (B.9)$$

The left-hand side can be transformed using $x = y^2$ to:

$$2\int_0^{\infty} y^{2\mu} e^{-\alpha y^2} I_{2\nu}(2\beta y)dy \;\triangleq\; 4\left(\frac{\beta}{\pi}\right)^{1/2} \int_0^{\infty} y^{2\mu+1/2} e^{-\alpha y^2} i_{2\nu-1/2}(2\beta y)dy \quad , \qquad (B.9a)$$

using DN's definition of i_m given in Eqn. (B.1a).

The right-hand side contains the Whittaker function $M_{-\mu,\nu}$, which obeys the relation (GR, p. 1059):

$$M_{-\mu,\nu}(z) \;=\; z^{\nu+1/2}\, e^{-z/2}\Phi(\nu+\mu+\tfrac{1}{2};2\nu+1;z) \quad .$$

Thus the right-hand side of Eqn. (B.9) can be written:

$$\frac{\Gamma(\mu+\nu+\frac{1}{2})}{\Gamma(2\nu+1)}\,\beta^{2\nu}\alpha^{-(\mu+\nu+1/2)}\Phi(\mu+\nu+1/2;2\nu+1;\beta^2/\alpha) \quad . \qquad \text{(B.9b)}$$

Now set

$$\alpha \rightarrow \gamma^2 \quad ,$$

$$\beta \rightarrow \alpha/2 \quad ,$$

$$\nu \rightarrow \frac{1}{2}(m + \frac{1}{2}) \quad ,$$

$$\mu \rightarrow \frac{1}{2}(\rho - \frac{3}{2}) \quad ,$$

i.e.,

$$(\mu + \nu + \frac{1}{2}) \rightarrow \frac{1}{2}(m + \rho) \quad ,$$

$$(2\nu + 1) \rightarrow m + \frac{3}{2} \quad .$$

With these substitutions, by Eqns. (B.9a) and (B.9b) we get our relation (B.3):

$$\int_0^\infty y^{\rho-1}e^{-\gamma^2y^2}i_m(\alpha y)dy = (\frac{\pi}{8})^{1/2}(\frac{\alpha}{2\gamma})^{m+\frac{1}{2}}\left\{\alpha^{-\frac{1}{2}}\gamma^{\frac{1}{2}-\rho}\right\}\frac{\Gamma(\frac{m+\rho}{2})}{\Gamma(m+3/2)}\cdot\Phi\left(\frac{m+\rho}{2};m+\frac{3}{2};(\frac{\alpha}{2\gamma})^2\right)$$

$$= \frac{\sqrt{\pi}}{4}(\frac{\alpha}{2\gamma})^m\gamma^{-\rho}\,\frac{\Gamma(\frac{m+\rho}{2})}{\Gamma(m+\frac{3}{2})}\cdot\Phi\left(\frac{m+\rho}{2};m+\frac{3}{2};(\frac{\alpha}{2\gamma})^2\right) \quad .$$

In Deshpande and Narasimha, the first version of this result is given incorrectly as Eqn. (2.13), in which the expression in curly brackets above is replaced by $\gamma^{-1/2}$. This appears to be only a misprint, as DN's later results are correct.

Appendix C

Outline of the Mott-Smith Method

The Boltzmann equation and the associated boundary conditions for the plane shock problem are given in Eqns. (2.1-13). The solution involves evaluation of the molecular distribution function $f(\underline{c},x)$ defined in (2.1). Mott-Smith [14] proposed a simple ansatz for f, namely:

$$f(\underline{c},x) \doteq f^{(0)}(n_\alpha(x),u_\alpha,T_\alpha) + f^{(0)}(n_\beta(x),u_\beta,T_\beta) \quad , \qquad (C.1)$$

where $f^{(0)}$ is the Maxwellian function defined by (2.2a) and the parameters u_α, u_β, T_α, T_β are independent of position x.

All the six unknown parameters are to be found by enforcing as many moment equations of (2.1) as may be required. Initial use of the moments m_i, $i = 1$ to 3 of (2.15), for which the collision contribution vanishes, leads to the Rankine-Hugoniot relations (2.5-7) and the results that:

(a) The fixed parameters u_α, u_β, T_α, T_β reduce to the endpoint parameters u_1,u_2,T_1,T_2 of (2.13).

(b) Only one of the space-dependent parameters $n_\alpha(x)$ and $n_\beta(x)$ is independent.

Thus the Mott-Smith ansatz reduces in effect to:

$$f(\underline{c},x) \triangleq f_{MS} \doteq (1-\nu(x))f_1^{(0)} + \nu(x)f_2^{(0)} \quad , \qquad (C.2)$$

with $\nu(x)$ still to be determined and $f_1^{(0)}$ and $f_2^{(0)}$ being the endpoint Maxwellian functions defined by (2.1a). The relations between Mott-Smith's parameters n_α and n_β and our own parameter ν can be written:

$$\left.\begin{aligned} n_\alpha(x) &= (1-\nu(x))n_1 \quad , \\ n_\beta(x) &= \nu(x)n_2 \quad , \\ \nu(x) &= \frac{n_\alpha(x)+n_\beta(x)-n_1}{n_2-n_1} = \frac{n_{MS}(x)-n_1}{n_2-n_1} \quad . \end{aligned}\right\} \tag{C.3}$$

As soon as $\nu(x)$ is determined, the Mott-Smith approximate solution f_{MS} is known and all the moments m_i may be calculated: those defined by (2.15) can be written as:

$$n_{MS} = n_\alpha + n_\beta \quad , \tag{C.4a}$$

$$n_{MS}u_{MS} = n_\alpha u_1 + n_\beta u_2 \quad , \tag{C.4b}$$

$$n_{MS} \cdot 3RT_{MS} = n_\alpha(u_1^2+3RT_1) + n_\beta(u_2^2+3RT_2) - n_{MS}u_{MS}^2 \quad , \tag{C.4c}$$

$$n_{MS} \cdot \frac{3}{2}\tau_{MS} = n_\alpha(u_1-u_{MS})^2 + n_\beta(u_2-u_{MS})^2 \quad , \tag{C.4d}$$

$$\begin{aligned} n_{MS} \cdot 2q_{MS} = {} & n_\alpha(u_1-u_{MS})[5R(T_{MS}-T_1) - (u_1-u_{MS})^2] \\ & + n_\beta(u_2-u_{MS})[5R(T_{MS}-T_2) - (u_2-u_{MS})^2] \quad . \end{aligned} \tag{C.4e}$$

All the results so far apply without regard to the detailed form of the collision term in the Boltzmann equation. The solution for $\nu(x)$, however, requires the solution of one moment equation for which the collision term is nonzero, and thus a collision law must now be assumed. The solution for $\nu(x)$ was found by Mott-Smith to be:

$$1 - \nu(x) = \left[1 + e^{Bx/\Lambda_1}\right]^{-1} \quad , \tag{C.5}$$

with $\Lambda_1 \triangleq$ upstream mean free path, where the quantity B depends both on the assumed collision law and on which moment equation is selected to

be satisfied. Mott-Smith gave results for B for hard sphere and Sutherland molecules, and for both the c_x^2 and c_x^3 moments. Other authors have looked at the general set of moments c_x^n for a wide range of n values [15], and at Maxwell and Lennard-Jones molecules [16].

The quantity B is obtained as follows. The c_x^n moment of the Boltzmann equation with the Mott-Smith ansatz can be written as:

$$\frac{d}{dx}\int d\underline{c}\; c_x^{n+1}\left\{(1-\nu(x))f_1^{(0)} + \nu(x)f_2^{(0)}\right\} \tag{C.6}$$
$$= \nu(x)\cdot(1-\nu(x))\int d\underline{c}\int d\underline{c}_1\int gbdbd\varepsilon(c_x'^n+c_{x_1}'^n-c_x^n-c_{x_1}^n)f_1^{(0)}(\underline{c})f_2^{(0)}(\underline{c}_1)\quad .$$

Using the Rankine-Hugoniot relations to express the endpoint parameters in terms of the upstream conditions, Eqn. (C.6) becomes, after cancellations:

$$\frac{d\nu(x)}{dx} = \nu(1-\nu)\cdot f(M)\cdot I\quad , \tag{C.7}$$

where $f(M)$ is a complicated function of the Mach number M only, and the quantity I is a definite integral[†] proportional to $T_1^{-1/2}n_1\phi^{(2)}(T_1^{1/2})$, where:

$$\phi^{(2)}(g) = \left(\frac{2\kappa}{m}\right)^{2/(r-1)}A_2(r)g^{(r-5)/(r-1)}\quad , \tag{C.8}$$

assuming point molecules with repulsion force κ/d^r at a separation distance d.

We now follow the approach of Muckenfuss [16]. A generalized mean free path Λ_1 is defined, analogously to the hard-sphere definition (5.1) but valid for all values of r:

$$\Lambda_1^{-1} \triangleq h\rho_1\bar{c}_1/\mu_1\quad ,\quad \text{c.f. (5.1)}\quad ;\quad h = \frac{5\pi}{32} \doteq 1/2\quad ,$$

[†] The quantity $f(M)\cdot I$ is written as $(4/X)$ by Muckenfuss in Ref. 16, and X is defined by his Eqns. 9 and 10.

which can be generalized to:

$$\Lambda_1^{-1} \triangleq n_1 \Omega^{(22)} \Big/ \sqrt{\frac{2RT_1}{\pi}} \quad , \tag{C.9}$$

with:

$$\Omega^{(22)} \triangleq \sqrt{\pi} \int_0^\infty z^6 e^{-z^2} \phi^{(2)}(2\sqrt{RT_1}\, z)\, dz \quad .$$

Because Λ_1^{-1} has exactly the same dependence upon n, T, κ and r as the integral I, the adoption of Λ_1 as a scale factor eliminates the dependence of all Mott-Smith solutions for point repulsion molecules upon κ and the thermodynamic state ahead of the shock. The results depend only on the Mach number M and a constant determined by r. (The moment c_x^n selected will also affect the results, but we henceforth restrict ourselves to the c_x^2 moment.) Equation (C.7) becomes:

$$\frac{d\nu(x)}{dx/\Lambda_1} = B(M,r) \cdot \nu(1-\nu) \quad , \tag{C.10}$$

which leads to the solution (C.5) already quoted above.

Appendix D

Correction for the Use of a Velocity-Independent Collision Frequency

We wish to derive an approximate correction for the effect of replacing the collision frequency $K(c)$ by $K(n,T)$ in our models. We shall do this here by applying the Mott-Smith method, outlined in the previous appendix, to the unmodeled equations and then to the models. We will treat the general case of molecules which are point centers of repulsion, and for this purpose will adopt the formulation of Muckenfuss [16] already discussed in Appendix C. Here, the normalizing mean free path Λ_1 is defined (ahead of the shock) in a consistent way for all values of the repulsion index r. This definition of Λ_1 via the upstream viscosity is entirely consistent with our own model formulation.

We adopt the notation of Appendix C, except that instead of $\nu(x)$ we choose $\chi(x) = \frac{1-\nu(x)}{n(x)/n_1}$ as the independent variable. This allows the temperature to be written conveniently as:

$$T(x)/T_1 = a + b\chi + c\chi^2 \quad , \tag{D.1}$$

with:

$$a = (5M^2-1)(M^2+3)/16M^2 \triangleq T_2/T_1$$

$$b = -(M^2-1)/2M^2$$

$$c = -5(M^2-1)^2/16M^2 \quad .$$

In the standard Mott-Smith theory, as shown by Muckenfuss [16], the quantity $\chi(x)$ obeys the ordinary differential equation:

$$\frac{d\chi(x)}{dx/\Lambda_1} = -B(M,r) \cdot \chi(1-\chi) \quad , \tag{D.2}$$

where the quantity B is given as $\Lambda_1/X \triangleq B/4$ in Figure 1 of Reference 16, as a function of Mach number M and force law exponent r.

For the models considered in this work, the approximation is made that K is independent of c but nevertheless has a dependence on local temperature T consistent with the local variation of viscosity with temperature, via the assumed relations: $\overline{K}(T) \sim \overline{c}/\overline{\Lambda}(T) \sim \frac{1}{2}\rho\overline{c}^2/\mu(T)$. Within the Mott-Smith formulation this corresponds to replacing the expression (C.8) for $\phi^{(2)}(g)$ by a quantity independent of g but proportional to $T^{-(r-5)/2(r-1)}$. Following through the use of $\phi^{(2)}$ in Eqns. (C.7) and (C.9) of the Mott-Smith formulation, it is easily seen that this results in the replacement of the quantity $B(M,r)$ in (C.10) and (D.2) by the quantity $B(M,5) \cdot (T/T_1)^{(r-5)/2(r-1)}$.

We will now confine ourselves to the case of hard spheres, for which the $K(c)$ effect is most pronounced. Equation (D.2) becomes:

$$\begin{aligned} \frac{d\chi(x)}{dx/\Lambda_1} &= -B(M,5)\left(\frac{T}{T_1}\right)^{1/2}\chi(1-\chi) \\ &= -B(M,5)(a+b\chi+c\chi^2)^{1/2}\chi(1-\chi) \quad , \end{aligned} \tag{D.3}$$

where we have used Eqn. (D.1) in the second line.

The solutions of both the standard (D.2) and modeled (D.3) Mott-Smith equations for $\chi(x)$ can be found analytically, choosing the origins in both cases at the point $\nu(0) = 1/2$ as usual:

Standard Hard Spheres: (H.S.)
$$\frac{x+x_0}{\Lambda_1} = \frac{1}{B(M,\infty)}\ln\left(\frac{1-\chi}{\chi}\right) \quad . \tag{D.2a}$$

Modeled Hard Spheres: (M.H.S.)
$$\begin{aligned} \frac{x+x_0}{\Lambda_1} = \frac{1}{\sqrt{a}B(M,5)}\Bigg\{&\ln\left(\frac{a+\frac{b}{2}\chi+a^{1/2}(a+b\chi+c\chi^2)^{1/2}}{\chi}\right) \\ &-\sqrt{a}\ln\left(\frac{1+(a+b\chi+c\chi^2)^{1/2}}{1-\chi}-\frac{b}{2}-c\right)\Bigg\} \quad . \end{aligned} \tag{D.2b}$$

In each case the quantity x_0/Λ_1 equals the respective RHS evaluated at $\chi_0 = 1/(1+\zeta)$, which corresponds to the point $\nu_0 = 1/2$. Here $\zeta \triangleq n_2/n_1 = 4M^2/(M^2+3)$.

In both cases the quantity χ falls from the value 1 at $x = -\infty$ to the value 0 at $x = +\infty$. Simple algebra shows that the point where the density slope (dn/dx) is maximum occurs at the origin χ_0 in the standard case. The modeled case is not so simple, leading to a quartic equation for the point of maximum slope, but for the case of large M which is of interest we can obtain the approximate point as $\chi_0^* = 1/(1+\zeta-b/2a)$. Using the conventional Prandtl definition of shock thickness, X:

$$X/\Lambda_1 \triangleq (n_2-n_1)/(dn/dx)_{max} ,$$

we then easily find that for large M the shock thicknesses for the two cases lie in the approximate ratio:

$$\frac{(X/\Lambda_1)_{MHS}}{(X/\Lambda_1)_{HS}} \doteq \frac{B(M,\infty)}{\sqrt{a}B(M,5)} . \qquad (D.4)$$

For large M, $a \to 5M^2/16$ and Muckenfuss [16] shows that the B values tend, respectively, to 0.4685 for $r = \infty$ and 0.9889/M for $r = 5$. Thus we see that Eqn. (D.4) predicts a limiting ratio of 0.847 for the two thicknesses, i.e., a model thickness approximately 15% less than the correct value.

More exact calculations for the particular case of $M = 10$ have been performed, using Eqns. (D.2a-b). The respective density profiles are presented in Fig. 13 and show a hard-sphere thickness of 2.134, a modeled hard-sphere thickness of 1.824, and the ratio equal to 0.854. Using these results, a correction for the TGF density profile of Fig. 8

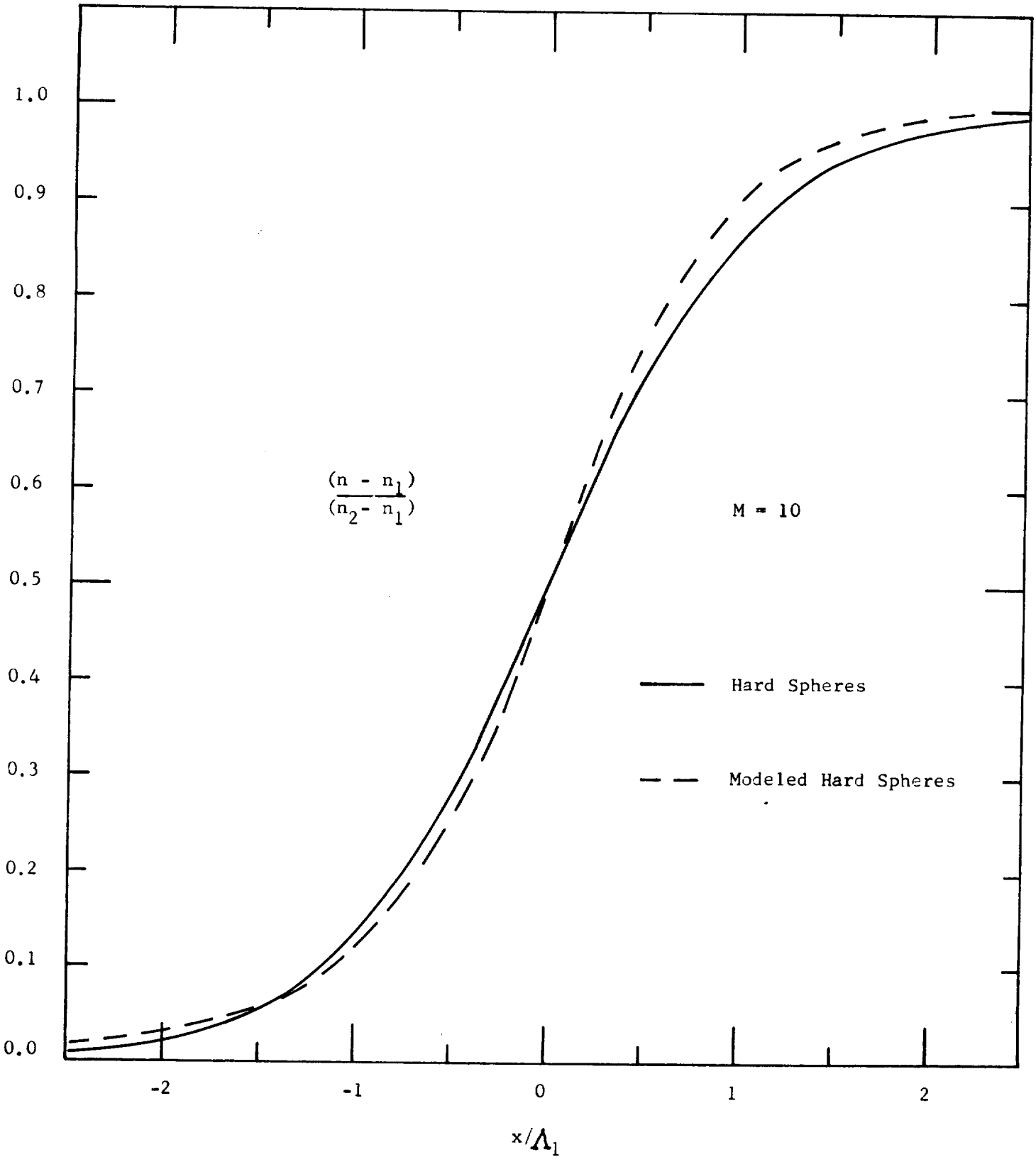

Figure 13: Mott-Smith Reduced Density Profiles vs. x/Λ_1 for Hard Sphere and Modeled Hard Sphere Molecules

has been evaluated as follows: at all ν values in Fig. 8 the x/Λ_1 scale of the TGF profile is increased in the ratio $\left(\frac{x}{\Lambda_1}\right)_{HS}/\left(\frac{x}{\Lambda_1}\right)_{MHS}$ measured in Fig. 13 at the χ value corresponding to ν. The corrected TGF profile is in greatly improved agreement with the Monte Carlo hard-sphere result, which appears to confirm the essential correctness of the present estimate.

Appendix E

Notes on Extending the Method to Allow a Velocity-Dependent Collision Frequency

The following notes outline the steps necessary to extend the present method to incorporate a velocity-dependent collision frequency. This is done here without proposing any detailed new models; we use simple yet realistic examples which point out the major sources of difficulty.

If we retain $K = K(\underline{c})$, we must make the following modifications to the treatment of Chapter II. The use of the t variable of Eqn. (2.16) must be abandoned and Eqn. (2.17) becomes:

$$c_x \frac{\partial f(\underline{c},x)}{\partial x} = K(\underline{c},x)\ \{\Psi(\underline{c},x) - f(\underline{c},x)\} \quad . \tag{E.1}$$

After formal integration in x, and taking moments with $\phi_i(\underline{c})$, we obtain the new form for Eqn. (2.19):

$$m_i(x) = \iiint d\underline{c} \int_{-\infty}^{\infty} dx' \phi_i(\underline{c}) \frac{K(\underline{c},x')\Psi(\underline{c},x')}{|c_x|} \exp - \left| \int_x^{x'} \frac{K(\underline{c},x'')dx''}{c_x} \right| . \tag{E.2}$$

We will restrict ourselves for this discussion to a BGK type of model with emission function:

$$\Psi(\underline{c},x) = f^{(0)} \triangleq N(x) \exp - [(c_x-u)^2+c_t^2]/2RT \quad , \tag{E.3}$$

where we have written for convenience $N(x) \triangleq n/(2\pi RT)^{3/2}$.

We note that the conservation relations now take the form:

$$0 = \iiint [Kf-K\Psi]\ \{\psi_i\} d\underline{c} \quad , \qquad i = 1 \text{ to } 5 \quad , \tag{E.4}$$

where $\{\psi_i\}$ are the collisional invariants $\{1,\underline{c},c^2\}$. In order to satisfy Eqns. (E.4) with the choice (E.3) for Ψ, our choice for K must contain

P suitable adjustable parameters $p_i(x)$, i = 1 to P; in general P = 5 but we confine ourselves to one space dimension, for which P = 3. Thus we can write:

$$K = K(c_x, c_t; p_i(x) \quad , \quad i = 1 \text{ to } 3) \quad . \tag{E.5}$$

Using Eqns. (E.3) and (E.5) in (E.2), with a suitable choice of $\phi_i(\underline{c})$ functions, we obtain a set of moment equations like (2.21):

$$m_i(x) = \int_{-\infty}^{\infty} N(x') \mathcal{K}_i(x,x') dx' \quad , \quad i = 1 \text{ to } M \quad , \tag{E.6}$$

with:

$$\mathcal{K}_i(x,x') = \int_0^{\infty} 2\pi c_t^{\ell+1} e^{-c_t^2/2RT} dc_t \int_{-\infty}^{\infty} c_x^m e^{-(c_x-u)^2/2RT} \frac{K(c_x,c_t,p_i(x'))}{|c_x|}$$

$$\cdot \exp - \left| \int_x^{x'} \frac{K(c_x,c_t,p_i(x''))dx''}{c_x} \right| \cdot dc_x \quad ,$$

and ℓ and m are integers determined by $\phi_i(\underline{c})$.

By comparing the kernels of the moment equations (E.6) with those of (2.21), we can see that three main sources of difficulty have now been added:

1. Instead of the kernels depending only on $|x-x'|$ and local quantities at x', they now contain integrals over the range x to x' which will require numerical quadrature for evaluation.
2. For all choices of $K(c_x,c_t)$, except for the trivial cases $K \sim \underline{C}$ or $K \sim C_x$, the conservation relations (E.4) for the p_i will involve moments of f outside the set m_i, i = 1 to 5 given in Eqn. (2.15). Thus more than two moment equations will have to be retained for solution, i.e., M in Eqn. (E.6) will be 3 or more.

3. Previously the c_t integration within the kernels was made analytically and the c_x integration led to the convenient H_n functions, as shown in Appendix A. For most physically interesting choices of $K(c_x,c_t)$ neither of these simplifications will hold, requiring additional numerical quadratures for the kernel evaluation.

In practice we would like to choose K to model the hard sphere loss function $\mathcal{L}^{(0)}$ (i.e., Eqn. (3.34a) defined with local Maxwellian parameters n, u, and T), or some similar function. For such a choice, all of difficulties 1 to 3 will hold, leading to a very expensive numerical calculation. Even a K of the form $a + b|C|$,† which models $\mathcal{L}^{(0)}$ very well at high $|C|$, will not lead to any simplifications. If simpler choices are made for K we can partly overcome difficulty # 3 as follows:

1. $K \sim a + bC^2$.

   This is a good model for $\mathcal{L}^{(0)}$ at low values of $|C|$, and it allows the c_t integration to be performed analytically; this is of the form:

$$\int_0^\infty c_t^{\ell+1} \exp-(b/|c_x| + 1/2RT)c_t^2 \cdot dc_t \sim (b/|c_x| + 1/2RT)^{-(1+\frac{\ell}{2})} .$$

   However, as this cannot be expressed as a polynomial in $|c_x|$, the integration over c_x will not lead to H_n functions.

2. $K \sim a + bC_x^2$, or $K \sim a + bc_x$.

   These forms both lead to kernels expressible in terms of H_n functions, but neither is a very good model for $\mathcal{L}^{(0)}$.

† Here a and b are independent of $\underline{c}$.

References

1. S. Earnshaw, Phil. Trans., 150, 133 (1858).
2. E. E. Stokes, Phil. Mag., 3, 23, 349 (1848).
3. W. J. M. Rankine, Phil. Trans., 160, 277 (1870).
4. A. Hugoniot, J. Ecole Polytechnique, 58 (1889).
5. Lord Rayleigh, Proc. Roy. Soc., A84, 247 (1910).
6. G. I. Taylor, Proc. Roy. Soc., A84, 371 (1910).
7. R. Becker, Z. Physik, 8, 321 (1922).
8. L. H. Thomas, J. Chem. Phys., 12, 449 (1944).
9. D. Gilbarg and D. Paolucci, J. Ratl. Mech. Anal., 2, 617 (1953).
10. L. M. Schwartz and D. F. Hornig, Phys. Fl., 6, 1669 (1963).
11. C. S. Wang-Chang, Univ. of Michigan, Dept. of Eng., Report UMH-3-F (APL/JHU CM-503), (1948).
12. H. Grad, Comm. Pure Appl. Math., 5, 257 (1952).
13. L. H. Holway, Jr., Phys. Fl., 7, 911 (1964).
14. H. M. Mott-Smith, Phys. Rev., 82, 885 (1951).
15. D. L. Rode and B. S. Tanenbaum, Phys. Fl., 10, 1352 (1967).
16. C. Muckenfuss, Phys. Fl., 5, 1325 (1962).
17. H. Salwen, C. E. Grosch and S. Ziering, Phys. Fl., 7, 180 (1964).
18. M. Krook, J. Fl. Mech., 6, 523 (1959).
19. M. Krook, in Rarefied Gas Dynamics, L. Trilling and H. Y. Wachman, Eds. (Acad. Press, Inc., N. Y.), Vol. I, p. 129 (1969).
20. H. K. Macomber, Harvard Univ., Eng. Sci. Lab. Tech. Report 13 (1964).
21. L. H. Holway, Jr., in Rarefied Gas Dynamics, J. H. DeLeeuw, Ed., (Acad. Press, Inc., N. Y.), Vol. I, p. 193 (1965).
22. S. H. Radin and D. Mintzer, Phys. Fl., 9, 1621 (1966).
23. K. Muraoka, T. Murakami and T. Ikui, Phys. Fl., 12, 2522 (1969).
24. W. A. Gustafson, Phys. Fl., 3, 732 (1960).
25. P. Glansdorff, Phys. Fl., 5, 371 (1962).
26. S. Ziering, F. Ek and P. Koch, Phys. Fl., 4, 975 (1961).
27. D. Baganoff and M. Nathenson, Phys. Fl., 13, 596 (1970).
28. P. L. Bhatnagar, E. P. Gross and M. Krook, Phys. Rev., 94, 511 (1954).
29. H. W. Liepmann, R. Narasimha and M. T. Chahine, Phys. Fl., 5, 1313 (1962).
30. M. T. Chahine in Rarefied Gas Dynamics, J. Laurmann, Ed., (Acad. Press, Inc., N. Y.), Vol. I, p. 260 (1963).

31. M. T. Chahine and R. Narasimha in Rarefied Gas Dynamics, J. H. DeLeeuw, Ed., (Acad. Press, Inc., N. Y.), Vol. I, p. 140 (1965).

32. D. G. Anderson, Ph.D. Thesis, Harvard University (1963).

33. D. G. Anderson, Harvard Univ., Engr. Sci. Lab. Tech. Report 15 (1965).

34. D. G. Anderson, J. Fluid Mech., 25, 271 (1966).

35. L. H. Holway, Jr., Ph.D. Thesis, Harvard University (1963).

36. _____ Phys. Fl., 9, 1658 (1966).

37. _____ in Rarefied Gas Dynamics, C. L. Brundin, Ed. (Acad. Press, Inc., N. Y.), Vol. I, p. 759 (1967).

38. D. P. Giddens, A. B. Huang and Y. C. Young, Proc. 20th Intl. Cong. Astronautics, Mar del Plata, Argentina (1969).

39. _____ in Rarefied Gas Dynamics (Proc. 7th Intl. Symp. RGD), (Acad. Press, Inc., N. Y.), to be published (1971).

40. J. E. Broadwell, Phys. Fl., 7, 1243 (1964).

41. A. Nordsieck and B. L. Hicks in Rarefied Gas Dynamics, C. L. Brundin, Ed. (Acad. Press, Inc., N. Y.), Vol. I, p. 695 (1967).

42. B. L. Hicks and M. A. Smith, J. Comp. Physics, Vol. 3, 1, 58 (1968).

43. B. L. Hicks and S. M. Yen, in Rarefied Gas Dynamics, L. Trilling and H. Y. Wachman, Eds. (Acad. Press, Inc., N. Y.), Vol. I, p. 313 (1969).

44. J. K. Haviland, in Methods in Computational Physics, B. Alder, Ed. (Acad. Press, Inc., N. Y.), Vol. 4, p. 109 (1965).

45. M. Perlmutter, in Rarefied Gas Dynamics, L. Trilling and H. Y. Wachman, Eds. (Acad. Press, Inc., N. Y.), Vol. I, p. 327 (1969).

46. G. A. Bird, J. Fl. Mech., 30, 479 (1967).

47. _____, in Rarefied Gas Dynamics, L. Trilling and H. Y. Wachman, Eds. (Acad. Press, Inc., N. Y.), Vol. I, p. 85 (1969).

48. _____, Phys. Fl., 13, 1172 (1970).

49. _____, Phys. Fl., 13, 2676 (1970).

50. B. Schmidt, J. Fl. Mech., 39, 361 (1969).

51. R. A. Matula, J. Heat Transfer (Trans. ASME), 90c, 319 (1968).

52. M. T. Chahine and R. Narasimha, J. Math. Phys., 43, 163 (1964).

53. D. G. Anderson and H. K. Macomber, Harvard Univ., Engr. Sci. Lab. Tech. Report 10 (1964).

54. E. M. Shakhov, Akad. Nauk. SSSR, Mekh. Zh. Gaza, 1, 156 (1968).

55. G. E. Uhlenbeck and G. W. Ford, Lectures in Statistical Mechanics, American Math. Soc. (1963).

56. S. Chapman and T. G. Cowling, The Mathematical Theory of Non-Uniform Gases, Cambridge University Press (1964).

57. C. S. Wang-Chang and G. E. Uhlenbeck, Univ. of Michigan, Engr. Res. Inst. Project M999 (1952).

58. E. P. Gross and E. A. Jackson, Phys. Fl., 2, 432 (1959).

59. D. Enskog, Doctoral Dissertation, Uppsala (1917).

60. P. Welander, Arkiv Fysik, 7, 507 (1954).

61. C. Cercignani and G. Tironi, in Rarefied Gas Dynamics, C. L. Brundin, Ed. (Acad. Press, Inc., N. Y.), Vol. I, p. 441 (1967).

62. S. M. Deshpande and R. Narasimha, J. Fl. Mech., 36, 545 (1969).

63. J. H. Ahlberg, E. N. Nilson and J. L. Walsh, Theory of Splines and Applications (Acad. Press, Inc., N. Y.), (1967).

64. M. Abramowitz and I. Stegun (Eds.), Handbook of Mathematical Functions, AMS 55, Natl. Bureau of Standards, Wash., D. C., p. 920 (1964).

65. D. G. Anderson, Math. Comp., 19, 477 (1965).

66. _____, J. ACM, 12, 547 (1965).

67. G. S. Deiwert, NASA-Ames Research Center, private communication (1970).

68. L. H. Holway, Jr., Phys. Fl., 8, 1905 (1965).